

Plant nitrate reductase and its isoform specific roles in nitrate and nitrite reduction



Inaugural-Dissertation
zur Erlangung des Doktorgrades
der Mathematisch-Naturwissenschaftlichen Fakultät
der Universität zu Köln

vorgelegt von

Marie Agatha Mohn
aus Borrisokane, Irland

Köln, März 2019

Marie Mohn

Berichterstatter: Prof. Dr. Guenter Schwarz
Gutachter Prof. Dr. Stanislav Kopriva

Tag der mündlichen Prüfung: 17th April 2019

Marie Mohn

Publications

- 2019 Marie Mohn, Besarta Thaqi, and Katrin Fischer-Schrader. *Isoform-specific NO synthesis by Arabidopsis thaliana nitrate reductase*. Plants Special Edition NO

Conference participation, poster contributions

- 2017 Marie Mohn, Katrin Fischer-Schrader. *Biochemical characterization of plant nitrate reductase isoform 1*. MoTEC X, Santa Fe, USA, June 2017
- 2018 Marie Mohn, Katrin Fischer-Schrader. *Biochemical characterization and comparison of isoform 1 and 2 Arabidopsis thaliana nitrate reductase*. Chemistry symposium, Department of Chemistry, University of Cologne, April 2018
- 2018 Marie Mohn, Besarta Thaqi, Dimitri Niks, Russ Hille, Katrin Fischer-Schrader. *Biochemical characterization of plant nitrate reductase isoform 1 and 2 in nitric oxide synthesis*. 10th International Conference on the Biology, Chemistry and Therapeutic Applications of Nitric Oxide, Oxford, UK, September 2018
- 2018 Marie Mohn, Besarta Thaqi, Dimitri Niks, Russ Hille, Katrin Fischer-Schrader. *Isoform specific function of nitrate reductase 1 and 2 in Arabidopsis thaliana*. 7th Plant Nitric Oxide International Meeting, Nice, France, October 2018

List of Figures	VIII
List of Tables	IX
Abbreviations	X
Zusammenfassung	XII
Abstract	XIII
1 Introduction	1
1.1 Nitrogen.....	1
1.2 Ammonium or nitrate?.....	1
1.3 Nitrate as a nutrient	2
1.3.1 Nitrate uptake by plants.....	2
1.3.2 Nitrate assimilation	3
1.4 Nitrate as a signal	3
1.5 Nitric oxide in plants.....	5
1.5.1 Sources of NO [•]	5
1.5.2 Biological functions of NO [•]	7
1.5.3 Mechanism(s) of action of NO [•]	8
1.6 The enzyme nitrate reductase.....	9
1.6.1 Structure of NR.....	10
1.6.2 Electron transport in NR.....	12
1.6.3 Functional domain fragments of NR	13
1.6.4 Isoforms of NR	14
1.6.4.1 Transcriptional differences between NR isoforms.....	14
1.6.4.2 Differences between NR isoforms on the protein level.....	17
1.6.5 Regulation of NR.....	20
1.6.5.1 Regulation of NR in nitrate reduction	20
1.6.5.2 Regulation of NR in nitrite reduction	23
1.6.5.3 14-3-3 proteins	23
1.7 Aim of this project.....	26
2 Results	27
2.1 Production of full-length AtNR.....	27
2.1.1 Expression of AtNR1-fl in KM71	27
2.1.2 Expression of codon-optimized AtNR1-fl in KM71	28
2.1.3 Expression of codon-optimized AtNR1-fl in GS115	30
2.1.4 C-terminal His-tagged AtNR1-co fl	32
2.1.5 Full-length NR2	34

2.2	Production of functional domain fragments of <i>AtNR</i>	36
2.2.1	Expression and purification of <i>AtNR1</i> -Mo-heme	36
2.2.2	Expression of <i>AtNR</i> -FAD fragments.....	39
2.2.3	Expression of <i>AtNR</i> -Mo fragments.....	39
2.3	Other constructs cloned for expression in <i>P. pastoris</i>	41
2.4	Nitrate reduction activity of recombinant NR.....	42
2.4.1	NADH:nitrate activity of full-length NR	42
2.4.2	The methyl viologen:nitrate activity of NR-Mo-heme	43
2.5	Re-constitution of full-length NR-activity from domain fragments	46
2.5.1	Establishing re-constituted NR activity	46
2.5.2	NADH:nitrate activity of re-constituted-NR	47
2.5.3	Pre-steady-state kinetics of NR1 and NR2 in nitrate reduction using re-constituted NR activities	48
2.6	Nitrite reducing activity of recombinant NR	52
2.6.1	Establishing a procedure for benzyl viologen nitrite activity determination (BV:nitrite)	52
2.6.2	NR-Mo-heme BV:nitrite activity	54
2.6.3	Nitrite reductase activity measured with an NO-Analyzer.....	55
2.6.4	Interplay of nitrate and nitrite as substrates of NR.....	58
2.6.5	Stoichiometry of NO [*] generation	60
2.7	Regulation of NR by 14-3-3 proteins	62
2.7.1	Regulation of NR activity of NR1 and NR2.....	62
2.7.2	Regulation of nitrite reductase activity of NR1 and NR2	65
2.8	Structure model of NR.....	68
3	Discussion	71
3.1	Recombinant NR expression	71
3.2	Functional domain fragments of NR	73
3.2.1	Nitrate reduction activity of NR-Mo-heme fragments.....	75
3.2.2	Nitrite reduction activity of NR-Mo-heme fragments.....	76
3.2.3	A comparison of NR isoforms from <i>Arabidopsis</i> and Soybean.....	80
3.3	Reconstitution of full-length NR activity	80
3.4	Pre-steady-state kinetics	82
3.5	Nitrite reduction activity with the nitric oxide analyzer	83
3.6	Stoichiometry of NO [*] generation by NR.....	86
3.7	14-3-3-mediated inhibition of NR1 and NR2.....	86
3.8	Structure model of NR.....	88
4	Conclusion and outlook	90

5	Materials and Methods	92
5.1	DNA cloning	92
5.2	Yeast methods	94
5.3	Full-length NR expression in <i>Pichia</i> and affinity purification	97
5.4	Recombinant protein expression in <i>E. coli</i>	99
5.5	Other biochemical techniques	102
5.6	Enzyme activity measurements.....	103
6	References.....	108
	Appendix 1	121
	Appendix 2	126
	Appendix 3	132
	Acknowledgements.....	133
	Erklärung.....	134

List of Figures		Page
Figure 1	Schematic illustration of a plant cell showing nitrate uptake and assimilation.	2
Figure 2	Schematic representation of the domain structure of NR	10
Figure 3	Model of NR structure	12
Figure 4	Comparison of <i>NIA1</i> and <i>NIA2</i> expression in publicly available transcriptomics data for wild type <i>Arabidopsis</i>	15
Figure 5	Factors influencing NR1 and NR2 expression and activity in <i>A. thaliana</i>	16
Figure 6	Model of inhibition of NR by 14-3-3 proteins	22
Figure 7	Structure model of 14-3-3 ω from <i>A. thaliana</i>	24
Figure 8	Clone selection of <i>P. pastoris</i> KM71 transformed with (natural) <i>AtNR1</i> DNA for expression	28
Figure 9	Clone selection of <i>P. pastoris</i> KM71 transformed with the codon-optimized <i>AtNR1</i> DNA for expression	30
Figure 10	Clone selection of <i>P. pastoris</i> GS115 with the codon-optimized <i>AtNR1</i> DNA for expression	31
Figure 11	Absence of binding to Ni-NTA resin by <i>AtNR1</i> -co expressed <i>Pichia pastoris</i> GS115	32
Figure 12	Expression in <i>Pichia pastoris</i> GS115 and purification of <i>AtNR1</i> -co with C-terminal his-tag	34
Figure 13	Purification of full-length NR2 expressed in <i>P. pastoris</i> KM71	35
Figure 14	Purification of NR-Mo-heme fragments expressed in <i>E. coli</i> TP1004	38
Figure 15	Purification FAD-domain fragments of NR1 and NR2	39
Figure 16	Purification NR-Mo-domain fragments of NR1 and NR2	40
Figure 17	NADH:nitrate activity of full-length NR1 and NR2 expressed in <i>P. pastoris</i>	43
Figure 18	MV:nitrate reduction activity of NR1-Mo-heme and NR2-Mo-heme	45
Figure 19	NADH:nitrate activity of re-constituted full-length NR1 and NR2	47
Figure 20	Pre-steady-state kinetic measurements of nitrate reduction by NR2	50
Figure 21	Pre-steady-state kinetic measurements of nitrate reduction by NR1	52
Figure 22	Stability of MV and BV in the presence of nitrate and nitrite. Determination of optimal pH for measuring BV:nitrite activity	53
Figure 23	BV:nitrite steady-state activity measurement	55
Figure 24	Substrate concentration dependent NO [•] generation measured using the NO-analyzer	57
Figure 25	Interplay of nitrate and nitrite on NO [•] generation	59
Figure 26	Stoichiometry of NO [•] generation by pre-reduced NR2-Mo-heme	61

Figure 27	Phosphorylation of NR1-Mo-heme by CPK3 kinase and MV:nitrate activity measurement	62
Figure 28	Inhibition of MV:NR activity by 14-3-3 isoforms	64
Figure 29	Test of 14-3-3 inhibition of BV:nitrite activity	67
Figure 30	Cryo-EM for determination of molecular structure of NR2	70
Figure 31	Substrate binding funnel of NR1 and NR2 compared in models based on <i>Pichia angusta</i> NR-Moco crystal structure	76
Figure 32	Chemical structures of Methyl viologen (MV) and benzyl viologen (BV) each shown with its single electron reduced radical	77

List of Tables

Page

Table 1	List of constructs cloned for expression in <i>P. pastoris</i>	41
Table 2	Michaelis Menten kinetic parameters of NR1 and NR2 NADH:nitrate activity	43
Table 3	Kinetic constants for MV:nitrate activity using NR-Mo-heme fragments	45
Table 4	Michaelis Menten kinetic parameters for NADH:nitrate activity of re-constituted NR1 and NR2	48
Table 5	Michaelis Menten kinetic parameters of BV:nitrite activity for NR1-Mo-heme and NR2-Mo-heme	55
Table 6	Pseudo Michaelis Menten kinetic parameters of NR1-Mo-heme and NR2-Mo-heme determined using the NO analyzer	57
Table 7	NR1-Mo-heme and NR2-Mo-heme summarized 14-3-3 inhibition-kinetic parameters	65
Table 8	Kinetic parameters for NR1- and NR2-Mo-domain and NR2-H600A heme free mutant	68

Abbreviations

Abbreviation	Definition	Abbreviation	Definition
ABA	Abscisic acid	mM	millimolar
[M]	Molar concentration	mm	millimeter
AHA2	<i>Arabidopsis</i> plasma membrane H ⁺ -ATPase isoform 2	MM	Michaelis Menten
<i>At</i>	<i>Arabidopsis thaliana</i>	MMH	Minimal methanol medium
ATH1	<i>Arabidopsis</i> genome array	Mo	Molybdenum
<i>Atnoa1</i>	<i>Arabidopsis thaliana</i> nitric oxide associated 1 mutant plant	Moco	Molybdenum cofactor
<i>Atnos1</i>	<i>Arabidopsis thaliana</i> nitric oxide synthase 1 mutant plant	mRNA	messenger RNA
ATP	Adenosine triphosphate	MS	Mass Spectrometry
BH4	Tetrahydro-biopterin	mV	Millivolt
BMMY	Buffered methanol medium yeast extract (complex)	MV	Methylviologen (N,N'-dimethyl-4,4'-bipyridinium dichloride)
bp	Base pairs of DNA	mV	Millivolt
BSA	Bovine serum albumin	MW	Molecular weight
BV	Benzyl viologen	n.d.	not determined
Ca ⁺⁺	Calcium ions	N ₂	Nitrogen
CaCl ₂	Calcium chloride	NaCl	Sodium Chloride
cDNA	copy DNA	NADH	Nicotinamide adenine dinucleotide
CO	Codon optimized	NADPH	Nicotinamide adenine dinucleotide (phosphate)
CO ₂	Carbon dioxide	NaOH	Sodium hydroxide
CPK	Calcium-dependent protein kinase family	NEB	New England Biolabs
CPK3-GST	Calcium dependent protein kinase with Glutathione S Transferase tag	NH ₄ ⁺	Ammonium
Cryo-EM	Cryo Electron microscopy	<i>NIA</i>	The gene for nitrate reductase
CSO	Chicken sulfite oxidase	<i>nia1</i>	Mutant defective in <i>NIA1</i> gene
ddH ₂ O	distilled, deionized water	<i>nia2</i>	Mutant defective in <i>NIA2</i> gene
DMSO	Dimethyl Sulfoxide	Ni-NTA	Nickel Nitrilotriacetic acid
DNA	Deoxyribonucleic acid	NiR	Nitrite reductase
<i>E. coli</i>	<i>Escherichia coli</i>	NLP	Nodule inception-like proteins
ECL	Enhanced chemiluminescence	nm	Nanometer
EDTA	Ethylenediaminetetraacetic acid	NO [•]	Nitric oxide
ε ₄₁₃	Extinction coefficient at 413nm	NO ₂ ⁻	Nitrite
FAD	Flavin adenine dinucleotide	NO ₃ ⁻	Nitrate
FeMoco	Iron-Molybdenum cofactor	NOG	Nitric oxide generating
Fig	Figure	NOS	Nitric oxide synthase
FL	Full-length	NR	Nitrate reductase
FMN	Flavine mono nucleotide	NR-Mo-heme	Molybdenum-heme domain fragment of NR

GE	General electric	NUE	Nitrogen use efficiency
GOGAT	Glutamate synthase	O ₂	Molecular oxygen
GS	Glutamine synthetase	O ₂ ⁻	Superoxide anion
GSH	Glutathione	OD	Optical density
GSNO	S-Nitrosoglutathione	Os	<i>Oryza sativa</i>
GTP	Guanosine triphosphate	PAGE	Polyacrylamide gel electrophoresis
h	hour	PCR	Polymerase chain reaction
H ⁺	Hydrogen ion/ Proton	PDB	Protein Data Bank
H ⁺ ATPase	Proton Adenosine triphosphate-ase (Cell membrane proton pump)	PEG	Polyethylene glycol
H ₂ O ₂	Hydrogen peroxide	PNR	Primary nitrate response
H ₂ S	Hydrogen sulfide	pNR	phosphorylated nitrate reductase
HATS	High affinity transport system	PP2A	Protein phosphatase 2
HCl	Hydrochloric acid	pSer	Phosphorylated serine
His	Histidine	RNA	Ribonucleic acid
HRP	Horse radish peroxidase	ROS	Reactive oxygen species
IC ₅₀	Inhibitory concentration leading to half maximal activity	RT	Room temperature
ID	Identify	S	Sulfur
IMAC	Immobilized metal affinity chromatography	s / sec	second
IPTG	Isopropyl β-D-1-thiogalactopyranoside	SA	Salicylic acid
<i>k_{cat}</i>	Enzyme turnover number	SDS	Sodium dodecyl sulfate
KCl	Potassium chloride	SEC	Size exclusion chromatography
K _D	Dissociation constant	SEM	Standard error of the mean
kDa	Kilo Dalton	Ser	Serine
K _M	Michaelis constant	SNF	Sucrose non-fermenting
<i>k_{obs}</i>	Observed rate of re-oxidation	SNRK1	SNF1 resembling kinase family
<i>k_{ox}</i>	Reoxidation constant	SO	Sulfite oxidase
KPO ₄	Potassium phosphate buffer	So	<i>Spinacia oleracea</i>
LATS	Low affinity transport system	t _{1/2}	Half-life
LB	Lauria bertani medium	T _A	Annealing temperature
M	Molar	TAE	Tris Acetate EDTA buffer
mARC	mitochondrial amidoxime reducing component	UV/vis	UV/visible
MCS	Multiple cloning site	wt	Wild type
Mg ⁺⁺	Magnesium ions	XOR	Xanthine oxidoreductase
MgAc	Magnesium acetate	YPD	Yeast peptone dextrose medium
min	minute	YPDS	Yeast peptone dextrose sorbitol medium
ABA	Abscisic acid	mM	millimolar
[M]	Molar concentration	mm	millimeter
AHA2	<i>Arabidopsis</i> plasma membrane H ⁺ -ATPase isoform 2	MM	Michaelis Menten
<i>At</i>	<i>Arabidopsis thaliana</i>	MMH	Minimal methanol medium

Zusammenfassung

Viele Pflanzen, unter anderem *Arabidopsis thaliana*, exprimieren zwei Isoformen der Nitrat Reduktase (NR1 und NR2). Dieses Enzym katalysiert die Reduktion des Nitrats zu Nitrit, und damit die schrittlimitierende Reaktion in der Nitratassimilation. Zudem ist NR eine wichtige enzymatische Quelle des universellem Signalmoleküls NO[•].

NR bildet ein Dimer mit drei redox-Cofactoren je monomer; am N-Terminus, ein Molybdän-Cofactor (Moco), in der Mitte eine Häm-*b5* und am C-Terminus ein FAD Cofactor. Elektronen werden übertragen vom zellulärem NADH, über FAD und Häm zu dem Substrat, das von Moco reduziert wird.

Die Regulierung der NR Aktivität ist komplex und vielschichtig. Tagsüber wird die Transkription hochreguliert, angepasst an der photosynthetischen Aktivität, nachts wird es herunterreguliert. Zudem wird NR über ein komplexes System der post-translationalen Regulation gesteuert in dem ein regulatorisches 14-3-3 Protein an einem phosphorylierten Serin-Rest bindet und Domän-Bewegungen und damit Aktivität verhindert. Diese Form der Regulierung ist schnell und reversible und verhindert ein toxischen Überschuss an Nitrit. Interessanterweise ist es in genau diesen Situationen in denen die Nitrit-Konzentration kurzfristig steigt, in welchen NO[•] Produktion beobachtet wird.

Obwohl es bekannt ist, dass NR in der Pflanze eine wichtige Quelle für NO[•] ist, wurden die kinetischen Parameter der Nitritreduktion durch rekombinante NR noch nicht untersucht. Zudem wurde noch nicht untersucht ob die zwei (oder mehr) Isoformen der NR vielleicht unterschiedlich beteiligt sein könnten an den zwei Reaktionen die das Enzym katalysiert.

In dieser Arbeit wurden die zwei Isoformen der NR rekombinant exprimiert und in verschiedene kinetische Analysen verglichen. Es konnte gezeigt werden, dass NR1 einen hohen K_M für Nitrat besitzt und eine vielfach niedrigere katalytische Effizienz für das Substrat Nitrat, verglichen mit NR2. In der Nitritreduktion hat NR1 ein etwa 10-fach höherem k_{cat} verglichen mit NR2. Zudem wurden Unterschiede zwischen den Isoformen in der 14-3-3 Regulation festgestellt. Diese Ergebnisse zeigen dass NR1 ein spezialisiertes Enzym der Nitrit-Reduktion ist, während NR2 eine Nitrat Reduktase ist. Zudem wurde mittels cryo-EM ein Model der NR generiert. Diese Methode könnte in Zukunft helfen die Molekularstruktur des NR's zu ermitteln.

Abstract

Many plants, including the model plant *Arabidopsis thaliana*, express two isoforms of the enzyme nitrate reductase (NR1 and NR2). This enzyme catalyses the first and rate-limiting step of nitrate assimilation by conversion of nitrate to nitrite. Furthermore, by reduction of nitrite to NO[•], NR is also a major enzymatic source of this universally important signalling molecule in the plant.

NR is a large, dimeric, multi-domain protein containing three redox-active cofactors per monomer – a Moco at the N-terminus, a *b5*-type heme located centrally, and an FAD cofactor at the C-terminus. NR transfers electrons from the cellular electron donor NADH through the FAD cofactor, then the heme, to the Moco where the substrates nitrate or nitrite bind and are reduced.

Regulation of NR activity is complex and takes place on multiple levels. Transcriptional regulation mainly functions to serve the diurnal requirement for NR in the plant with up-regulation to match photosynthetic activity during daylight, and down-regulation at night. In addition, a complex post-translational regulation mechanism for NR is known in which a regulatory 14-3-3 protein binds to a phosphorylated serine and arrests domain movement and activity. This means of regulation is fast and reversible allowing the plant to respond within minutes to darkness or lack of CO₂ and avoid long-term, toxic nitrite accumulation. On the other hand, there is evidence, that in situations in which a short-term spike in nitrite concentration is observed, NO[•] generation occurs.

The kinetic parameters for nitrite reduction have never been determined before for pure recombinant NR protein. In addition, it has not been tested, whether the two or multiple isoforms of NR in many plant species may have distinct catalytic roles in the plant.

To examine these questions, the two NR isoforms of *Arabidopsis* were separately expressed and compared in multiple kinetic studies. It could be shown that NR1 has a very large K_M for nitrate and a far lower catalytic efficiency compared with NR2, while NR1 has a 10-fold higher k_{cat} for nitrite and a five-fold higher catalytic efficiency compared with NR2. Additionally, differences were observed in the post-translational regulation of NR1 and NR2 via 14-3-3 proteins. These results show that NR2 is a dedicated nitrate reductase and NR1 a nitrite reductase. In addition, a model of the NR structure could be obtained by cryo-EM and this method offers a promising possibility to determine the molecular structure of NR in the future.

1 Introduction

1.1 Nitrogen

Nitrogen is the fourth-most abundant structural element of living organisms after carbon, oxygen and hydrogen. The earth's atmosphere is composed of about 78% nitrogen gas, but in this triple-bonded N_2 form it is extremely inert and requires energetically expensive fixation before it can be used by lifeforms (Erisman et al., 2008). In the natural nitrogen cycle, only bacteria containing nitrogenase enzymes (diazotrophs) are capable of fixing gaseous nitrogen into the inorganic forms that can be used by plants (besides an additional small amount of nitrogen fixed by lightning in the atmosphere) (Canfield et al., 2010). This means that plants growing on natural soils are frequently limited in their growth due to low nitrogen availability (Vitousek and Howarth, 1991). The discovery in 1908 of the Haber Bosch process for industrial nitrogen fixation has massively boosted crop productivity worldwide by provision of fixed inorganic nitrogen to plants for food production (Smil, 2002, 2011). Nitrogen compounds within plants – mainly generated by uptake and conversion of nitrate and ammonium into organic forms – represent the main source of organic nitrogen for heterotrophic organisms (Beevers and Hageman, 1983).

1.2 Ammonium or nitrate?

The two main sources of nitrogen nutrients available in the soil for plant growth are ammonium (NH_4^+) and nitrate (NO_3^-) (Miller et al., 2007). Ammonium requires less energy for plants to incorporate it into amino acids, however, excess NH_4^+ is in fact toxic to many plant species because it causes an energetically expensive transport cycling into and out of the cell (Britto et al., 2001). Certain plant species such as rice which grows on lowland, water-logged soils preferentially uptakes ammonium and is resistant to ammonium toxicity (Kronzucker et al., 2000). Nevertheless, even for rice, a strong benefit in growth and productivity is seen when nitrate is also available (Kronzucker et al., 2000). The vast majority of higher plant species growing in aerobic temperate soils including most agricultural crop plant species use nitrate as the preferred source of nutrient nitrogen (Wang and Macko, 2011).

1.3 Nitrate as a nutrient

1.3.1 Nitrate uptake by plants

The availability of nitrate in the soil can vary widely from <1 mM up to 70 mM in heavily fertilized agricultural soil (Crawford and Glass, 1998; Forde and T. Clarkson, 1999). Uptake of NO_3^- into the plant root cells is an active process. Specialized transporter proteins have evolved to fulfil this function in both cases of low nitrate supply (High affinity nitrate transporters, HATS) and high nitrate supply (low affinity nitrate transporters, LATS) (Miller et al., 2007) (Fig. 1). The nitrate transporter proteins efficiently capture available nitrate and transport it into the cells in a system in which H^+ ions are simultaneously transported in (Buchanan et al., 2015). H^+ ions for this uptake are maintained at a locally high concentration outside the cell by the action of the membrane H^+ -ATPase (Michelet and Boutry, 1995). Once inside the cytosol, nitrate may follow one of several pathways: Firstly, it may immediately be reduced to nitrite by the enzyme NR as discussed in detail in the coming sections or secondly, it may be stored in the vacuole. Alternatively, it may be exported into the xylem and translocated to aerial plant cells where it may be stored in the vacuole or assimilated.

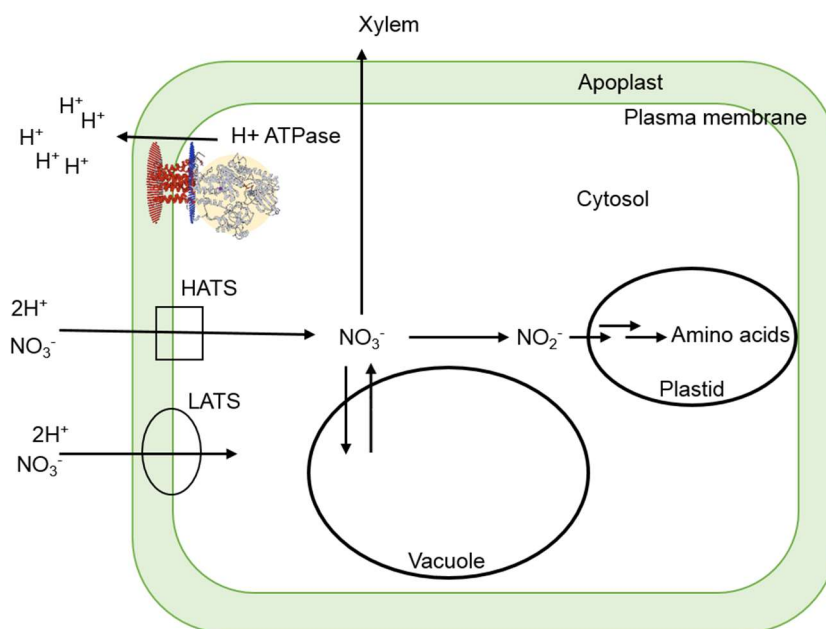


Figure 1: Schematic illustration of a plant cell showing nitrate uptake and assimilation. Proton ATPase AHA2 is shown using its crystal structure (PDB 5ksd) (Focht et al., 2017), it functions in maintaining an excess of protons outside the cell for symport of NO_3^- into the cell. HATS and LATS are the high- and low- affinity nitrate transporters. Inside the cell NO_3^- is reduced to NO_2^- in the cytoplasm then transported to the plastids for further assimilation, or is stored in the vacuole or loaded in the xylem for transport to other plant parts.

1.3.2 Nitrate assimilation

The first committed step of nitrate assimilation in the plant cytosol is the reduction of nitrate to nitrite by the enzyme NR (Campbell, 2001). This enzyme was first recognised and partially purified from soybean in 1953 (Evans and Nason, 1953). The two electrons required for reduction of nitrate are supplied in the plant by either NADH or NADPH. Some plants have a bispecific NADH/NADPH NR such as barley (Dailey et al., 1982), rice (Shen, 1972) and soybean (Dean and Harper, 1988) but the majority of higher plants utilize only NADH. There was a clear allocation in one study, with 15 of 16 NRs tested using the substrate NADH (Ritenour et al., 1967). The reaction catalysed is as follows:



The nitrite thus formed is rapidly transported to the plastids (in roots) or to the chloroplasts (in leaves) for assimilation. Further reduction of nitrite to ammonium in the plastid requires six electrons which, originate from photosynthetic activity and are supplied in the form of reduced ferredoxin (Solomonson and Barber, 1990). Finally, the ammonium is coupled to the carbon skeleton of a glutamate (also a product of photosynthesis) by the enzyme glutamine synthetase to yield glutamine. Glutamate oxoglutarate aminotransferase then transfers the alpha amino group to 2-oxoglutarate to yield two molecules of glutamate (Masclaux-Daubresse et al., 2006). Transamination reactions result in the formation of all the nitrogenous compounds required by the plant (Lam et al., 1996). The need for carbon skeletons and electrons derived from photosynthesis mean that nitrogen assimilation ultimately depends on photosynthesis. In fact, it is estimated that 25% of the energy of photosynthesis is used for nitrogen assimilation (Solomonson and Barber, 1990).

1.4 Nitrate as a signal

Besides the primary role of nitrate as a nutrient for plants, nitrate is also a powerful signalling molecule that controls many aspects of plant growth and development, (reviewed in Fredes et al., 2019). In fact, a report in 1983 about the effects of nitrate seen on plants led the author to describe nitrate as a 'plant hormone' (Trewavas, 1983). Meanwhile, the pathways and processes that are controlled by nitrate have been extensively examined and many details understood. Nitrate effects on the plant start

with the sensing of nitrate in the soil by the root cells causing root growth toward the source of the nutrient (Forde and Zhang, 1998; Mlodzinska et al., 2015). Nitrate is also a signal that releases seed dormancy and induces seed germination (Fredes et al., 2019). High nitrate supply stimulates vegetative growth and delays flowering, while plants grown under low nitrate supply accelerate flowering (Castro Marín et al., 2011; Stitt, 1999).

For the model plant *A. thaliana*, it is interesting to look at the scale of nitrate signalling effects using the publicly available transcription data obtained using the whole genome microarray chip ATH1 from Affymetrix (GeneChip® Arabidopsis ATH1 Genome Array). It was shown that 20 minutes of nitrate application to previously nitrate-starved plants resulted in up- or down-regulation of up to 10% of all genes (of 22500 in total) (Wang et al., 2003). In another study, an NR knock-out mutant of *Arabidopsis* was used, in order to exclude that downstream metabolites of nitrate reduction (such as nitrite or ammonium) exerted influence on gene expression. This study could pinpoint that 595 genes (~2% of the genome) were directly influenced by nitrate (Wang et al., 2004) and indirectly implying that the remaining 8% of gene transcription was influenced by downstream metabolites of nitrate (such as nitrite and ammonium).

Up-regulation for some genes (including NR) takes place already only 15 – 30 minutes following nitrate application (Krouk et al., 2010), cannot be inhibited by cyclohexamide (a protein synthesis inhibitor) and is therefore part of the Primary Nitrate Response (PNR) (Medici and Krouk, 2014). There are multiple definitions of PNR, but one definition includes responses stimulated by applied nitrate that do not require *de novo* protein synthesis (Medici and Krouk, 2014). PNR also comprises transcription of genes for nitrate transport, for nitrite reduction and the gene encoding for Glucose-6-phosphate 1-dehydrogenase 3 which, catalyses the rate-limiting step of the oxidative pentose-phosphate pathway (Medici and Krouk, 2014).

How exactly nitrate influences gene expression leading to this metabolic reprogramming is not fully understood, however a nitrate responsive *cis*-element has been found in the regulatory DNA sequence of some nitrate responsive genes (Konishi and Yanagisawa, 2011b). In addition, NODULE INCEPTION-like proteins (NLP's) have been identified that are post-translationally modified by nitrate and then act as transcription factors influencing the transcription of nitrate responsive genes (Yanagisawa, 2014).

1.5 Nitric oxide in plants

Up until the late 1980's and early 1990's the free radical gaseous molecule NO[•] was mainly recognised as an environmental toxin (Yamasaki, 2005). It had been observed emitted from plants under certain conditions – such as upon herbicide treatment (Klepper, 1979) – but the concept of NO[•] functioning as a signalling molecule in plants was only recognised after the discovery that NO[•] serves as a signalling molecule in animals (Ignarro et al., 1987). In animals this observation was followed by the discovery that NO[•] was enzymatically generated by a dedicated family of nitric oxide synthase enzymes (NOS) (Bredt and Snyder, 1990; Lamas et al., 1992; Moncada et al., 1989; Xie et al., 1992).

1.5.1 Sources of NO[•]

The early observation of NO[•] emission from plants was thought to be the result of a chemical reaction between nitrite, that had accumulated because of herbicide treatment, and plant metabolites (Klepper, 1979). Further research revealed that the NO[•] generation was enzymatic, and used nitrite as substrate, (Harper, 1981). Subsequently, NR was identified as the enzyme responsible for NO[•] production from nitrite (Dean and Harper, 1988) and thus it was recognised for the first time that NR catalyses not just the reduction of nitrate to nitrite but also reduction of nitrite to NO[•].

Despite these early findings about an important source of NO[•] in plants, the focus of much research turned instead to the search for a NOS in plants. It was thought that NOS proteins in plants must exist similar to the NOS in animals. Measurements of L-arginine oxidation by plant extracts in the presence of known NOS cofactors (tetrahydrobiopterin (BH₄), calmodulin, Ca²⁺, NADPH, FAD and FMN), resulted in detectable NO[•] production and the formation of L-citrulline. However higher plants do not produce the cofactor BH₄ and therefore, this cannot be a natural cofactor for putative NOS enzymes in plants, nevertheless, it was described as being strictly required for NO[•] synthesis (Corpas et al., 2004). Furthermore, this NO[•] generation could be pharmacologically modulated by animal NOS inhibitors (Barroso et al., 1999; Corpas et al., 2004; Delledonne et al., 1998; Modolo et al., 2002). This NO[•] synthesising activity was detected in association with cellular organelles such as peroxisomes and chloroplasts (Barroso et al., 1999; Prado et al., 2004) or mitochondria (Modolo et al., 2005). Other studies showed cross-reactive protein bands in crude plant

extracts to antibodies raised against animal NOS isoforms (Barroso et al., 1999; Modolo et al., 2002; Ribeiro et al., 1999). This was later proven in some cases to be unspecific cross reaction of the antibody as the protein(s) identified had no similarity with NOS enzymes (Butt et al., 2003).

In 2003, Guo *et al.* published the discovery of a plant NOS sequence (Guo et al., 2003), which was hailed as a breakthrough. NOS-activity in the mutant plant (*Atnos1*) as measured by L-citrulline formation in leaf extract was reported to be only 25% of the NOS activity in wild type (wt) plants. Another study showed that lipopolysaccharides (mediators of innate immune responses) caused a burst of NO[•] release that was not inhibited by sodium azide (an NR inhibitor), but could be associated with NOS activity since the *Atnos1* mutant had 80% reduced levels of NO[•]-burst (Zeidler et al., 2004).

Later however, doubts arose about the direct participation of *AtNOS* in NO[•] generation in plants and, the gene had to be renamed from 'NOS' to 'nitric oxide associated' (NOA1) because NOS activity of the recombinant protein could not be detected (Zemojtel et al., 2006) and the protein was homologous to a GTPase protein (Sudhamsu et al., 2008). *Atnoa1* mutant plants have altered NO[•] levels, but this is no longer thought to arise from a direct activity of NOA1 protein in NO[•] synthesis, rather the effect appears to be indirect.

In summary, it can be said that no NOS gene or enzyme has been detected in plants to date – despite the sequencing of the genomes of 1000 plant species (Matasci et al., 2014). Most recently it has been proposed to cease using the term 'NOS activity' in plants and instead to use the term 'nitric oxide generating (NOG)' to more accurately name the observed NO[•] generation in the absence of any NO-synthase (Hancock and Neill, 2019). However, because such a body of data exists showing oxidative NO[•] generation, it has been proposed that NO[•] is generated by a NOS/NOG activity putatively composed of multiple subunits (with no similarity to animal NOS, and having no requirement for BH₄), but with a conserved function in oxidative NO[•] generation (Crawford, 2005). Confirmation of this proposal is outstanding.

In addition, other NO[•] sources in plant cells exist, for example, a non-enzymatic low-pH dependent NO[•] release from nitrite, which was shown for the aleurone layer in the apoplast of barley grains (Bethke et al., 2004). Other nitrite-reductive mechanisms involving components of the mitochondrial electron transport chain (most likely Complex III) or other heme-containing proteins have been demonstrated to produce

NO[•] (Alber et al., 2017; Benamar et al., 2008; Planchet et al., 2005). Finally, other molybdenum-containing enzymes, besides NR have the capacity to produce NO[•] via reduction of nitrite (Bender and Schwarz, 2018). In animal systems xanthine oxidoreductase (XOR) is recognised as an NO[•] source (Harrison, 2002), however studies with recombinant plant XOR revealed no NO[•] production (Planchet, 2006). Mitochondrial amidoxime reducing component (mARC) is a further Moco enzyme with nitrite to NO[•] catalytic activity with *in vitro* activity shown for the plant enzyme (Yang et al., 2015). In conclusion, a wide range of sources for NO[•] exist in plants depending on the context and signal that triggers NO[•] production.

1.5.2 Biological functions of NO[•]

Despite the described controversy concerning the NO[•] source in plants, NO[•] is now clearly established as a crucial signalling molecule in plants involved in various processes. These include physiological responses, pathogen defence responses and abiotic stress responses and are described in detail below.

Looking more closely at studies showing physiological effects of NO[•], treatment of lettuce seeds with the NO[•] donor SNP led to a stimulation of seed germination and chlorophyll production, while hypocotyl elongation was 20% reduced (Beligni and Lamattina, 2000). NO[•] modulated the expression of cell cycle regulatory genes in a model examining formation of lateral root primordia (Correa-Aragunde et al., 2006). Pollen tube orientation as it grows through the pistil toward the female gametophyte was shown to be steered by NO[•] (Prado et al., 2004). NO[•] also plays a role in flowering induction, with the concentration of NO[•] in the floral parts increasing until anthesis (Seligman et al., 2008). The aleurone layer cells of *Arabidopsis* seeds have been shown to be NO[•] responsive and thus to function as a primary determinant of seed dormancy (Bethke et al., 2007). In addition, NO[•] regulates the expression of several genes involved in the response to wounding by leaf excision or mechanical damage (Jih et al., 2003; Orozco-Cardenas and Ryan, 2002).

Abscisic acid (ABA) is sometimes referred to as the plant 'water stress hormone' that regulates the response to drought by causing stomatal closure. It was found that NO[•] is required as a signal in the response to ABA in the guard cells causing them to lose turgor and close, thus enhancing drought tolerance (Garcia-Mata et al., 2003; Neill et al., 2002). Many pathogen responses have also been shown to require NO[•] signalling

(Delledonne et al., 1998; Shi and Li, 2008), and NO[•] along with a burst of reactive oxygen species (ROS) initiates cell death in the plant hypersensitive response (Delledonne et al., 1998).

In some of the above mentioned NO[•]-signalling responses, the source of the NO[•] could be specifically attributed to NR. This is the case for example, in the induction of flowering (Seligman et al., 2008) and for the response of guard cells to ABA (Neill et al., 2002). Other examples will be discussed in section 1.6.4.

Finally, using the whole genome microarray chip ATH1 to detect *Arabidopsis* transcripts affected by NO[•] treatment, 342 genes were found to be upregulated while 80 genes were down-regulated. This number of genes represents about 2% of the *Arabidopsis* transcriptome, however about 10% of those are transcription factors (Parani et al., 2004). In sum, NO[•] signalling is involved in a variety of different physiological pathways that are vital for plant survival.

1.5.3 Mechanism(s) of action of NO[•]

Despite its relatively simple chemical nature, NO[•] is well suited to function as signalling molecule (Wilson et al., 2008). Firstly, it is a small non-charged molecule that is highly mobile within biological systems due to its lipophilic nature. Secondly, it can easily pass through biological membranes and thus effectively transfer the signal from its source to its target. Thirdly, its reactive, free radical characteristics engages NO[•] in a wide variety of chemical reactions, which can be additive or redox in nature (Del Castello et al., 2019). Finally, NO[•] has a rather short $t_{1/2}$ in biological tissues – estimated at about 2 s (Thomas et al., 2001) - resulting in a fast and self-sufficient ending of the signalling cascade.

One of the breakthroughs in the field of NO[•] signalling in animals was the discovery that NO[•] binds to the ferrous heme iron of soluble guanylyl cyclase and upregulates its activity 100 – 200 fold (reviewed in Childers and Garcin, 2018). This reaction exemplifies one important mode of action of NO[•] – that of binding to metal centres. In principle, NO[•] will react with any metal center containing an unpaired electron (Thomas, 2015).

Another common mode of action of NO[•] is the reaction with reactive cysteine thiols of a target protein leading to a covalent modification called S-nitrosylation (reviewed in Feng et al., 2019). Tyrosine residues can also be modified by covalent binding of an

NO[•] to the phenolic hydroxyl group resulting in tyrosine nitration (reviewed in Corpas et al., 2013). Both of these protein modifications regulate protein function by changing the stability, conformation, subcellular localization or activity of the protein (Feng et al., 2019).

Another important pathway of NO[•] signalling involves the reaction of NO[•] with glutathione to form S-nitrosoglutathione (GSNO). This molecule is considered a storage pool of NO[•] within cells and can react with thiol groups of target proteins to mediate S-nitrosylation as part of a signal transduction (Guerra et al., 2016).

NO[•] that is generated in the biological setting co-exists with other similar reactive signalling molecules such as hydrogen sulfide (H₂S), reactive oxygen species, for example superoxide anion (O₂^{•-}) or hydrogen peroxide (H₂O₂) and additionally, antioxidants such as glutathione (GSH) or ascorbic acid. All forms likely compete for reactions with reactive thiol groups of proteins, with different modifications resulting in different regulatory outcomes (e.g. reduction of the thiol by GSH, or S-nitrosylation of the thiol by NO[•]) (Wilson et al., 2008). In addition, NO[•] is highly reactive with these reactive signalling species resulting in either signal quenching, or formation of additional signal molecules (reviewed in Hancock and Neill, 2019). For example, reaction of NO[•] with O₂^{•-} results in the formation of peroxynitrite, which is generally considered to be highly toxic, however some plant cells are resistant to it and it has been suggested to function as a further signalling molecule (reviewed in Gross et al., 2013; Wilson et al., 2008). Overall it can be said that the reaction between NO[•] and ROS represents an important part of natural ROS metabolism and an intricate balance exists between different reactive species in the plant maintaining redox homeostasis.

1.6 The enzyme nitrate reductase

NR is the enzyme that links two major fields in plant biology, the assimilation of nitrate and thus biomass production and the generation of an important molecule of signal transduction pathways (NO[•]). The control of carbon and nitrogen nutrition are tightly linked by the requirement for the energy from photosynthesis and the enzyme NR plays a large role in balancing these two processes. At the same time, NR is a major source of NO[•] in plants by reduction of nitrite and the NO[•] formed plays roles in many physiological and stress response signalling pathways in the plant.

1.6.1 Structure of NR

NR is a dimeric protein of about 100 kDa per monomer (Redinbaugh and Campbell, 1985) (Fig. 2). In total there are three, modularly folded cofactor binding domains made up by eight functional sequence motifs arranged from N to C terminus as follows: (i) The N-terminal peptide is thought to be unstructured and is not conserved between isoforms and species, however a type-conserved acidic sequence motif in the N-terminal tail is involved in NR activity regulation (Chi et al., 2015). (ii) The dark blue sequence depicted in Fig. 2 incorporates the molybdenum cofactor (Moco), which consists of a molybdenum atom co-ordinated in a specialized pterin structure that is the only known form of catalytic molybdenum found in eukaryotes. (iii) Adjacent is the dimerization region (light blue) that is responsible for the interaction between two monomers forming a functional dimer. The Mo and dimerization segments together make up the Moco domain. (iv) The hinge 1 is probably an unstructured sequence segment and plays a key role in NR catalysis and in activity regulation by phosphorylation of the highly conserved, highlighted serine residue (Bachmann et al., 1996b; Lambeck et al., 2010). (v) The *b*₅-type heme bound in the central domain (heme domain) is the cofactor that gives NR its typical deep red colour (Redinbaugh and Campbell, 1985). (vi) hinge 2 is another less flexible and non-conserved region connecting the heme domain to the C-terminal FAD cofactor binding domain. This domain consists of (vii) the FAD-cofactor binding lobe and (viii) a lobe where NADH or NADPH binds to supply electrons to the FAD.

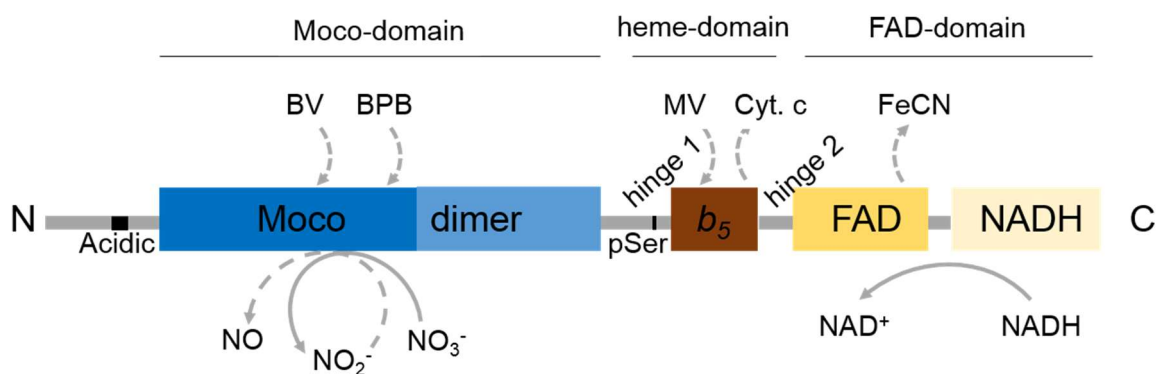


Figure 2: Schematic representation of the domain structure of NR. The three domains are highlighted in different colours (blue: Mo domain, red: heme domain, yellow: FAD domain). In addition, important regulatory sequences are highlighted in the N-terminal peptide (Acidic) and in the hinge 1 (pSer). Artificial electron donors and acceptors are shown above (section 1.6.3), physiological electron donors and acceptors below. Abbreviations: Moco, Moco-binding motif; dimer, dimerization region; *b*₅, heme domain, FAD, FAD-binding region, NADH, NADH-binding motif, BV, benzyl viologen, BPB, Bromphenol blue, MV, methyl viologen, Cyt.c, cytochrome c, FeCN, potassium ferricyanide.

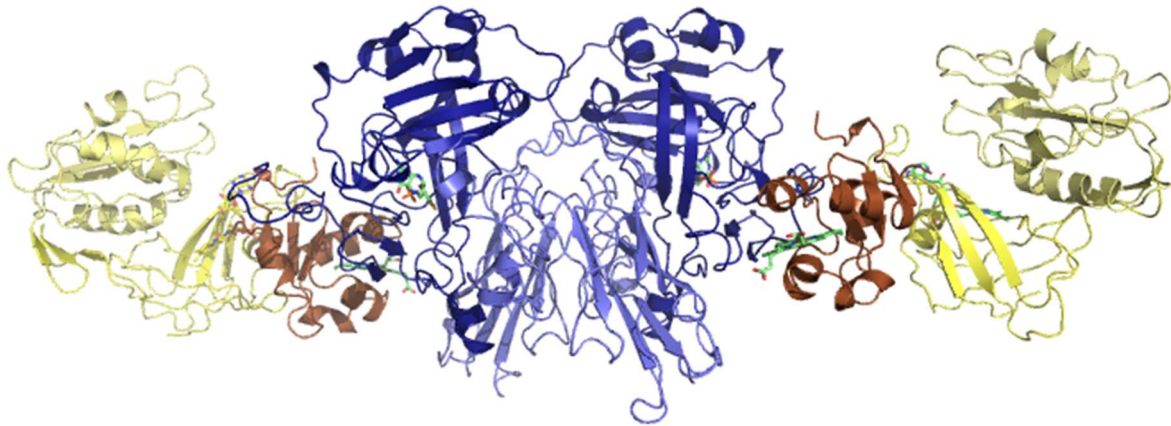
Crystallization of full-length NR has not been successful to date. The large size of the 100 kDa monomer, its instability, the requirement for three bound cofactors and intervening unstructured protein sequences between the domains probably all collectively contribute to the difficulty in obtaining ordered crystals of NR (Campbell, 1999; Chi, 2012). Added to this is the practical difficulty in obtaining large quantities of purified and highly concentrated full-length protein. The crystal structures of some of the domains of NR have however, been determined and taken together with the crystal structures of proteins and domains homologous to NR, can be used to develop a model of the NR structure (Fig. 3).

The crystal structure of the FAD domain of corn leaf NR in complex with FAD-cofactor was determined (Lu et al., 1994). Likewise, the Moco domain of *Pichia angusta* NR has been crystalized and the structure determined (Fischer et al., 2005). Animal sulfite oxidase (SO) is a Moco and heme domain-containing protein with high sequence identities to the Moco and heme domains of NR (about 40% identity between the Moco domains and 29% identity between the heme domains (determined based on Clustal Omega alignment of residues 1-483 of *AtNR2* (Uniprot P11035) with chicken SO (CSO)(Uniprot P07850)).

Functionally, SO catalyses the oxidation of sulfite to sulfate in the liver of animals as the final step in the degradation of sulfur containing amino acids. The crystal structure of CSO has been determined (Kisker et al., 1997). The homology of the domains may be helpful in modelling the structure of NR, however SO differs from NR in that the heme domain of SO is at the N-terminus (i.e. opposite to the orientation relative to Moco-domain found in NR (Fig. 2)). Also, the position/orientation of the linker in SO was not clearly defined in the CSO crystal structure and therefore the heme position observed in the CSO crystals may not reflect the physiological heme position in CSO (or NR). In fact for both proteins, large domain movements between heme and Moco are thought to play a role in catalytic turnover, as viscous media during catalysis slowed enzyme turnover (Barbier and Campbell, 2005; Feng et al., 2002; Lambeck et al., 2012). Finally, NR contains an additional FAD domain that SO does not have, and the positioning of this C-terminal domain relative to the central heme and N-terminal Moco domain is unknown. However a model has been proposed (Campbell, 1999), in which the C-terminal FAD-domain is arranged next to the heme in such a way that electron transfer from the NADH-reduced FAD to the heme-cofactor could occur (Fig. 3).

Subsequent to the model in 1999, the crystal structure for *Pichia angusta* Moco domain was determined (Fischer et al., 2005) and proved a different orientation of the dimer to the head to toe orientation proposed (Campbell, 1999). The corrected dimer-orientation is shown in Fig. 3.

A



B

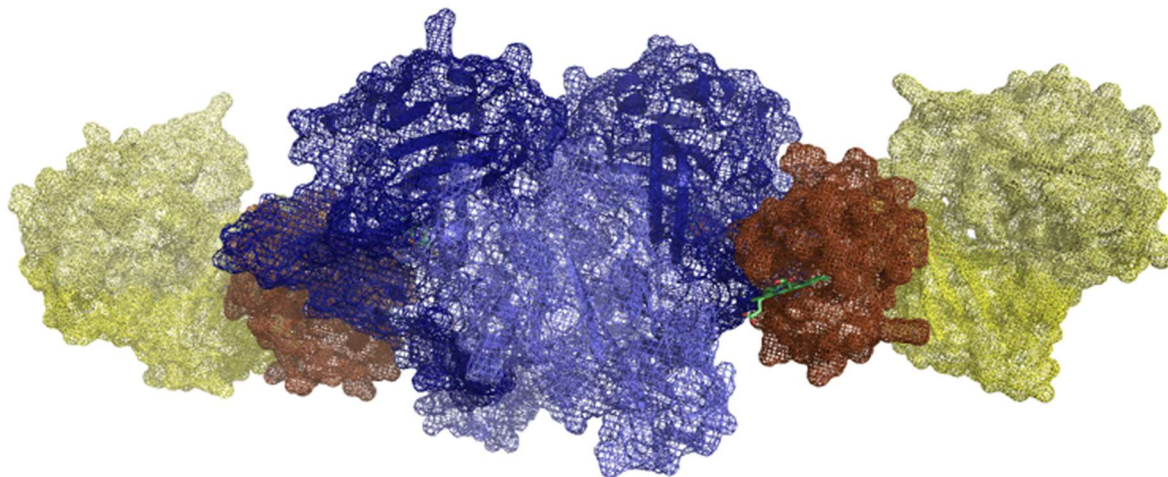


Figure 3: Model of NR structure. The domains of AtNR2 were individually modelled using Swiss-Model (Waterhouse et al., 2018). Moco domain modelled on CSO (1sox, 40% identity), heme domain on fly cytochrome *b5* (2ibj 1A, 42% identity) and FAD domain on corn NR-FAD-domain (1cne, 65% identity). The Moco and heme domains are arranged in the orientation that was observed in CSO. The FAD-NADH was placed as suggested (Campbell, 1999). Visualization was performed using PyMOL (DeLano, 2002). **A:** Cartoon representation of the protein, cofactors (Moco, heme and FAD) are shown in ball and stick. **B:** Mesh representation. Dark blue: Moco domain, light blue: dimerization motif, brown: heme-domain, dark yellow: FAD binding motif, light yellow: NADH binding motif

1.6.2 Electron transport in NR

NR is considered to function as a mini-electron transport chain (Campbell, 1988). The cellular reductants NADH or NADPH bind at the C-terminal FAD domain (Fig. 2) and

transfer two electrons to the FAD cofactor. The electrons are then passed one at a time to the central heme domain and onward to the Moco. It is at the Moco domain, which carries one or two electrons in the partially or fully reduced state (Mo (V) or (IV)), where nitrite or nitrate reduction takes place. Based on the redox potentials of the redox-active cofactors, a 'downhill' electron flow is thought to occur in NR from FAD (~ -280 mV) to heme (~ -160 mV) to Moco (~ 0 mV) (Campbell, 2001; Ratnam et al., 1996). Evidence for this was seen in the full reduction of the heme cofactor by UV/vis spectroscopy, before reduction of the FAD cofactor could be spectroscopically observed using a heme-FAD fragment of NR (Campbell, 2001; Lambeck, 2009; Ratnam et al., 1996).

While nitrate reduction is a two-electron process that must start with the fully reduced Mo (IV), it is unclear whether nitrite reduction is possible with Mo (V) or only with Mo (IV) as the fully reduced Mo (IV) redox state has been reported compulsory for nitrite reduction by SO (Bender, 2017; Wang et al., 2015). A single electron is required for the reduction of nitrite to NO[•] and the reaction is thought to be as follows:



1.6.3 Functional domain fragments of NR

The full-length NR protein is rather unstable and difficult to work with; probably for the same reasons stated above that full-length protein has not yet been crystallized. Nonetheless, some studies in the literature exist using full-length NR extracted from native tissue or recombinantly expressed. These studies were used, for example, to generate NR-specific antibodies (Campbell and Remmler, 1986), to determine the steady-state and pre-steady state kinetic parameters for the enzyme (Barber and Notton, 1990; Skipper et al., 2001) and to study post-translational regulation of NR (Lambeck et al., 2010).

It was realized early-on, however that the proteolytic digested or separately recombinantly expressed domain fragments of NR retain the partial activity of the respective domain(s) in the full-length enzyme (Campbell, 1996; Kubo et al., 1988). These studies offered the advantage of working with the more stable protein fragments and have helped to define the individual electron transfer steps during catalysis. Domain fragments such as the isolated FAD-domain (Hyde and Campbell, 1990; Lu et al., 1994), the heme-FAD fragment ('Mo-reductase fragment') (Mertens et al., 2000),

and the Moco-heme fragment (NR-Mo-heme) (Lambeck et al., 2012) have been successfully recombinantly expressed and display activity similar to parts of the full-length protein – if suitable artificial electron donors or acceptors are provided (Fig. 2). For example, the FAD-domain fragment displays diaphorase activity by using NADH/NADPH for reduction of ferricyanide (Kubo et al., 1988), the Mo-reductase fragment can be used to reduce ferricyanide or cytochrome c (Mertens et al., 2000) and the NR-Mo-heme can reduce nitrate when artificial electron donors are supplied, such as methyl viologen (MV) or bromphenol blue (Lambeck et al., 2012).

1.6.4 Isoforms of NR

Many plant species express more than one isoform of NR. This includes the model plant *A. thaliana* (2 isoforms), but also barley (*Hordeum vulgare*, 3 isoforms), soybean (*Glycine max*, 3 isoforms), rice (*Oryza sativa*, 2 isoforms), tobacco (*Nicotiana tabacum*, 4 isoforms), and maize (*Zea mays*, 3 isoforms). Other plants express just one isoform, for example spinach (*Spinacea oleracea*), squash (*Curcubita pepo*) and tomato (*Solanum lycopersicum*). For plants with multiple isoforms, differences have been discerned on the level of transcription, on the protein expression level and in the role of one or other isoform in a particular function. For example, differences have in some cases been determined between the isoforms in their specificity for the co-substrate NADH or NADPH (Beevers et al., 1964; Dailey et al., 1982) while other NR isoforms in a species are either constitutively or inducibly expressed (Wu et al., 1995). Soybean is thought to be unique in that it expresses two constitutive and one inducible NR isoform (Wu et al., 1995). The greatest number of comparisons has been performed for the model plant *A. thaliana*, which expresses 2 isoforms; NR1 and NR2 encoded by the genes *NIA1* (GenBank accession Z190520) and *NIA2* (GenBank accession J03240) respectively.

1.6.4.1 Transcriptional differences between NR isoforms

The largest body of information about differences between transcription of NR isoforms has been gleaned from transcriptome data. Using the Genevestigator software (Hruz et al., 2008) the transcripts for *NIA1* and *NIA2* in wild type *Arabidopsis* were compared for their expression in various plant tissues. This tool accesses publicly available Affymetrix ATH1 transcriptomics data and allows a visual depiction of the expression result. The expression of *NIA2* in this analysis is higher in all tissues, except for the

inflorescence (which includes the ovule, seed and embryo) (Fig. 4). Although overall *NIA* expression is lower in this tissue, *NIA1* was more highly expressed than *NIA2*.

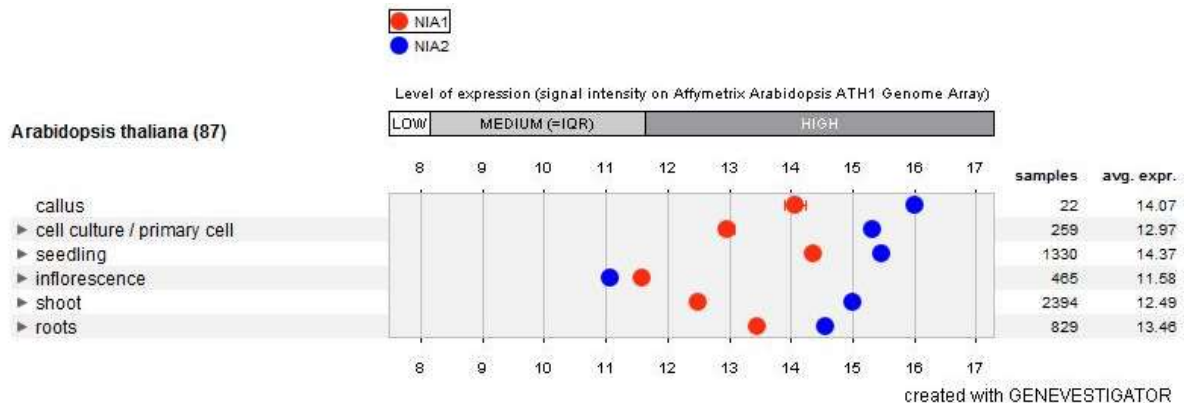


Figure 4: Comparison of *NIA1* and *NIA2* expression in publicly available transcriptomics data for wild type *Arabidopsis*. *NIA2* expression is higher compared to *NIA1* in all tissues except the inflorescence.

Besides looking at the transcriptomics data for the entire plant, many studies have focussed on looking at *NIA* expression in particular tissues or under certain conditions. One of the first observations was that *NIA1* and *NIA2* expression oscillates diurnally and is linked to the circadian clock (Fig. 5) (Cheng et al., 1991). The nutrient nitrate is a major signal inducing expression of NR and many other genes involved in nitrate uptake and assimilation, and in the case of *Arabidopsis*, nitrate supply leads to massive upregulation of both *NIA1* and *NIA2* (Cheng et al., 1991). In fact, both genes have nitrate responsive elements in the 5' promoter region (Lin et al., 1994), *NIA1*, however has an additional nitrate responsive *cis*-element in the 3' genomic sequence that renders *NIA1* even more nitrate responsive compared to *NIA2* (Konishi and Yanagisawa, 2011a). Another group looked only at the promoter sequence for *NIA1* and found that it contained elements responsive to nitrate, nitrite and ammonium (Wang et al., 2010).

In the presence of nitrate, light also has a profound effect on *NIA1* and *NIA2* expression because nitrate assimilation is closely linked to photosynthesis (Cheng et al., 1991). Later, the same group of researchers found that sucrose could mimic the effect of light-stimulation on NR transcription (Cheng et al., 1992). While these effects were general for transcription of both *NIA1* and *NIA2*, isoform-specific differences have also been reported. Under conditions of nitrogen starvation, low levels of *NIA1* are basally expressed while *NIA2* is absent (Cheng et al., 1991) and in certain specific pathways of light signalling, differences have been discerned in the induced expression of *NIA1*

and *NIA2*. In the *cr88* mutant *Arabidopsis*, red light signalling that controls *NIA2* expression was lost, while no effect on *NIA1* expression was seen (Lin and Cheng, 1997). Similarly, an *Arabidopsis* mutant lacking HY5 (LONG HYPOCOTYL 5) and HYH (HOMOLOG OF HY5) lost light induction of *NIA2* expression while no effect on *NIA1* expression was seen (Jonassen et al., 2009a; Jonassen et al., 2009b). On the other hand, the cytokinin benzyladenine induced a ~14-fold increase in NR activity in *Arabidopsis*. This correlated with increased *NIA1* transcription and mRNA levels while *NIA2* transcript level was unchanged (Yu et al., 1998). To summarize, there are factors controlling the transcription of *NIA1* and *NIA2* that are common to both isoforms, and there are also factors that result in individual expression patterns that points toward specialized requirements in the plant for one or other isoform under particular environmental conditions or in certain tissues (Fig. 5).

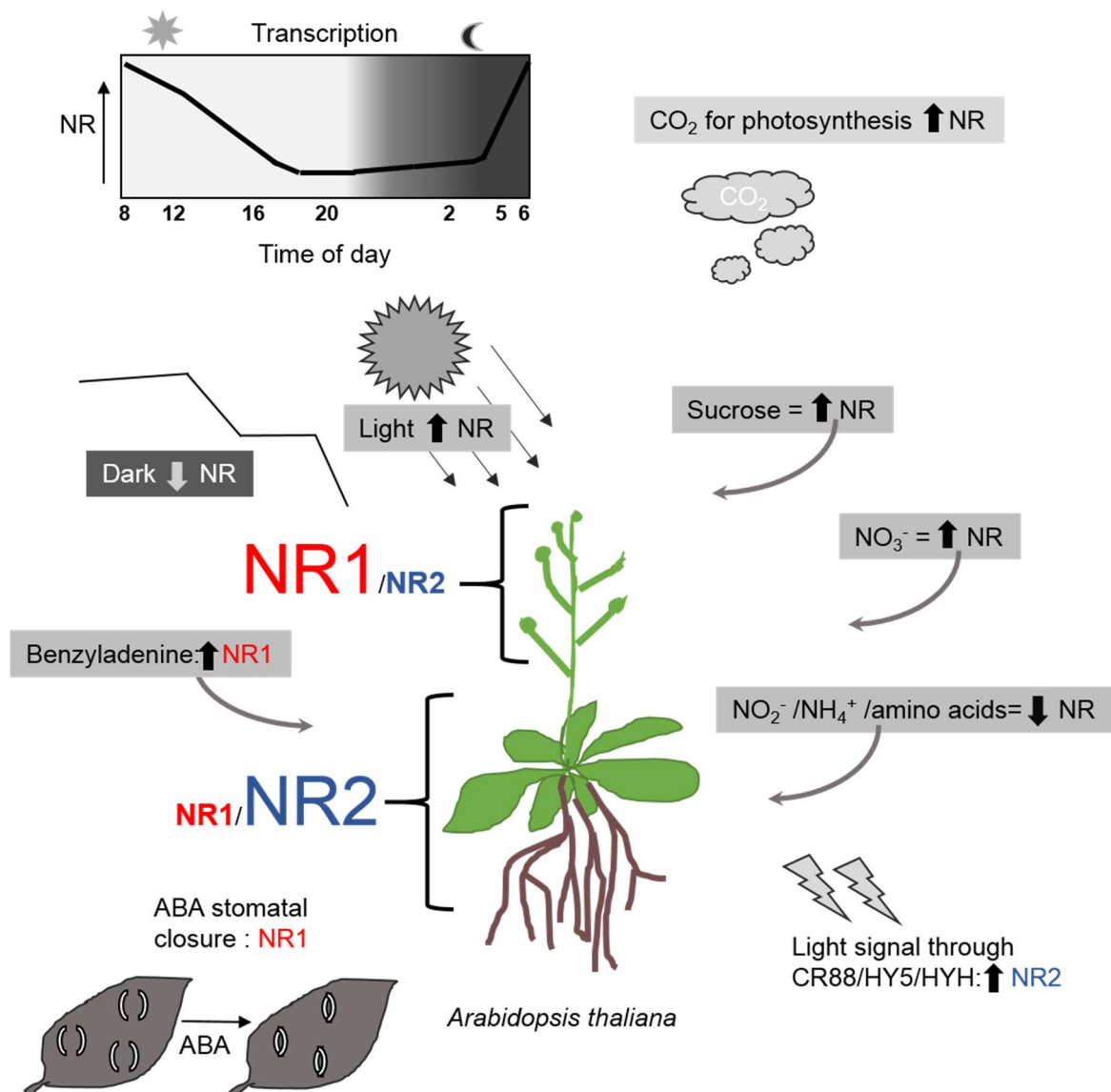


Figure 5: Factors influencing NR1 and NR2 expression and activity in *A. thaliana*.

1.6.4.2 Differences between NR isoforms on the protein level

Directly measured differences between the quantities of NR-isoform-proteins in a plant tissue or plant extract, for example by immunoblot analysis are not known. This is likely due to the high level of identity between NR isoforms on the protein level. By alignment using Clustal Omega of UniProt entry P11832 for *Arabidopsis* NR1 and P11035 for *Arabidopsis* NR2, the identity at the amino acid level between the two proteins is 78%. Therefore, available NR antibodies (e.g. AS08 310 from Agrisera) frequently cross-react with both isoforms.

Mutant plants in general offer an alternative tool to study the effects of specific genes on the activity of a protein on the whole-plant level. Such studies were very useful in the 1970's and 1980's for comparing soybean plants lacking one or other *NIA* gene. As already mentioned, soybean expresses three isoforms of NR two constitutive (cNR1 and cNR2) and one inducible (iNR). The early discovery of a mutant plant lacking both cNR isoforms compared with wildtype (not induced) allowed for biochemical studies of the properties of individual purified NR isoforms (Robin et al., 1985). Later, methods were developed to further separate the two constitutive isoforms based upon a differing co-substrate preference and here it was revealed that cNR1 has a preference for NADPH, has an optimum of pH 6.5 and has a high K_M^{nitrate} (5 mM). The other two isoforms had K_M^{nitrate} in the range of 0.13 – 0.19 mM (Streit et al., 1985). At the same time it was known that the mutant lacking both cNR isoforms was unable to evolve NO[•] (Dean and Harper, 1986). Later it was shown using a further mutant, this time lacking only cNR2 that cNR1 was specifically responsible for NO[•] generation (Dean and Harper, 1988).

In *A. thaliana*, mutant plants are available with one or the other NR isoforms knocked out, *nia1* or *nia2* plants, respectively. By comparing the NR activity of these mutant plant extracts a major difference was observed between the two isoforms: *nia1* plants lack a functional gene for NR1 expression, however they have NR activity similar to the wild type. The *nia2* mutant on the other hand, retains only about 10% of NR activity that may be attributed to the functional NR1 isoform (Cheng et al., 1988; Wilkinson and Crawford, 1991) (Fig. 5). However, this seems to be sufficient for the plant because all single knock-out NR mutant plants retain the ability to grow without a phenotype on nitrate as the sole nitrogen source. This is the case for *Arabidopsis* (Wilkinson and Crawford, 1991) and also for barley (Savidov et al., 1997).

Double knock-out *Arabidopsis* mutants also exist; one of these carries a point mutation in the *NIA1* gene and deletion of the entire *NIA2* gene (*nia1-1/nia2-5*). This mutant retains about 0.5% of the NR activity of wild type plants (Wilkinson and Crawford, 1993) or as determined by another study, retains 1% of NR activity in the shoot and 5 – 10% of root activity (Lejay et al., 1999; Wang et al., 2004). This mutant can grow, but is impaired on nitrate as sole nitrogen source. The second double-*nia* mutant carries a deletion of the *NIA2* gene and a transposon insertion in the *NIA1* gene (*nia1-2/nia2-5*). This mutant expresses no NR transcript displays no detectable NR activity and cannot grow on nitrate (Parinov et al., 1999; Wang et al., 2004).

Using double knock-out *nia* mutant plants it has been possible to quantify the role of NR in NO generation on the whole-plant level, compared with the other NO[•] sources described (1.5.1). In two studies that fluorescently visualized NO levels in untreated *nia1-1/nia2-5* mutant plants, the residual level of NO[•] was estimated to be about 40-65% (Lozano-Juste and Leon, 2010; Xie et al., 2013). Functional differences have also been discerned between *nia* mutant plants, for example, in the process of regulating stomatal apertures. First, it was seen that the mutant *nia1-1/nia2-5* had impaired stomatal closure in response to ABA signalling due to lowered NO[•] levels in the guard cells (Desikan et al., 2002). Later, it was shown that *AtNOA1* was not involved in this process but by using the single *nia1* knock-out it was discovered that NR1 is the isoform of NR that is apparently involved in ABA induced NO[•] generation and stomatal closure (Bright et al., 2006) (Fig. 5). The *nia2* single knock out plants behaved as wildtype in this system (Neill et al., 2008). An additional phenotype that may be related to NO-signalling was seen in the *nia1* plants: upon transition from light to darkness this mutant plant failed to close the stomata (Ribeiro et al., 2009; Wilson et al., 2008).

In contrast to those findings, a study in 2010 studied the triple mutant *nia1-1/nia2-5/noa1-2* and concluded that NO[•] is actually not needed for stomatal closure, because *nia1nia2noa1* stomata closed efficiently despite undetectable levels of NO[•] in the guard cells and that rather ABA acts directly upon the guard cells to induce stomatal closure (Lozano-Juste and Leon, 2010). The authors concluded that the triple mutant is simply more sensitive to ABA than the wildtype, and that the phenotype is independent of the lower NO[•] levels in the mutant plant. Another group found that salicylic acid (SA)-induced stomatal closure required NO[•] produced by *AtNOA1*, NR1 and NR2, and in

fact showed that NR2 appeared to play a greater role in NO[•] generation in response to SA (Hao et al., 2010).

To summarize, there are conflicting reports on both the sources and the effects of NO[•] in plants. NO is difficult to measure *in planta*, and some reports specifically criticise inappropriate use of methodologies for detecting and quantifying NO[•] (Arita et al., 2006; Planchet, 2006). It has been suggested for example that DAF-fluorescence measurement to detect NO[•] in the plant tissue is not specific for NO[•], but rather reacts with more oxidised forms of NO[•] (such as NO⁺ or N₂O₃) (Planchet, 2006). Studies in mutant plants have yielded partially conflicting results such as those described above and are also criticised for the fact that the entire metabolism of a plant may be changed by a gene knock-out. This may lead to indirect outcomes that are not related to the absent gene. An example for this would be that by gene knock-out of both *nia1* and *nia2* in a plant, the levels of all nitrate metabolites are altered – including L-arginine (Modolo et al., 2006), which is the substrate for a putative oxidative NOS method of NO[•] generation and in addition, nitrite concentration is lowered, which is the substrate for all means of reductive NO generation in the plant (Planchet et al., 2005).

Despite these controversies, altogether, evidence exists for functional differences between NR isoforms within a plant species, and implies that the functions of multiple isoforms are not completely redundant. Studies comparing the isoforms of NR on the level of the pure/purified protein may be helpful in further clarifying the roles for NR1 and NR2 as this would avoid the issues described in NO[•] detection *in vivo* and the use of mutant plants.

Because of its greater abundance, expression and contribution to NR activity, NR2 is by far the better characterized isoform of NR on the biochemical level. Recombinant expression of the protein has been performed and many biochemical studies undertaken. In fact, this isoform has served as a reference and a model for studying NR biochemistry, function and regulation for many years (Campbell, 1999; Chi et al., 2015; Lambeck et al., 2010; Lambeck et al., 2012; Skipper et al., 2001; Su et al., 1996; Su et al., 1997). Biochemical studies of NR isoform 1 using purified protein have not been performed to date.

1.6.5 Regulation of NR

We have seen so far that NR is linked to many important processes in the plant such as controlling nitrate concentration in the cytosol, being the rate limiting enzyme of nitrogen assimilation (by reduction to nitrite), production of nitrite as the substrate for reductive NO[•] generation and finally, by itself being a producer of NO[•]. NR activity is therefore strictly regulated in order to balance these roles.

1.6.5.1 Regulation of NR in nitrate reduction

Most information concerning the regulation of NR was obtained in relation to its function in nitrate reduction. This is because nitrogen for plant growth is the nutrient most limiting and therefore it has long been of interest to plant breeders and researchers trying to find ways to improve nitrogen utilization by plants (Tischner, 2000). Supplying excess nitrogen fertilizer to crop plants is not completely successful in this regard as different crop species and strains have individual 'nitrogen use efficiency' (NUE) values: That is the percentage of supplied nitrogen that the plant can successfully incorporate into biomass. For example, for the important crop plant rice, this value is estimated to be only about 30 – 50% (Kronzucker et al., 2000). It was observed by plant breeders early on that a correlation exists between NR activity and NUE, and therefore measurement of NR activity became part of the standard repertoire of tests comparing newly bred crop strains.

NR, and consequently its activity, is very tightly regulated on the level of transcription, by the stability and amount of the protein, and by post-translational modifications. Transcription of NR is primarily induced by the signal and availability of nitrate. Other factors regulating transcription (section 1.6.4 and reviewed in Yanagisawa, 2014) are light, CO₂, circadian rhythm and downstream metabolites of nitrate assimilation. Upregulated transcription is typically followed by increased amounts of NR protein. However, NR is not active at first (probably due to slow incorporation of Moco) and is then followed by increased NR activity (Remmler and Campbell, 1986). Effects of transcription on NR activity levels tend to work on the timescale of hours or within the daily diurnal cycle (Deng et al., 1990). One study that compared the effects of transcription and post-translational control mechanisms on NR activity showed that transcriptional regulation is secondary to post-translational mechanisms (Lea et al., 2006). Overexpression of NR transcript, by placing it under the control of the

cauliflower mosaic virus 35S RNA promoter led only to small increases in nitrate metabolites and free amino acid concentrations in the plants. Additional deactivation of post-transcriptional regulation, by mutation of the regulatory pSer in the hinge 1, led to 9 – 14-fold accumulation of the amino acids glutamine and asparagine.

Therefore, the most important layer of NR regulation is at the post-translational level and occurs on the timescale of minutes. This can be observed upon placement of plants that were in light into darkness. Studies of corn leaf NR showed that within one hour after transfer into darkness, NR activity dropped by 30% although the amount of NR protein was unchanged (Remmler and Campbell, 1986). Another study defined this time scale even more tightly with inhibition being observed already after 5 minutes (Lillo et al., 2003). When plants are returned to light after a short time in darkness (~1.5 hrs), the activity is quickly restored without any change in NR protein level. Following longer periods of darkness, NR degradation plays a role and NR amount decreases parallel to NR activity (Remmler and Campbell, 1986).

The rapid and reversible inactivation of plant NR on the protein level is the result of phosphorylation of a highly conserved serine residue of NR within the hinge 1 sequence (Fig. 2) (Bachmann et al., 1996b; Su et al., 1996). This phosphorylated serine then binds to a 14-3-3 regulatory protein and NR activity is arrested (Bachmann et al., 1996a). 14-3-3 proteins constitute a group of highly conserved regulatory proteins in eukaryotes and will be described in more detail in section 1.6.8. Millimolar concentrations of divalent cations such as Mg^{2+} or Ca^{2+} are required in *in vitro* tests, either for the phosphorylation of NR and binding of 14-3-3 (or both) and must be available for inactivation to be observed (Provan et al., 2000). Phosphorylation alone does not influence NR activity (Lambeck et al., 2010). Furthermore, mutation of the conserved serine to aspartic acid or glutamic acid, which usually mimics a phosphorylated serine residue, but in the case of NR is not phosphomimetic, results in constitutively active NR as was shown in *Arabidopsis* (Lambeck et al., 2010; Pickenhahn, 2015; Su et al., 1996) and *Nicotiana plumbaginifolia* (Lea et al., 2006).

An additional interaction site between NR and 14-3-3 is an acidic region of residues at the N-terminal tail of NR that is type-conserved between NR of different isoforms and species. Binding of 14-3-3 to the phosphorylated pSer in the hinge 1 and to the N-terminal acidic region inhibits NR activity up to 97% (Chi et al., 2015).

It has not yet been shown, which kinase is responsible for NR phosphorylation *in vivo*, however several calcium dependent kinases (CPK) and also some calcium independent SNF1 (sucrose non-fermenting) resembling kinases, have been shown *in vitro* to be capable of phosphorylating NR (Lambeck et al., 2012; Sugden et al., 1999). Post-translational inhibition of NR by 14-3-3 is completely reversible by de-phosphorylation of the hinge 1 serine. The phosphatase that performs this function *in vivo* is PP2A phosphatase (Lillo et al., 2004).

It has been determined that the molecular mechanism of inhibition by 14-3-3 proteins is by hindering domain movement between the heme and Moco domains that is required for electron transfer (Lambeck et al., 2012). A model of this mechanism, further refined by the additional binding of the NR N-terminus to 14-3-3 was proposed (Chi et al., 2015) and is shown in Fig. 6. The phosphorylated and 14-3-3 bound NR displays an 18-fold lower nitrate turnover k_{cat} , and an apparent decrease in $K_M^{nitrate}$ from 280 μM to 141 μM (Lambeck et al., 2010).

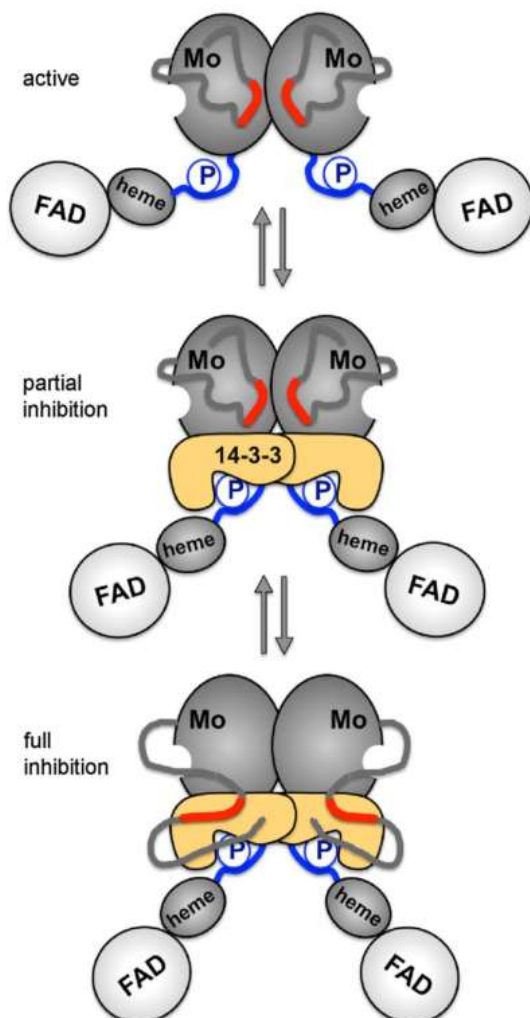


Figure 6: Model of inhibition of NR by 14-3-3 proteins (Chi et al., 2015). The upper panel depicts NR phosphorylated in the hinge 1 (blue) but still active, with domain movement between the heme and Moco (Mo) domain freely possible. In the middle panel, 14-3-3 binding to the phosphorylated sequence hinders domain movement and inhibits NR activity. In the lower panel, 97% inhibition of NR is achieved by the additional binding of the N-terminal acidic region of NR (red).

1.6.5.2 Regulation of NR in nitrite reduction

Few studies have been performed that directly looked at the regulation of NR activity in nitrite reduction to NO[•]. Of note in the literature is one study that focussed specifically on this question (Rockel et al., 2002). The authors used detached leaves of spinach and (whole) sunflowers or purified protein from spinach and commercial maize leaf NR to measure NO[•] release to the gas phase under different conditions. In summary, it was found that purified NR extracts could generate NO[•] *in vitro* when nitrite and NADH were supplied in excess. The K_M for nitrite was determined to be approximately 100 μ M, which was considered to be high relative to the concentration of nitrite in the leaves at about 10 μ M (Rockel et al., 2002). The authors found that under conditions in which nitrite concentration spiked (such as after turning off the light), NO[•] emission was boosted. They also saw that anoxia or feeding uncouplers, which resulted in sharply increased nitrite concentrations, increased by 100-fold the amount of NO[•] released. Finally, it was seen that several treatments that result in activation or deactivation of NR activity (such as phosphorylation and binding of 14-3-3 proteins for inhibition), resulted in paralleled nitrite reductase activity and thus concluded that this mechanism of post translational regulation is also valid for nitrite reductase regulation.

In another study, it was seen that mutating the pSer phosphorylation site in tobacco NR to aspartic acid resulted in increased formation of nitrite and high NO[•] emission *in vivo* (Lea et al., 2004; Lillo et al., 2004), thus also suggesting that phosphorylation and interaction with 14-3-3 normally regulates this activity.

1.6.5.3 14-3-3 proteins

14-3-3 proteins are a highly conserved family of proteins found in all eukaryotes. The name relates to the fraction number in bovine brain extracts in which they were first discovered (Moore and Perez, 1967). 14-3-3 proteins participate in the regulation of a wide range of cellular processes such as cell cycle, apoptosis, metabolism and the DNA damage response (Obsil and Obsilova, 2011). Three main modes of action are known in 14-3-3 interactions with target proteins, which cause (i) conformational change in the target protein, (ii) masking a sequence specific feature of the target, or (iii) acting as a scaffold to bridge interacting protein partners (Obsil and Obsilova, 2011). In the case of NR, which is a well-studied target of 14-3-3, the binding to pSer in the hinge 1 causes conformational change and activity inhibition as described in the

foregoing sections (Jaspert et al., 2011; Lambeck et al., 2012). In fact, this binding is an example of the most commonly observed mode of 14-3-3 regulation: that of binding to the general phosphoserine binding motif R-S-X-phosphoS-X-P. 14-3-3 proteins are highly conserved and the dimer forms a concave structure (Fig. 7). The phosphoserine of the target protein binds inside in this deep binding groove. Two key arginine residues per monomer play an important role in this interaction (Fig. 7). In the case of NR, the binding stoichiometry is 1:1 (one NR dimer binds to one 14-3-3 dimer) (Kaiser and Huber, 2001). The second interaction between the N-terminal acidic region of NR and 14-3-3 is probably a more unconventional mode of 14-3-3 binding and the exact binding site in the 14-3-3 has not yet been identified. Other examples have shown that binding to the 'outer side' of the C-terminal helices (shown in orange in Fig. 7) of 14-3-3 can occur as was seen for Hd3A (florigen) in complex with phosphorylated OsFD1 (a transcription factor in rice) (Taoka et al., 2011).

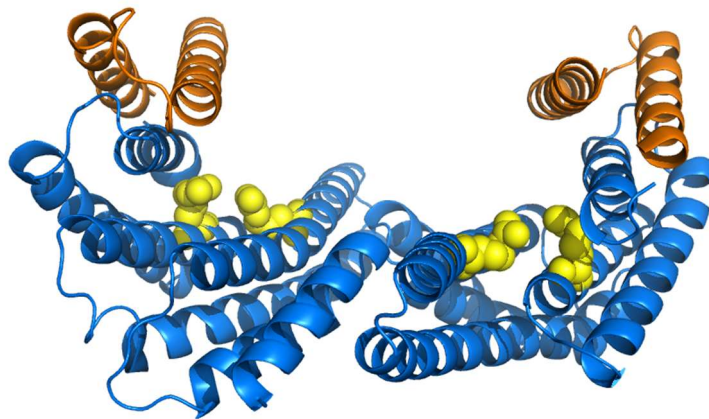


Figure 7. Structure model of 14-3-3 ω from *A. thaliana*, generated by sequence homology to crystal structure PDB 3e6y (14-3-3 from tobacco) using <http://proteinmodelportal.org/> and visualized using PyMOL. The arginine residues involved in interaction with the phospho-peptide of the target protein are highlighted in yellow. C-terminal helix 8 and 9 are highlighted in orange.

Even though all eukaryotes express multiple 14-3-3 isoforms, *Arabidopsis* is remarkable in having a total of 13 isoforms (DeLille et al., 2001). It is thought that plants have a need for very complex and branched regulatory circuits in order to deal with the range of environmental and stress signals that they are exposed to. In addition, localization of expression of certain 14-3-3 isoforms inside organelles is consistent with the idea that there is a diversity of function for individual isoforms (DeLille et al., 2001; Sehnke et al., 2002). The 14-3-3 isoforms in *Arabidopsis* can be divided into two major

evolutionary branches: Rho, Omicron, Mu, Epsilon and Pi belong to the 'epsilon' group (based on amino acid sequence and gene intron/exon structure and named after the human 14-3-3 epsilon) while Kappa, Lambda, Phi, Chi, Omega, Psi, Upsilon and Nu belong to the 'non-epsilon' group (DeLille et al., 2001). Some reports suggest that the ancient epsilon family of 14-3-3 proteins may regulate basic cellular functions, while the non-epsilon proteins regulate organism specific functions (Keicher et al., 2017).

Altogether, eight isoforms of 14-3-3 proteins from *Arabidopsis* were tested for inhibition of AtNR2 *in vitro* and although seven of the eight isoforms could inhibit NR, isoform Epsilon could not. It was suggested that only non-epsilon 14-3-3 isoforms may function in NR inhibition (Lambeck et al., 2010). However, other epsilon group members have not been tested to date.

1.7 Aim of this project

Two important facts paved the way for this thesis. First, many plants express multiple isoforms of the enzyme NR, still mostly uncharacterised. Second, NR catalyses two different reactions in the plant: the well characterized reduction of nitrate to nitrite and the more recently discovered and less-well characterized reduction of nitrite to NO[•].

Thus, this project was to address the following aims:

- To closely examine the steady-state and pre-steady state kinetic parameters of nitrate reduction by NR. To this end, recombinantly expressed and purified NR1 and NR2 of *A. thaliana* and active domain fragments thereof were to be used. NR2 has been characterized for nitrate reduction extensively in the past, however NR1 has never been expressed or analysed before.
- To measure how phosphorylation and 14-3-3 binding regulate the activity of NR1. Here, a MV:nitrate activity-determination system is to be used, which has been implemented in the past to measure the post-translational regulation of NR2.
- To establish suitable systems for determination of the kinetic parameters of nitrite reduction by NR1 and NR2.
- To establish and compare the kinetic parameters of nitrite reduction for both NR isoforms. In fact, *in vitro* nitrite reduction or NO[•] production have not been measured for either NR isoform from *Arabidopsis* before.
- To examine possible regulatory mechanisms controlling NR activity *in vitro*, which may play roles in tuning NR activity/nitrite reductase activity *in vivo*. This would include substrate effects and 14-3-3 mediated inhibition.
- To obtain a model of NR structure using cryo electron microscopy.

2 Results

2.1 Production of full-length AtNR

For a detailed comparison of the two isoforms AtNR1 and NR2, it was first required to establish protocols for the expression and purification of NR1, as the expression of full-length *A. thaliana* NR1 (or any fragments thereof) has not been reported to date. As expression and purification for NR2 has only been successful in the yeast *Pichia pastoris*, the first aim was to establish a protocol for recombinant expression of NR1-fl in *P. pastoris*.

2.1.1 Expression of AtNR1-fl in KM71

When transforming yeast cells, the linearized plasmid DNA containing the gene of interest is integrated into the yeast genome. Due to this integration event, transformed yeast clones typically exhibit variable expression levels of the protein of interest and a positive clone expressing the protein of interest has to be selected (Cregg et al., 2009). Development of the protocol for expression of AtNR1 in *Pichia* was performed as follows: The native *A. thaliana* NR1 DNA sequence containing an N-terminal His tag was cloned into the pPICZb vector (Invitrogen) and transformed into *P. pastoris* strain KM71 using PEG (see materials and methods). Transformed clones were selected by growth on zeocin-containing medium. Six clones were randomly chosen for further testing. It was additionally confirmed by colony PCR that the NR1 gene had been successfully introduced into the host cells (data not shown).

Next, small-size test-expression cultures were performed for 12 h – 72 h. Cells were lysed and 15 µg of total lysate protein for each condition were subjected to SDS-PAGE gel and immunoblot analysis (Fig. 8A, B). On the Coomassie-stained gel no clear band was seen in any of the lanes which indicated that the total amount of desired recombinant protein in the cells was low. On the immunoblots it can be seen that in fact all six clones expressed NR1 to different degrees, but that already after 12 h basically only a 70 kDa (and smaller) truncation product was seen, and degradation was ever increasing during prolonged culture. It was not possible to identify whether the NR1 truncation product was due to internal degradation after translation or due to premature stop of transcription due to suboptimal codon usage. Therefore, before

continuing with the optimization of the expression conditions, it was decided to switch to a gene sequence of *AtNR1* that had been codon-optimized for expression in *P. pastoris*.

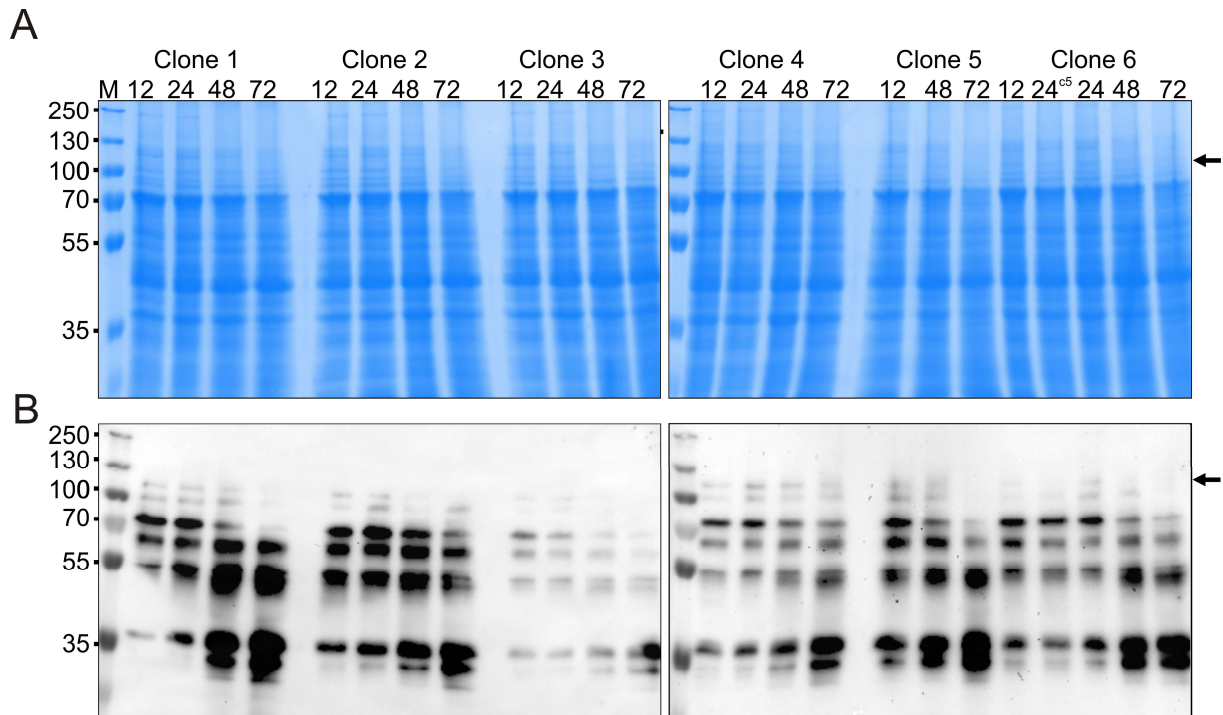


Figure 8: Clone selection of *P. pastoris* KM71 transformed with (natural) *AtNR1* DNA for expression. A. 15 µg/lane of raw lysate of transformed *Pichia* clones 1 – 6 at four different time points (12, 24, 48, and 72 h, as indicated over the lanes) following induction, on Coomassie blue stained gel. Arrows indicate the expected band of fl-NR1 at ~103 kDa. **B.** Immunoblot of the samples in A using anti-NR antibody.

2.1.2 Expression of codon-optimized *AtNR1*-fl in KM71

Codon optimization of a transgene for expression in a foreign host can overcome the problems associated with rare codons prematurely halting heterologous protein expression and can result in a more stable, full-length protein product (Hedfalk et al., 2008). Considering the difficulties that were seen with the expression of NR1-fl in *Pichia*, the natural sequence of *AtNR1* fl was analysed using the software ‘Graphical Codon Usage Analyser’ (Fuhrmann et al., 2004). The graphical result of this analysis is shown in Appendix 1. It was seen that within the first ~1/3 of the gene sequence, about 10 codons were found to be limiting in *Pichia* for expression of NR1-fl. The codon optimized synthetic DNA sequence (*AtNR1*-co) was therefore purchased (Genscript, NJ, USA) in the pPICZa vector ready for expression.

Pichia strain KM71 was transformed by electroporation and after selective growth on a gradient of zeocin-containing medium, eight clones (with higher zeocin resistance) were selected for analysis. Colony PCR indicated that all the clones contained the codon optimized NR1 sequence in contrast to the clone transformed with the empty pPICZa vector (right-most lane, Fig. 9A). Small-scale, 4 h test expression was performed and the cells were lysed with raw lysate (10 µg/lane) analysed by Coomassie staining and immunoblot (Fig. 9B, C). On the immunoblot it can be seen that five of the eight clones express NR1 to a greater or lesser extent, however there is more degraded than full-length protein visible which may have been due to overheating in the incubator during culture (which is also why culture was only performed for 4 h). Expression of NR1 using the codon optimized construct was confirmed.

Next, it was attempted to optimize the duration of expression time and induction conditions by choosing one clone from the previous experiment, six expression times (4h, 6h, 8h, 14h, 19h and 24h), and two methanol concentrations for induction (0.5% and 1%). Raw lysate (10 µg/lane) was analysed by Coomassie staining and immunoblot (Fig. 9D, E). Once again, strong expression was absent as no clear band on the Coomassie gel can be attributed to the NR1 protein. On the immunoblot, a positive band can be seen for all conditions. The NR-specific band on the immunoblot indicated that 1% methanol resulted in somewhat stronger induction. In this experiment, the degradation of the protein that had been seen using the natural *AtNR1* DNA or for the 'overheated' culture was absent (Fig. 8B, Fig. 9C).

Further expression condition tests that were performed with KM71 transformed with pPICZa:*AtNR1-co* included comparison of 'rich' peptone and yeast extract containing expression medium (BMMY), compared with 'minimal' expression medium without those components (MMH). However, all attempts resulted in only trace expression levels that could be detected only by immunoblotting (data not shown).

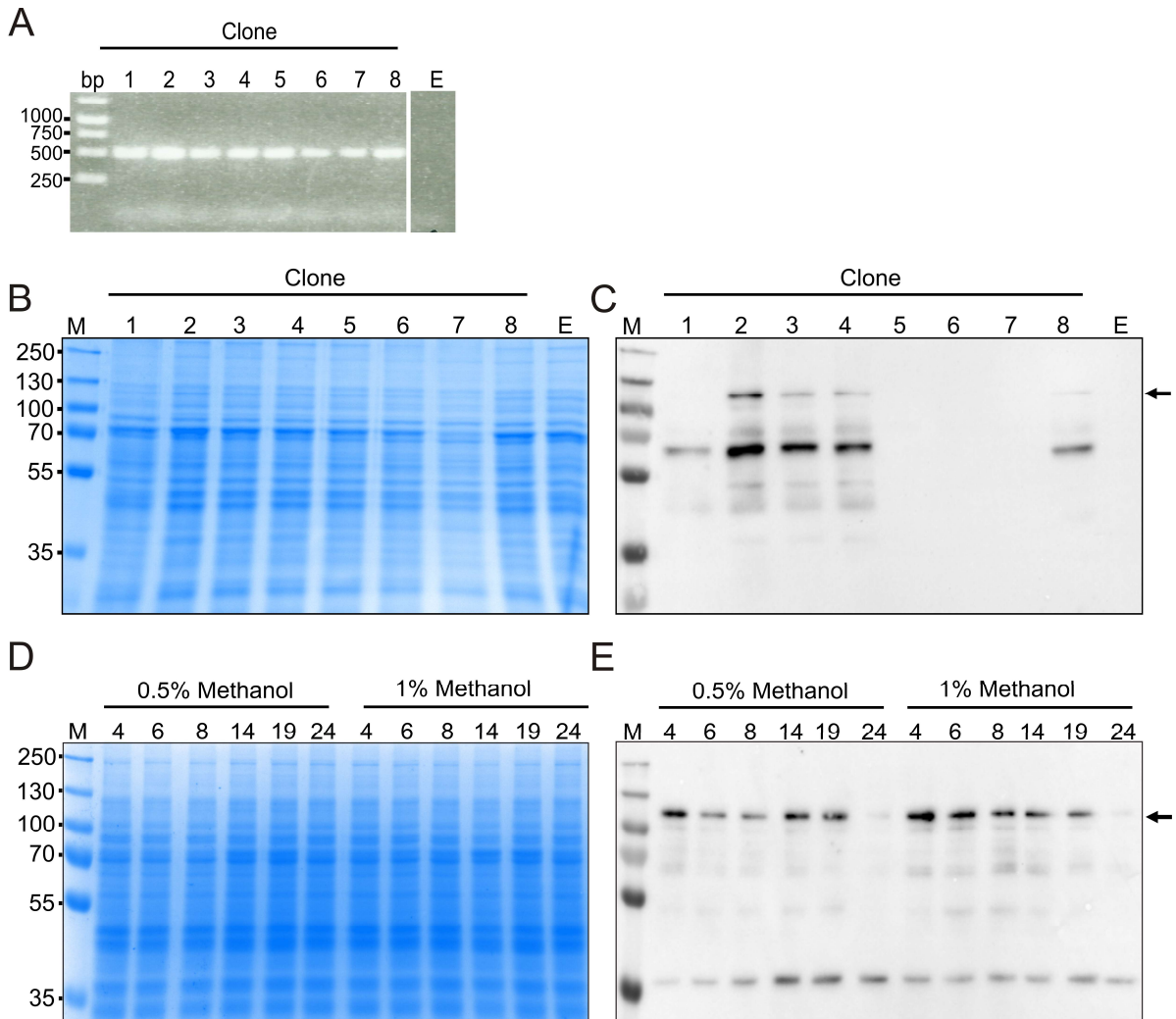


Figure 9: Clone selection of *P. pastoris* KM71 transformed with the codon-optimized *AfNR1* DNA for expression. **A: 1% agarose gel of colony PCR of transformed yeast clones 1 to 8 (numbers above lanes) and one clone transformed with empty pPICZa plasmid (E). The band at ~500 base pairs is specific for *AfNR1*-co. **B and C:** Four-hour test expression analysed by Coomassie stained gel and anti-NR immunoblot. **D and E:** Clone 3 from panel B/C was used for expression of various duration (numbers above the lanes in hours). Two methanol concentrations were tested for induction. Abbreviations: bp, base pairs of DNA marker, M, protein molecular weight marker, E, empty pPICZa transformed yeast clone.**

2.1.3 Expression of codon-optimized *AfNR1*-fl in GS115

The yeast strain used for expression and the genotype of the yeast can influence the success in expression of a certain heterologous protein (Krainer et al., 2012). Therefore, it was next attempted to express the *AfNR1*-co sequence in the alternative *P. pastoris* strain GS115. In contrast to KM71, which has the Mut^s (Slow methanol utilization phenotype), GS115 has the Mut⁺ phenotype (Grows quickly on methanol). GS115 cells were grown and transformed similarly to KM71. Zeocin resistant clones

were selected and subjected to small-scale expression culture for three times of expression (6 h, 24 h and 30 h) and analyzed as before (Fig. 10A, B).

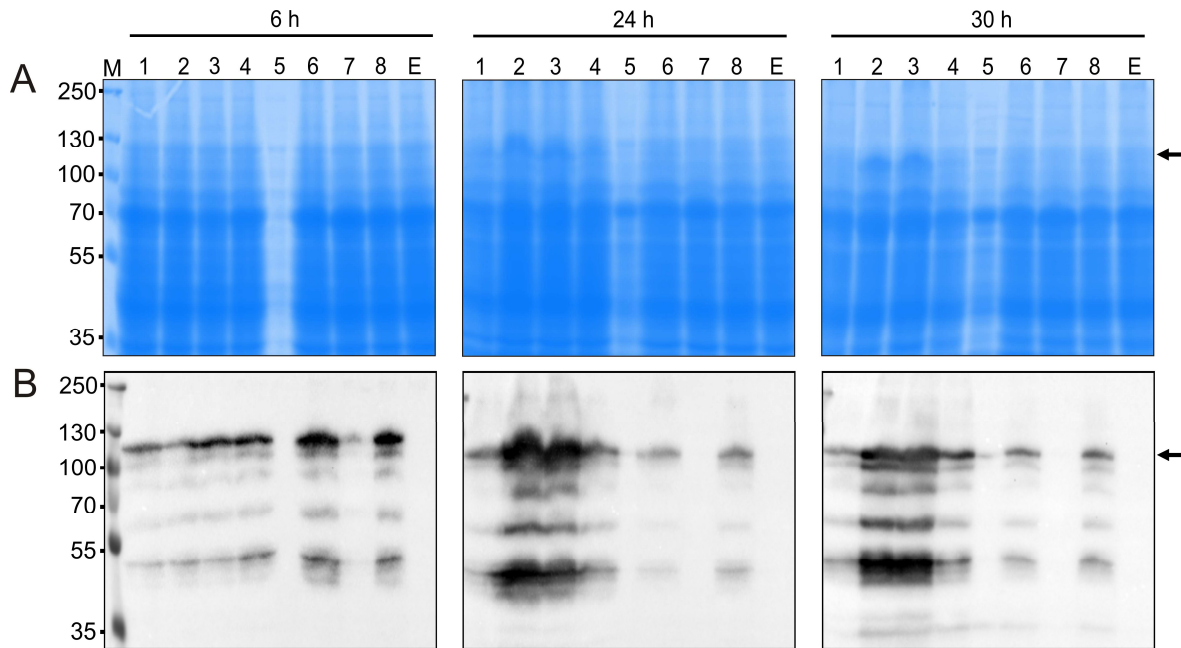


Figure 10: Clone selection of *P. pastoris* GS115 with the codon-optimized *AtNR1* DNA for expression. **A: Equal volumes of raw lysate of eight selected clones (labelled 1 – 8) were analysed by Coomassie blue staining at 6 h, 24 h and 30 h post-induction – compared with a clone transformed with empty pPICZa vector (E). **B:** Anti NR immunoblotting of the samples shown in A. Abbreviation: h, hour**

In general, the amount of NR expressed by the GS115 clones appeared to be greater compared to KM71 as a specific NR1 protein band could be seen on the Coomassie gel. Testing different clones and durations of expression yielded important insights into the expression of *AtNR1-co* and was individual for different clones. For example, clones 6 and 8 expressed strongly at 6 h but expression was reduced again at 24 h (Fig. 10B). Clones 2 and 3, on the other hand had the strongest signal for NR at 24 h, but much weaker signals with shorter or longer expression times. There was evidence that longer duration of expression resulted in increased amounts of degraded protein relative to full-length protein, therefore as a next step, clones 2 and 3 were chosen for larger scale culture with expression times of 14 h and 18 h respectively. Small samples of cells were taken at various timepoints during the culture and confirmed the expression kinetic of clone 2: no NR was seen at 8.5 h, but it was present at 14 h (harvest), data not shown. Clone 3 showed expression at 12 h and was harvested at 18 h.

Both clones expressed full-length NR with minimal degraded protein present and therefore it was attempted to purify the protein by Ni-NTA affinity chromatography. Even though the lysis and wash buffers contained no imidazole, the recombinant full-length NR1 did not bind to the Ni-NTA matrix (Fig. 11A, B). The same result was obtained for both clones. It was confirmed that the DNA used for transformation contained the intended 6xHis tag, however this tag was integrated into the NR1 sequence after the first two residues (MA-HHHHHH-TSVDNR.....) similar to the NR2 expression construct (originally donated by Prof. N. Crawford, University of California, San Diego, USA). Therefore, it can be concluded that the N-terminus of NR1 adopts a conformation in which the His-tag is not surface-exposed and accessible to the Ni-NTA matrix for affinity purification, which contrasts to NR2, which can be purified via its intrinsic His-tag without difficulties (Section 2.1.5). This gives an indication that the folding of the N-terminus of NR1 may be different to NR2.

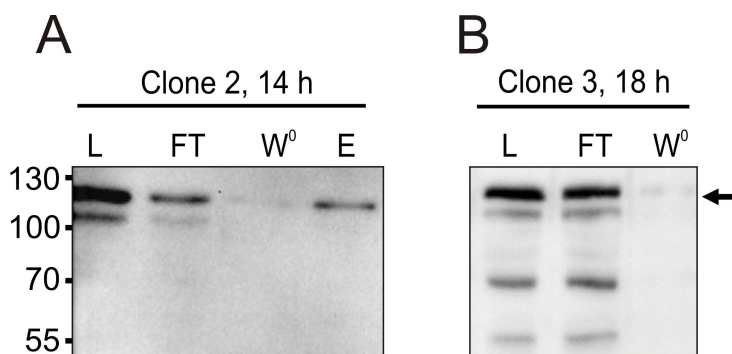


Figure 11: Absence of binding to Ni-NTA resin by AtrNR1-co expressed *P. pastoris* GS115 **A:** Anti NR immunoblot of samples of raw lysate (L), flow through (FT) wash (W⁰) and elution fraction (E) of Ni-NTA column. **B:** Immunoblot of Ni-NTA affinity purification of a second GS115 clone. The elution fraction contained no protein as determined by spectrophotometry (not shown on immunoblot).

2.1.4 C-terminal His-tagged AtrNR1-co fl

A new strategy for expression of AtrNR1-co was developed. The purchased sequence of AtrNR1-co in pPICZa plasmid was excised and then re-introduced into the pPICZa plasmid, in such a way that the N-terminal His tag was removed and the NR1 was in-frame with a C-terminal 2xMyc and 6xHis tag. The resulting protein had an expected size of 108 kDa. *Pichia* GS115 were again transformed and 18 clones were obtained from zeocin selection agar plates. All were positive by colony PCR for AtrNR1-co. Small-scale test expressions for 24 h were performed. Of the 18 clones, six displayed weak expression at 24 h, and one clone displayed strong expression on the

immunoblot (data not shown). This clone was then subjected to more extensive expression testing with expression assessed at 4h, 8h, 24h, 32h, 48h, and 72h (Fig. 12A). A band of NR1 protein on Coomassie blue stained SDS PAGE gel indicated that longer time of expression was favourable. Other time course experiments with the same clone yielded partially conflicting results showing expression up to 24 h and decreased expression thereafter (data not shown).

Large scale culture (3L expression volume) was performed for 24 h and samples were taken at 7h and 24h (harvest) and confirmed the presence of NR1 (Fig. 12B) and therefore the bulk of cells were lysed in two portions. In each case, a small amount of full-length NR1 was purified. One example is shown (Fig. 12C). For one of the portions, size exclusion chromatography (SEC) was performed to further purify the protein as it could be seen on the Coomassie gel to contain bands besides the NR1 protein; however this resulted in loss of the protein. For the second portion preparatory scale SEC was not performed, rather it was directly buffer exchanged into storage buffer using a PD-10 column and after cofactor content determination was frozen in liquid nitrogen and stored at -80°C. Form A content was determined to be 2.4%. The recovery of cofactor saturated NR1-fl was 11.5 µg per liter expression culture.

Despite the low recovery of NR1-fl, the protein quantity was sufficient for some biochemical characterizations. Firstly, UV/visible spectroscopy was performed to determine the *At*NR1 spectrum and to compare it with other NR proteins reported in the literature. Indeed the *At*NR1 displayed a spectrum typical for NR proteins with the heme cofactor absorption dominating the spectrum. The oxidized protein displayed a prominent peak at 413 nm that is typical for a *b*-type-heme containing protein (Fig. 12D, dashed trace). When the protein was reduced by its co-substrate NADH the heme absorption changed as being typical for this type of cofactor; the peak at 413 nm shifted to a maximum at 423 nm and two additional peaks appeared at 528 nm and 555 nm (Fig. 12D, unbroken trace). The FAD-cofactor of NR also contributed to the absorption spectrum. The shoulder that was visible in the range from 450 nm to 500 nm in the oxidized protein can be attributed to this cofactor. Upon reduction by NADH, the absorption in this range disappeared. The third cofactor of NR, the Moco, also has a characteristic absorption at about 380 nm, however in the full-length protein containing the heme cofactor, Moco absorption was masked by the stronger heme absorption.

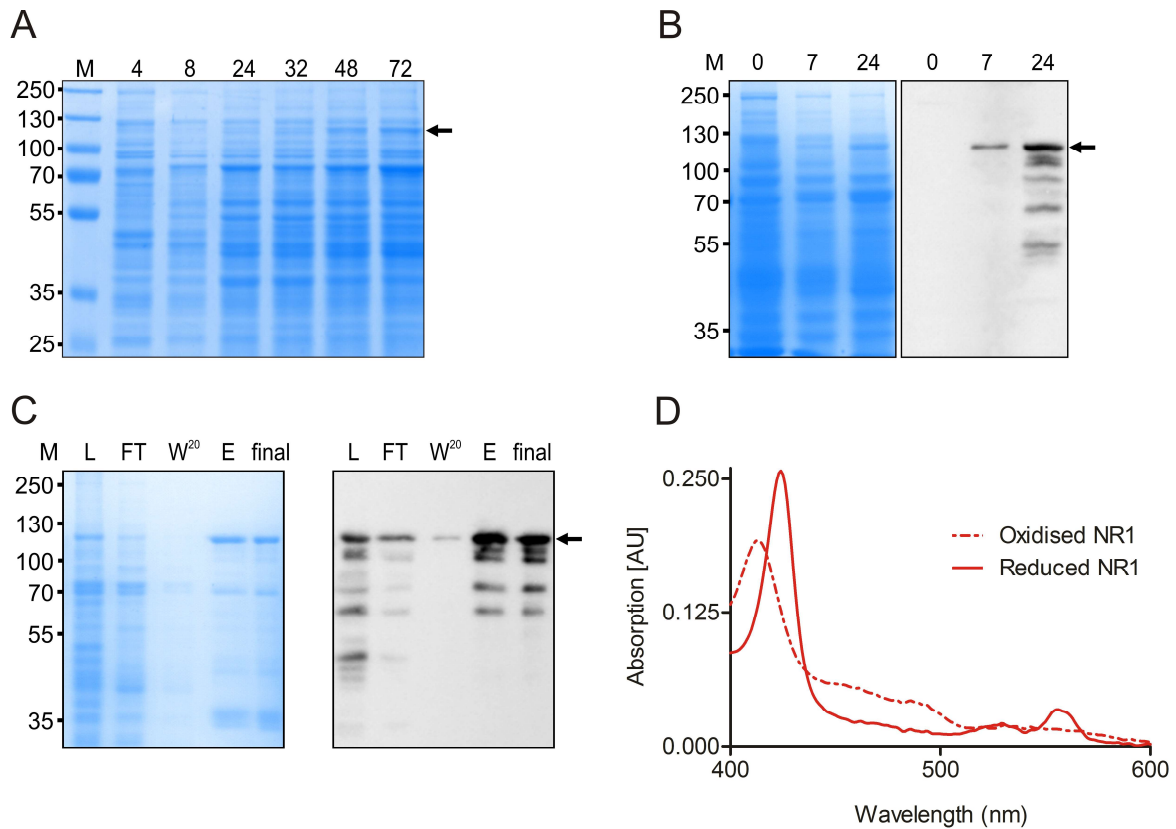


Figure 12: Expression in *P. pastoris* GS115 and purification of AtNR1-co with C-terminal his-tag. **A:** Positive NR1-expressing clone 8 from test expressions (not shown) was subjected to an expression experiment of 4 – 72 h induction (numbers above the lanes). **B:** 24 h expression culture (3L-scale) was performed with samples removed at 7 h and 24 h, and compared to the cells before induction 0 by Coomassie blue stained PAGE and anti NR immunoblot. **C:** Ni-NTA affinity chromatography to purify NR1-fl from the cells in B (24 h). **D:** UV/visible spectrum of 1.6 μ M (based on heme cofactor) NR-fl after purification (oxidised - dashed line, NADH reduced - unbroken line). In panels A-C, arrows indicate the size of NR1-fl. Abbreviations: M: Protein molecular weight marker, L: raw lysate, FT: Flow through, W²⁰: Wash with lysis buffer containing 20 mM imidazole, E: Elution fraction, final: buffer exchanged final purified protein

2.1.5 Full-length NR2

Full-length AtNR2 has been expressed in *P. pastoris* in the past (Lambeck et al., 2010; Skipper et al., 2001; Su et al., 1996) and was expressed in this work as a positive control for nitrate and nitrite reductase activity determination. Freshly prepared linearized pPICZb:AtNR2 DNA (Lambeck et al., 2010) was used for transformation of *P. pastoris* strain KM71. The *Pichia* cells were lysed and the 6xHis labeled NR protein was purified by standard Ni-NTA affinity chromatography. Samples of lysate and purification fractions were separated by SDS-PAGE and subjected to Coomassie staining and immunoblotting (anti NR antibodies and Ni-NTA conjugate) (Fig. 13).

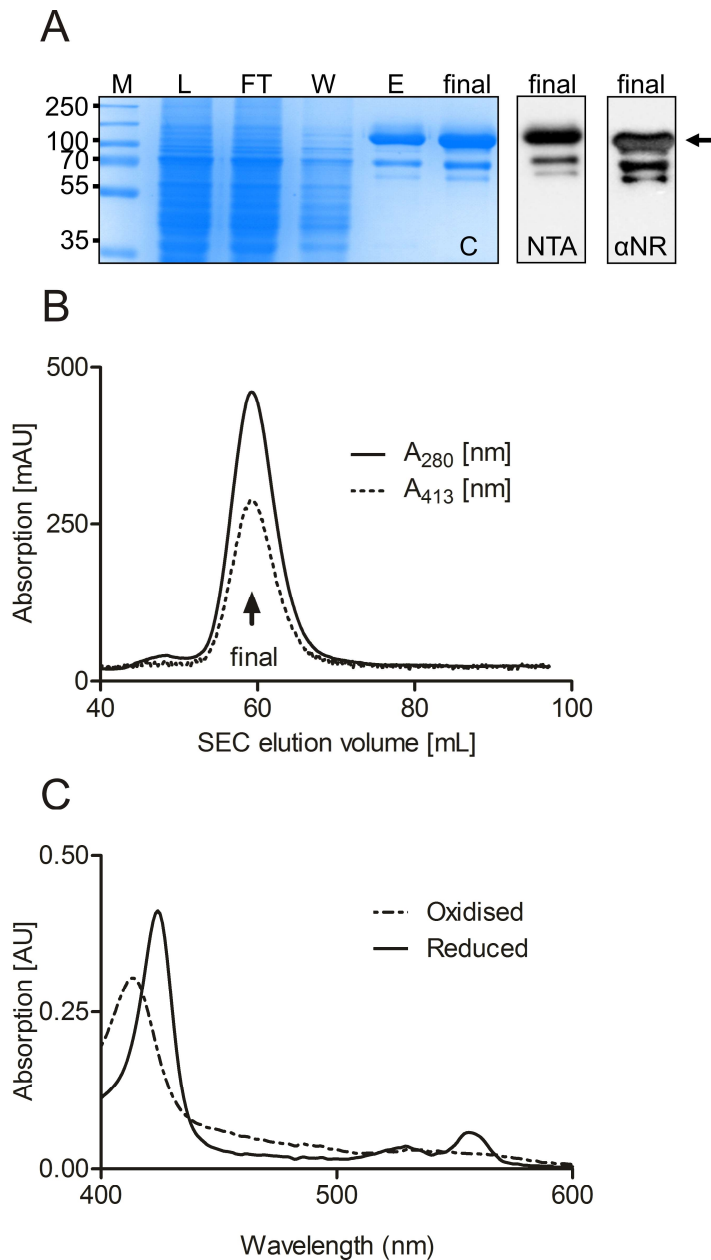


Figure 13: Purification of full-length NR2 expressed in *P. pastoris* KM71. **A:** Coomassie blue (C) stained samples of lysis and purification fractions and the final protein band on immunoblots using HRP conjugated Ni-NTA (NTA) detecting the His tag of the recombinant protein and anti-NR (α NR). **B:** SEC profile for the full-length NR2 protein. The pooled final peak is indicated (final). **C:** UV/visible spectrum of 2.5 μ M (based on heme cofactor) NR2-fl after purification (oxidised - dashed line, NADH reduced - unbroken line).

Full-length NR2 was obtained following Ni-NTA affinity separation. The peak indicated on the SEC plot corresponds with a calculated MW of about 507 kDa. NR2 is expected to form a dimer of two 100 kDa subunits, however a larger apparent size in SEC is commonly observed and is sometimes attributed to the fact that NR most likely has asymmetric dimensions (Fig. 3) and therefore a larger hydrodynamic radius than SEC size standard proteins (Mertens et al., 2000). Alternatively it has been proposed that

NR2 can easily form a tetramer (dimer of dimers) based on the SEC profile and native gradient PAGE results with NR2-fl (Mertens et al., 2000; Skipper et al., 2001; Su et al., 1997). Degradation product bands are seen in the Coomassie gel and immunoblots (Fig. 13A). The total amount obtained of cofactor saturated NR2 was 0.5 mg per liter of culture. Moco saturation was determined to be in the range of 23 – 35% (for different lots). For subsequent experiments the concentration of Moco saturated protein was used as reference (unless otherwise stated). The oxidized and NADH-reduced spectrum of full-length NR2 (Fig. 13C) was very similar to the spectrum for NR1-fl (Fig. 12D)

2.2 Production of functional domain fragments of AtNR

Despite testing various approaches described above to express NR1-fl protein in *P. pastoris*, recovery was extremely low. Therefore, the long-standing knowledge that the domain fragments of NR retain the partial activity of the respective reaction that they catalyse within full-length NR was utilized and an alternative approach to studying the biochemistry of NR1 in comparison to NR2 was developed. For this approach, domain-fragments of the two N-terminal domains of NR1 and NR2 were separately expressed in *E. coli* and then compared for their MV:nitrate and benzyl viologen (BV) :nitrite partial activities (NR-Mo-heme domains). In addition, the NR-FAD domain fragments of NR1 and NR2 were expressed and a functional reconstitution of the full-length NADH:nitrate /NADH:nitrite activity by combination of fragments was achieved as described below in section 2.5.

2.2.1 Expression and purification of AtNR1-Mo-heme

As already mentioned, AtNR1 or fragments thereof have not been expressed before. The NR-Mo-heme fragment of NR2 has been successfully expressed in the past, and has been the subject of several studies, particularly from our research group concerning its biochemistry and regulation (Chi et al., 2015; Lambeck et al., 2012). For a comparison of the two isoforms, NR1-Mo-heme was expressed and purified in *E. coli* strain TP1004 using a protocol modified from that described for NR2-Mo-heme (Lambeck et al., 2012). NR1-Mo-heme was observed to be very unstable in the expression host and following its expression, the bacteria proceeded rapidly to degrade the protein. Therefore the ideal expression conditions were found to be

shorter (22 h) compared to NR2-Mo-heme (70 h), and at a different temperature (25°C vs. 18°C for NR2) (Mohn, 2016).

Following Ni-NTA affinity chromatography for isolation of the N-terminally His-tagged protein, a subsequent SEC step was performed to separate protein pools containing dimers of one- or two- degraded NR1-Mo-heme subunits from dimers containing only non-degraded NR1-Mo-heme. Judging by the elution volume in the SEC, the apparent molecular weight of NR1-Mo-heme in the final pool is 360 kDa while the two peaks containing degraded NR1-Mo-heme run at apparent sizes of 120 kDa and 50 kDa respectively.

In the SEC it could be seen that the final pool of NR1-Mo-heme had a high ratio of A_{413} absorption (Fig. 14C, dashed trace) relative to A_{280} absorption (unbroken trace). The average value for this A_{413}/A_{280} ratio derived from 12 NR1-Mo-heme batches as measured with the spectrophotometer in the final pool was 0.804 ± 0.248 (mean \pm standard error of the mean (SEM)). Based on the specific extinction coefficient of the heme cofactor ϵ_{413} $120,000 \text{ M}^{-1} \text{ cm}^{-1}$ and the NR-Mo-heme specific ϵ_{280} $125,415 \text{ M}^{-1} \text{ cm}^{-1}$ (calculated using ProtParam) the heme saturation in the final pool was on average 84% while the peaks that eluted later in the SEC contained comparably less heme. This indicated that the surface exposed hinge 1 sequence between the Moco and heme domain is a site of proteolytic cleavage in NR1 expressed in *E. coli*.

The results of NR2-Mo-heme expression are shown for comparison with NR1-Mo-heme (Fig. 14B, D). In this case, only two pools of protein dimers were obtained by SEC; dimers of non-degraded NR2-Mo-heme "final", and dimers of degraded NR2-Mo-heme "P2". NR2-Mo-heme final-pool SEC elution volume corresponds with a MW of 327 kDa. P2 is shown on the gel and immunoblot and it can be seen to consist of a homogeneous ~57 kDa protein. This appears to run as a dimer with a calculated MW of ~110 kDa based on the elution volume from the SEC column. The average heme-saturation (n=7) for NR2-Mo-heme was 63%.

For both NR1-Mo-heme and NR2-Mo-heme the saturation with Moco was determined by oxidation to Form A and quantification via HPLC. In subsequent experiments (unless otherwise stated), protein concentration used refers to the concentration of Moco containing enzyme. Average levels of Moco saturation expressed as a percentage of heme-containing protein were 20% for NR1-Mo-heme (Range 9% to 33%, n=14) and 38% for NR2-Mo-heme (range 25% to 44%, n= 8).

The recovery of NR1-Mo-heme was $\sim 30 \mu\text{g}$ per liter of *E. coli* culture and of NR2-Mo-heme was $\sim 1 \text{ mg}$ per liter.

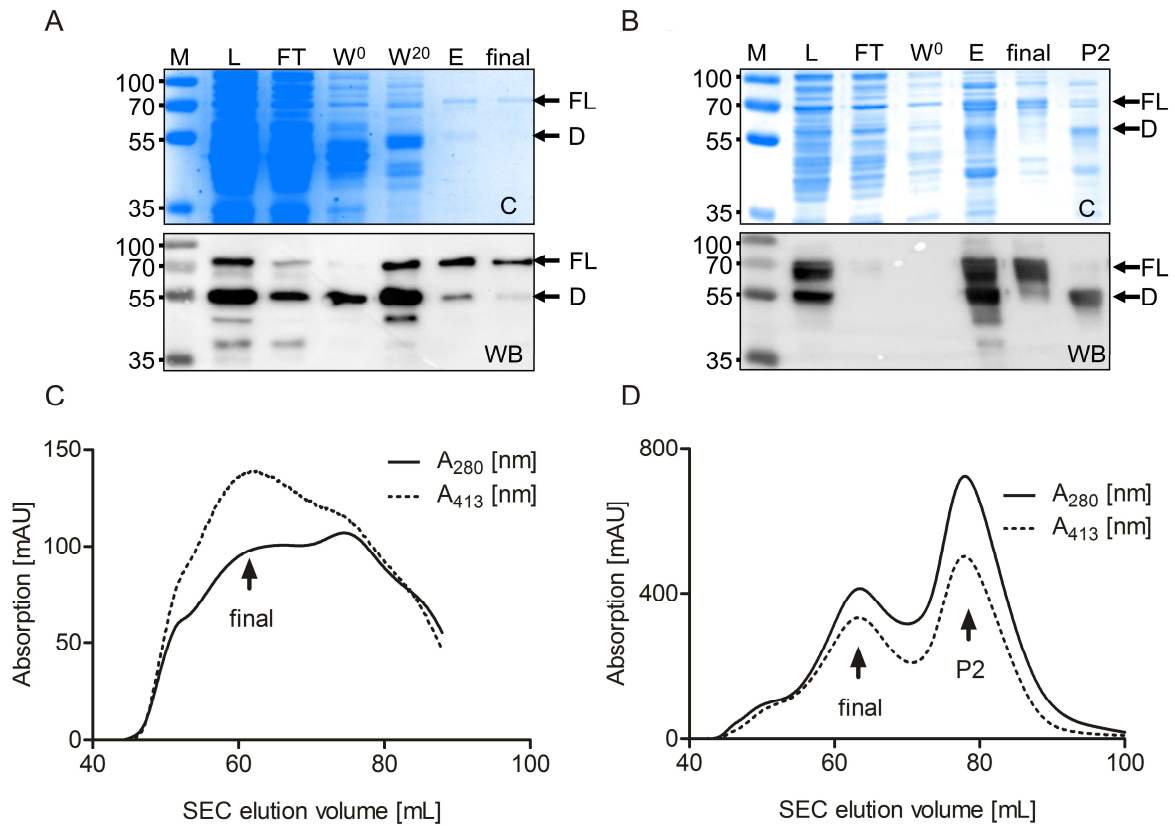


Figure 14: Purification of NR-Mo-heme fragments expressed in *E. coli* TP1004. **A:** SDS-PAGE Coomassie stained (C) and immunoblot (WB) using anti-NR antibody of NR1-Mo-heme purification. **B:** Purification of NR2-Mo-heme. **C and D:** SEC for purification of NR1-Mo-heme and NR2-Mo-heme respectively. Abbreviations: M, protein marker; L, *E. coli* lysate; FT, flow-through of Ni-NTA chromatography; W⁰, wash fractions without imidazole; W²⁰, wash fraction with 20 mM imidazole; E, eluted protein; final, final protein pool; P2, pool of degraded NR2-Mo-heme protein, FL, Full-length NR-Mo-heme, D, degraded NR-Mo-heme.

2.2.2 Expression of AtNR-FAD fragments

For experiments using re-constituted NR activity the FAD fragments of NR1 and NR2 were cloned and expressed in the *E. coli* expression host BL-21 (materials and methods). The 6xHis-tagged proteins were purified using Ni-NTA affinity chromatography. Coomassie blue-stained gels of the purified FAD-fragments are shown (Fig. 15). The fragment size following purification was 32 kDa, as expected. The expression and purification led to recoveries of 1.6 mg – 3 mg FAD fragment per liter of *E. coli* culture.

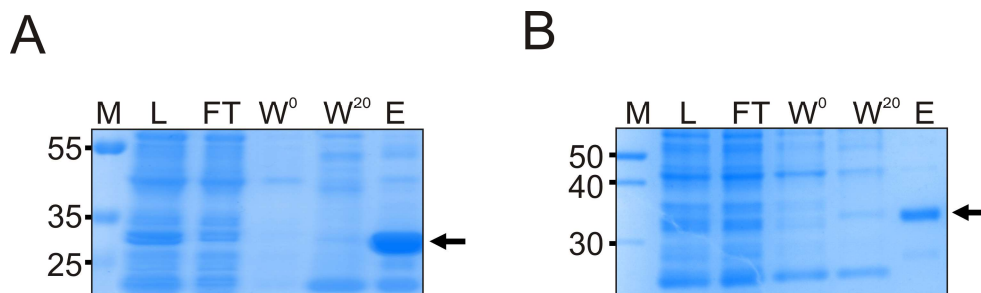


Figure 15: Purification FAD-domain fragments of NR1 and NR2. **A:** Purified NR1-FAD fragment **B:** Purified NR2-FAD fragment on 12% SDS-PAGE, Coomassie stained. Abbreviations: M, protein marker; L, *E. coli* lysate; FT, flow-through of Ni-NTA chromatography; W^0 , wash fractions without imidazole; W^{20} , wash fraction with 20 mM imidazole; E, eluted protein

2.2.3 Expression of AtNR-Mo fragments

The Mo-domain of NR1 was cloned from the NR1-Mo-heme sequence and placed in the pQE80L plasmid for expression in TP1004. Ni-NTA affinity chromatography was performed followed by SEC to purify the NR1-Mo domain fragments. The absorptions at wavelengths 280 nm and 380 nm were recorded during SEC as Moco-containing proteins exhibit a specific absorption maximum at 380 nm that can be attributed to Moco. (Fig. 16A). Samples of pooled fractions indicated in the SEC elution profile (P1 and P2) were analysed together with the Ni-NTA purification fractions on the Coomassie gel and immunoblot (Fig. 16C). Using the calculated extinction coefficient ϵ_{280} 108,330 $M^{-1} cm^{-1}$ the concentration of protein in the P1 pool was 10.64 μM , however it can be seen on the Coomassie gel that the protein is impure. The concentration of Moco-containing protein was 0.49 μM (4.6 %). The recovery (Moco saturated) of NR1-Mo per liter *E. coli* culture was 9.4 μg .

NR2-Mo-domain was likewise expressed in TP1004 using the appropriate construct (pQE80:AtNR2-Mo, kindly provided by K. Schrader) (Fig. 16B, D). Many bands of truncated or degraded NR2-Mo are seen on the immunoblot, and the purity was low (Fig. 16D, P1). Based on the signal on the immunoblot, and the activity of the pools that was later determined (section 2.7.2), P1 was most enriched for intact NR2-Mo. The concentration of total protein in the pool was 19.35 μ M but the concentration of Moco saturated protein was 8.44 μ M (44%). Recovery of NR2-Mo was 44 μ g/liter *E. coli* culture.

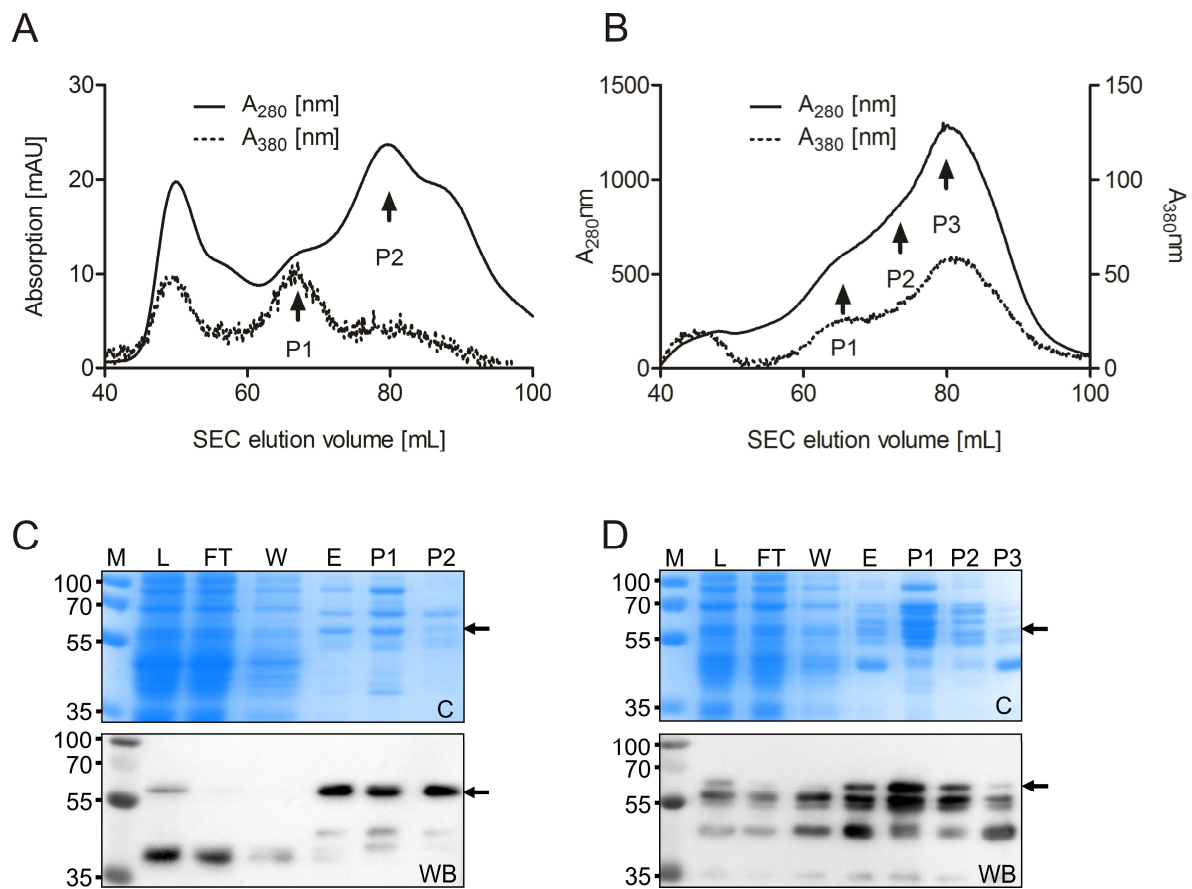

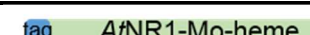
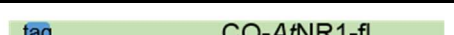





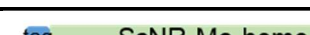
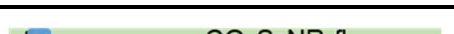


Figure 16: Purification NR-Mo-domain fragments of NR1 and NR2. **A:** NR1-Mo fragment SEC **B:** NR2-Mo fragment SEC P1, P2, P3, pools of SEC. **C:** NR1-Mo **D:** NR2-Mo, Coomassie stained gel of purification fractions (C), Anti NR immunoblot (WB). The arrow indicates the size of the expected Mo domain fragment at ~57 kDa, which was most enriched in P1. Note: In B, the absorption at wavelength 380 nm is shown on the right-y- axis as it was more than 10x smaller than the 280 nm absorption. Abbreviations: M, protein marker; L, *E. coli* lysate; FT, flow-through of Ni-NTA chromatography; W, wash fractions, E, eluted protein, P1, P2, P3, pools of protein collected.

2.3 Other constructs cloned for expression in *P. pastoris*

In total 10 different constructs of NR1 or NR2 and of NR from spinach (SoNR) have been generated for expression in *P. pastoris*. (Table 1). Transformation of *Pichia* KM71 or GS115, test expressions and clone selection have been performed for all constructs (as described for AtNR1-fl constructs). Glycerol stocks have been made and are in storage. Larger scale cultures and protein purification are outstanding due to time constraints.

Table 1: List of constructs cloned for expression in *P. pastoris*. Transformations and expressions using some of the constructs are described in the text.

	Gene	Expression plasmid	Position His tag	Cartoon of construct showing His-tag in blue
<i>A. thaliana</i> NR, isoform 1				
1	AtNR1-fl	pPICZb	N-terminus	
2	AtNR1-Mo-heme	pPICZb	N-terminus	
3	Codon optimized AtNR1-fl	pPICZa	Internal at N-terminus	
4	Codon optimized AtNR1-fl	pPICZa	C-terminus	
5	Codon optimized AtNR1-fl	pPICZb	N-terminus	
<i>A. thaliana</i> NR, isoform 2				
6	AtNR2-fl*	pPICZb	Internal at N-terminus	
7	AtNR2-Mo-heme	pPICZb	N-terminus	
<i>Spinacia oleracea</i> NR				
8	SoNR-fl	pPICZb	N-terminus	
9	SoNR-Mo-heme	pPICZb	N-terminus	
10	Codon optimized SoNR-fl	pPICZa	Internal at N-terminus	

*This construct is described in (Lambeck et al., 2010) and was provided for this work.

2.4 Nitrate reduction activity of recombinant NR

In order to fully characterize the nitrate reducing activity of NR1, NR1-fl and domain fragments were tested in various kinetic measurements. For comparisons, NR2 was measured in parallel.

2.4.1 NADH:nitrate activity of full-length NR

As described in section 2.1.1, the amount of purified NR1-fl protein was small with a low Moco saturation (Lot A: 11.5 µg, 2.4% Moco saturation (Fig. 12C) and Lot B: 14 µg, 5.0% Moco saturation (Fig. 17A)). However, the quantity was sufficient to determine the activity using the physiological substrates NADH and nitrate. Results are shown for Lot B (Fig. 17A, B). The activity for the two lots diverged strongly (Table 2). In fact, both the K_M and k_{cat} determined differed by a factor of ~five between the two batches of NR1 measured. Lot A was expressed from the C-terminal His-tagged NR1-co (construct #4, Table 1) in *Pichia* GS115, while Lot B was expressed with an N-terminal His-tag (construct #5, Table 1) in the same host strain. The biochemical properties of both protein preparations were similar and no clear explanation could be found for the divergent activities.

For comparison to NR1, the purity and activity of a batch of NR2 is shown (Fig. 17A and B, Table 2). It can be seen that the 'more active' Lot B of NR1-fl displayed NADH:NR activity that was very similar to NR2-fl determined here with K_M^{nitrate} 196 ± 9 µM and a k_{cat}^{nitrate} 32.3 s^{-1} . The data were also comparable to the values described in the literature (Lambeck et al., 2010) with a K_M^{nitrate} 197 ± 15 µM and a k_{cat}^{nitrate} 33 s^{-1} .

Due to the very small amount of NR1-fl obtained here and the fact that so far only two lots could be obtained, suggests that the kinetic parameters determined here for NR1 cannot be considered reliable. Further studies are required beyond this study.

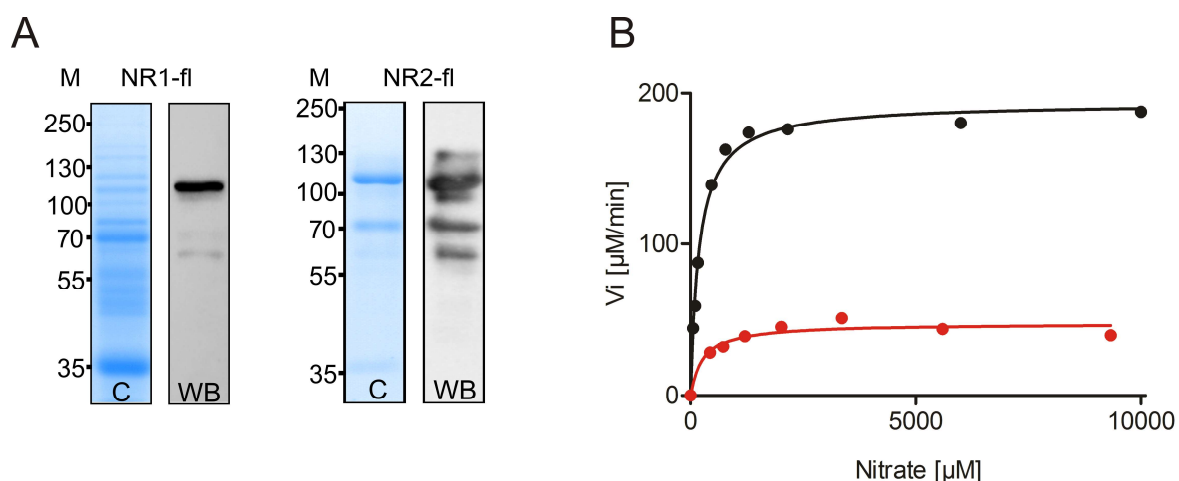


Figure 17: NADH:nitrate activity of full-length NR1 and NR2 expressed in *P. pastoris*. **A:** Coomassie gel (C) and anti NR-immunoblot (WB) of the NR1-fl and NR2-fl used in this experiment. **B:** NADH:nitrate activity of 25 nM NR1 (red) and 100 nM NR2 (black). The data have been fitted with a Michaelis Menten hyperbolic fit using GraphPad Prism 5 to yield K_M and k_{cat} for the two enzyme isoforms (Table 2)

Table 2: Michaelis Menten kinetic parameters of NR1 and NR2 NADH:nitrate activity

	K_M^{nitrate} [μM]	k_{cat}^{nitrate} [s^{-1}]	Catalytic efficiency [$k_{cat}/K_M \text{ s}^{-1}\text{mM}^{-1}$]
NR1 Lot A	56 ± 20	6.72	120
NR1 Lot B	283 ± 57	31.7	112
NR2	196 ± 9	32.3	164

2.4.2 The methyl viologen:nitrate activity of NR-Mo-heme

The domains of NR are independently folded and therefore retain a partial activity of the full-length protein if they are separated by partial proteolysis or are expressed separately as recombinant proteins (Kubo et al., 1988; Solomonson and Barber, 1990). It has been shown in the past for NR2, that the NR activity and 14-3-3-regulation of the N-terminal molybdenum and heme domains, linked by hinge 1 (residues 1-625) is similar to the full-length protein (Chi et al., 2015; Lambeck et al., 2012). In the absence of the FAD-domain, NADH – the physiological electron donor – is no longer able to function and instead the artificial electron donor methyl viologen can be used in its reduced form (see Fig. 2), that donates its electrons directly to the heme domain, which in turn passes them to the Moco domain, where nitrate reduction takes place. Nitrate

reduction activity may be followed by the decrease in absorbance at 595 nm as the pre-reduced MV becomes re-oxidised.

As a first step toward determining the NR activity of NR1-Mo-heme, it was first tested at which pH nitrate reduction by this enzyme isoform showed the highest rate. The optimum for NR2 is known to be pH 7.0 (Lambeck, 2009), spinach NR also has highest nitrate activity at pH 7.0 (Barber and Notton, 1990). It could be confirmed by performing a kinetic series at pH 6.5, 7.0, 7.5, and 7.9 and then plotting the V_{Max} obtained for each pH, that the optimum pH for nitrate reduction by NR1-Mo-heme was also pH 7.0 (Fig. 18A). Activity at pH 7.9 was almost absent.

Next, the MV:nitrate activity of multiple purified NR1-Mo-heme protein batches were measured (Fig. 18B-D). Some lot-to-lot variability was seen in the activity of both NR1 and NR2-Mo-heme batches, but the means \pm SEM were determined for a large sample size (Table 3). The K_M^{nitrate} for NR1-Mo-heme was found to be $2120 \pm 160 \mu\text{M}$, compared with $443 \pm 26 \mu\text{M}$ for NR2-Mo-heme and was thus almost five times higher (Fig. 18C). The k_{cat} values were $51 \pm 4 \text{ s}^{-1}$ for NR1-Mo-heme and $69 \pm 9 \text{ s}^{-1}$ for NR2-Mo-heme (Fig. 18D). Using the catalytic efficiency k_{cat}/K_M to compare both isoforms NR1-Mo-heme had a value of $24 \text{ s}^{-1} \text{ mM}^{-1}$ while NR2-Mo-heme was with $155 \text{ s}^{-1} \text{ mM}^{-1}$ more than six-times more efficient than NR1-Mo-heme in nitrate reduction.

Compared with the NADH:nitrate activities determined (Section 2.4.1), the kinetic parameters determined here are different; both the MV:nitrate K_M and k_{cat} for NR2 were about 2-fold higher, while the MV:nitrate K_M for NR1 was about a factor of ten- and the k_{cat} was 2 – 8-fold higher compared with the values for NADH:nitrate activity. It has been reported in the past that rates of reduction of nitrate by reduced MV can be greater than the rates observed with NADH (Mertens et al., 2000). Therefore, it is thought that a two-fold difference between the two methods could be plausible and may be explained by the shorter electron path involving ‘only’ the heme to Moco transfer, instead of transfer from FAD through the entire enzyme (NADH:nitrate activity). However, the discrepancy in the case of NR1 is more likely to reflect the “poor quality” of NR1-fl tested in the NADH:nitrate activity determination. It is thought that because of the large number of replicate samples for MV:nitrate tested activity that the values determined were more likely to reflect the real nitrate reduction activity of NR1.

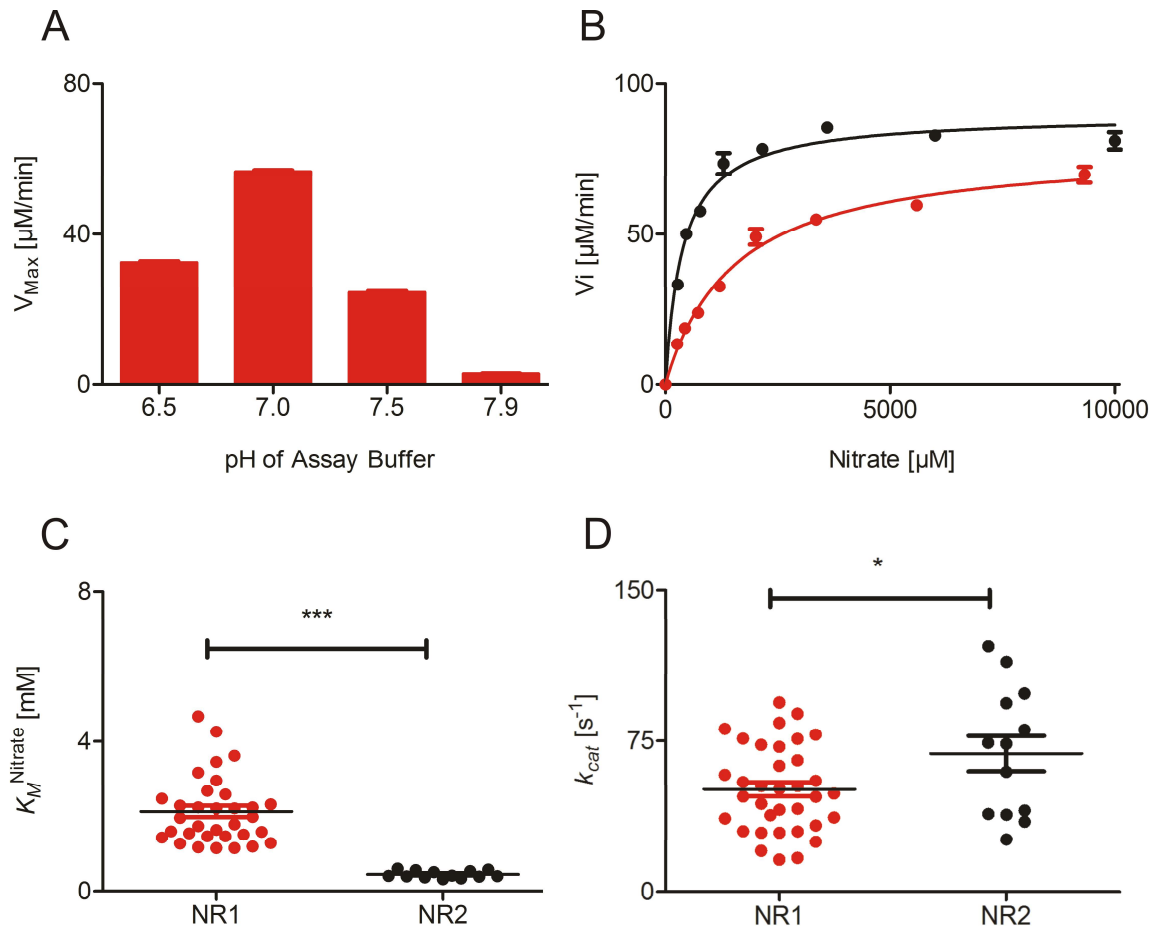


Figure 18. MV:nitrate reduction activity of NR1-Mo-heme and NR2-Mo-heme. **A:** Michaelis-Menten steady-state kinetic series at four different pH values. **B:** MV:nitrate activity comparing 25 nM NR1-Mo-heme (red) with 25 nM NR2-Mo-heme (black) and fitted with a Michaelis Menten hyperbolic curve using GraphPad Prism. **C:** The K_M^{Nitrate} of NR1-Mo-heme (red) and NR2-Mo-heme (black) are compared for multiple kinetic series. **D:** The $k_{\text{cat}}^{\text{Nitrate}}$ is compared. The means \pm SEM of $n = 33$ kinetic series for NR1-Mo-heme (made with 23 protein batches) and $n = 13$ kinetic series for NR2-Mo-heme (made with 8 protein batches) are shown. *** $p < 0.0001$, * $p < 0.05$. This figure is modified from Mohn et al 2019.

Table 3: Kinetic constants for MV:nitrate activity using NR-Mo-heme fragments.

	K_M^{Nitrate} [μM]	$k_{\text{cat}}^{\text{Nitrate}}$ [s^{-1}]	Catalytic efficiency [$k_{\text{cat}}/K_M \text{ s}^{-1} \text{ mM}^{-1}$]
NR1-Mo-heme (n=33)	2120 ± 160	51 ± 4	24
NR2-Mo-heme (n=13)	443 ± 26	69 ± 9	155

2.5 Re-constitution of full-length NR-activity from domain fragments

Although it has been proposed that hinge 2 is involved in intramolecular domain movement during electron-transfer (Barbier and Campbell, 2005) our own studies have indicated that the electron transfer between FAD and heme is not affected by viscosity (Lambeck et al., 2012) thereby suggesting that the intact hinge 2 might not be essential for NR activity. It was therefore tested, if the activity of full-length NR may be reconstituted by co-incubation of the domain fragments (NR-Mo-heme and NR-FAD) that have been expressed separately in *E. coli* (Mohn et al, 2019).

2.5.1 Establishing re-constituted NR activity

In preliminary tests it was observed that NADH:nitrate activity of re-constituted-NR required anaerobic conditions because otherwise the NR-FAD fragment displayed substantial diaphorase (NADH:O₂ oxidoreductase) activity (data not shown). These tests also confirmed that re-constitution of NR activity was possible and that the covalent link between the FAD and heme domain via hinge 2 is not essential for NR activity.

First, it was tested what ratio of Mo-heme fragment to FAD fragment resulted in a measurable level of NADH:nitrate activity (Fig. 19 – adapted from Mohn et al 2019). It was observed that the relationship between activity- and excess of NR-FAD fragment was dose dependent: the more FAD fragment that was supplied, the higher the activity measured (Fig 19A). For NR1-Mo-heme + NR1-FAD ratios of up to 1:100 were measured yielding a maximal apparent k_{cat} of 18 s⁻¹ and for NR2-Mo-heme ratios of up to 1:200 were measured, which resulted in a maximal apparent k_{cat} of 23 s⁻¹ (Fig. 19A). Because of the concentration of the protein solutions available, and the volume of reagents used for measurement it was not possible to test higher ratios of FAD. NADH and nitrate were both supplied in excess. Although these k_{cat} values were below the k_{cat} values for MV:nitrate activity (section 2.4.2), in the case of reconstituted-NR2, they were near the published k_{cat} for the full-length enzyme (33 s⁻¹ Lambeck et al., 2010).

Overall, however, it could be concluded that the rate of re-constituted enzyme activity was somewhat limited by supply of FAD-fragment – or more precisely, by supply of electrons from the separate NR-FAD domain to the NR-Mo-heme domain. It was decided to use a ratio of 1 Mo-heme to 50 – FAD fragments for subsequent steady-state kinetic activity measurements. The ratio 1:50 yielded measurable slopes of

NADH consumption and avoided protein foaming during measurement that would have been exacerbated by higher protein concentrations.

2.5.2 NADH:nitrate activity of re-constituted-NR

By performing steady state NADH:nitrate activity measurement for re-constituted NR1 and NR2 it was possible to again compare both isoforms. Because of the limitation in the rate of the reaction caused by the FAD-domain being a separate entity from the Mo-heme domain, the steady-state kinetic constants do not reflect the maximum activity of the full-length protein (at least for NR2, compared with the measured values (2.4.1) or the published values (Lambeck et al., 2010)). However, the activity measured is substrate (nitrate) concentration dependent and shows that the internal electron transport chain of NR has been successfully restored. The 1:50 ratio of Mo-heme:FAD reconstituted NR1-activity k_{cat} was 10 s^{-1} in the titration curve and the respective reconstituted NR2-activity k_{cat} was 13 s^{-1} . Because the k_{cat} values are lower as compared to the respective Mo-heme fragments, the resulting K_M values were also reduced with $K_M 17 \pm 1.2 \mu\text{M}$ for NR1-activity and $35 \pm 1.4 \mu\text{M}$ for NR2-activity (Table 4).

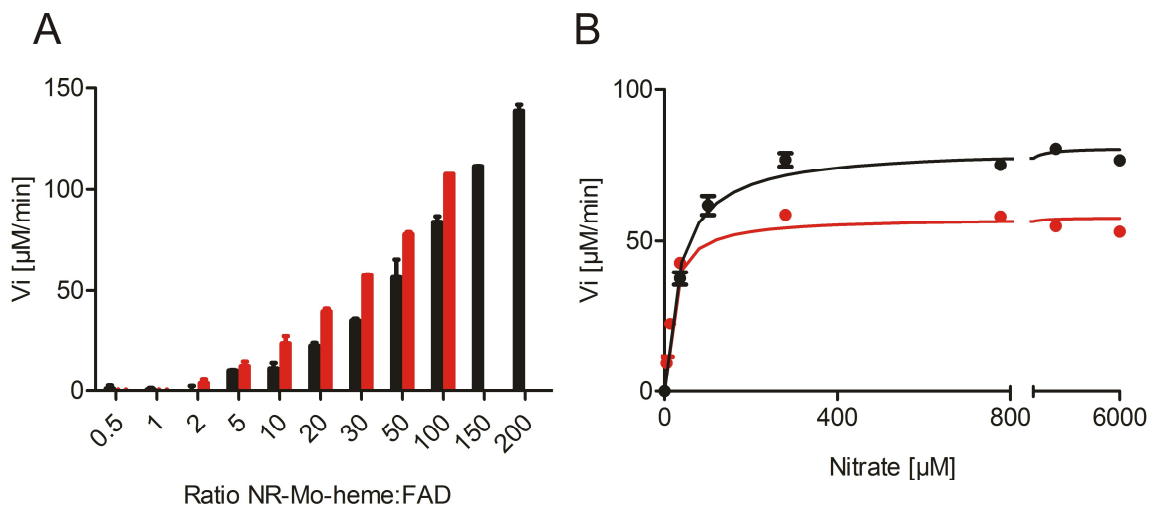


Figure 19: NADH:nitrate activity of re-constituted full-length NR1 and NR2. **A:** Titration of NR-FAD fragment (red – NR1, black – NR2) with 100 nM NR-Mo-heme fragment showing the V_i of NADH consumption. **B:** Steady-state NADH:nitrate activity of 100 nM NR1-mo-heme + 5 μM NR1-FAD (red) and 100 nM NR2-Mo-heme + 5 μM NR2-FAD (black). Figure adapted from Mohn, et al 2019

Table 4: Michaelis Menten kinetic parameters for NADH:nitrate activity of re-constituted NR1 and NR2

	K_M^{nitrate} [μM]	$k_{\text{cat}}^{\text{nitrate}}$ [s^{-1}]	Catalytic efficiency [$k_{\text{cat}}/K_M \text{ s}^{-1}\text{mM}^{-1}$]
NR1-Mo-heme + NR1-FAD	17	10	588
NR2-Mo-heme + NR2-FAD	35	13	371

2.5.3 Pre-steady-state kinetics of NR1 and NR2 in nitrate reduction using re-constituted NR activities

Using pre-steady state rapid kinetic measurements, it was next aimed to obtain a direct measurement of the rate of nitrate reduction when the enzyme is in the pre-reduced state. The rates of the various electron transfer steps during nitrate reduction and upon 14-3-3 inhibition have been studied extensively for NR2 in the past but not yet for NR1 (Lambeck et al., 2012; Skipper et al., 2001). Skipper et al. used *Pichia*-expressed full-length NR2 and an excess of NADH to obtain the initially reduced enzyme. Lambeck et al. used the NR2-Mo-heme fragment and pre-reduced the enzyme using sodium dithionite. Here, it was decided to test if the NR-Mo-heme fragment could also be pre-reduced using the physiological reductant NADH and by re-constituting the electron transfer chain with the separated FAD domain. Subsequently, the nitrate re-oxidation of the heme cofactor was measured on the stopped-flow apparatus.

Since the enzyme was to be pre-reduced – and therefore sufficient time was given to complete this reaction, a sub-stoichiometric ratio of 0.5 NR-FAD fragments to 1 NR-Mo-heme fragment was used. In initial tests using a spectrophotometer, it could be confirmed that the re-constituted NR was easily reduced by the addition of an excess of NADH, and remained stably reduced under anaerobic conditions for a long period of time (overnight). This is a great advantage over the reduction with dithionite, which is more sensitive to oxygen-dependent re-oxidation over time on the stopped-flow instrument. An excess of dithionite in the reaction mixture would not be desirable due to unspecific side-reactions and interference with the UV/visible spectrum of the enzyme.

Because the rate of reduction of the NR-Mo-heme fragment using the FAD-fragment was observed to be very slow (Section 2.5.1) the effect of potential re-reduction while measuring the rate of nitrate oxidation of the heme cofactor could be neglected. It was decided to measure only a single wavelength on the stopped flow apparatus using the

monochromator set to 412 nm, as this allows for more sensitive absorption measurement (compared to spectral mode) and it was seen in a preliminary experiment that the spectral change at 412 nm was largest between the reduced and oxidized protein (not shown). Before mounting the pre-reduced enzyme on the stopped flow instrument, a spectrum was measured in a sealed cuvette using a spectrophotometer to confirm that the enzyme was reduced (Fig. 20A, dashed trace). By addition of a 1:1 volume of nitrate (final concentration 250 μM) it could be confirmed that the heme spectrum became oxidized (Fig. 20A, unbroken trace). The concentration of NR2-Mo-heme used on the stopped-flow-apparatus was 3 μM , based on the heme absorption at 413 nm and using an extinction coefficient 91,000 $\text{M}^{-1} \text{cm}^{-1}$ for the NADH reduced enzyme (Skipper et al., 2001).

On the stopped-flow-apparatus, multiple concentrations of anaerobic nitrate solution were used for re-oxidation of the heme compared to a blank measurement with buffer. By fitting a single exponential equation to the first rapidly proceeding absorption increase (~ 0.04 sec, correlating with the first electron transfer from the heme domain to the Moco domain following nitrate reduction), the rate constant k_{obs} for each nitrate concentration was extracted (Fig. 20B). By plotting the k_{obs} at each concentration and fitting a hyperbolic curve to the data the maximal rate of re-oxidation k_{ox} of $253 \pm 15 \text{ s}^{-1}$ and a K_D^{nitrate} of $78 \pm 15 \mu\text{M}$ were obtained. This compares well with the rate constants determined previously of k_{ox} 310 s^{-1} and K_D^{nitrate} of $131 \mu\text{M}$ (Lambeck et al., 2012). It was thus confirmed that re-constituted NR-enzyme could be used to stably and conveniently pre-reduce the heme in a system similar to the physiological one, with NADH as electron donor.

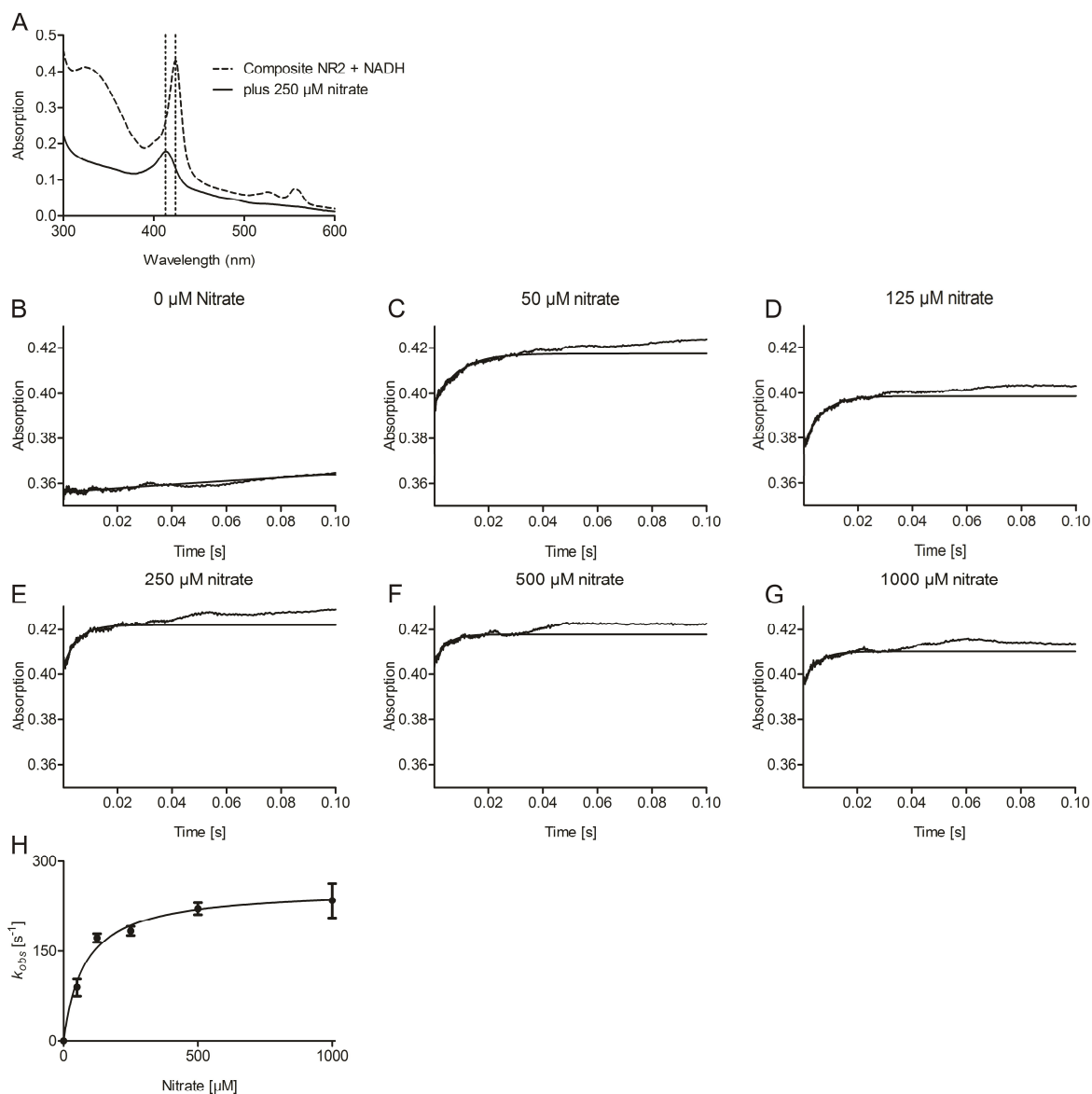


Figure 20: Pre-steady-state kinetic measurements of nitrate with NR2. **A:** Spectrum of NR2-Mo-heme+NR2-FAD (composite NR2) pre-reduced with an excess of NADH, and re-oxidised by addition of an equal volume of nitrate. Dotted lines indicate 412 nm and 424 nm **B – G:** A series of stopped flow 412 nm traces measured with the nitrate concentration indicated and with single exponential curves fit to the first ~0.04 sec. **H:** Hyperbolic curve fit using GraphPad Prism to the observed kinetic constants (k_{obs}) at each nitrate concentration to yield the kinetic constants K_D and k_{ox} .

The experiment described above for NR2-Mo-heme was repeated for NR1-Mo-heme + NR1-FAD, as the pre-steady state kinetics of this enzyme have not been determined to date. Unfortunately, due to the fact that NR1-Mo-heme cannot be obtained in a high concentration, the absorption at 412 nm on the stopped flow was very low and thus the absorption measurements had a small signal to noise ratio that rendered the evaluation difficult and a quantitative result impossible to formulate.

In one case, two peaks of the SEC for purification of NR1-Mo-heme, both of which were active were not separated (see Fig. 14C – NR1-Mo-heme pooled up to ~80 mL), – resulting in a far higher recovery and concentration of NR1-Mo-heme protein. This protein pool was pre-reduced using *A. thaliana* cytochrome b reductase (*AtCbR*, Recombinant protein kindly provided by L. Vohwinkel (Vohwinkel, 2017)), which functions similarly to the NR-FAD fragment in reducing the NR1-Mo-heme using NADH. The pre-reduced NR1-Mo-heme spectrum was measured using the stopped-flow-apparatus immediately after (0.001 sec) addition of 2 mM nitrate (Fig. 21A unbroken trace) and 10 sec later (Fig. 21A dashed trace). For the re-oxidation determination, two concentrations of nitrate were measured using the stopped-flow-apparatus and multiple replicate measurements. One trace for each concentration is shown (Fig. 21B-D). This experiment could confirm that nitrate re-oxidized NR1-Mo-heme but there were too few data points to determine K_D (The value based on the fit was 3.42 mM (Fig. 21E)). The k_{obs} for the 2 mM nitrate measurement based on the spectral change at 422 nm was $55.1 \pm 10.6 \text{ s}^{-1}$ (mean \pm SEM) and the k_{obs} for the 25 mM measurement was $131.4 \pm 20.9 \text{ s}^{-1}$. Based on the steady state K_M (MV:nitrate activity) of 2.1 mM nitrate for NR1-Mo-heme, it was assumed that a concentration of 25 mM nitrate is saturating and should yield a value close to the maximal rate of re-oxidation. The value based on the hyperbolic curve fit (Fig 21H) was 149 s^{-1} but requires further measurements.

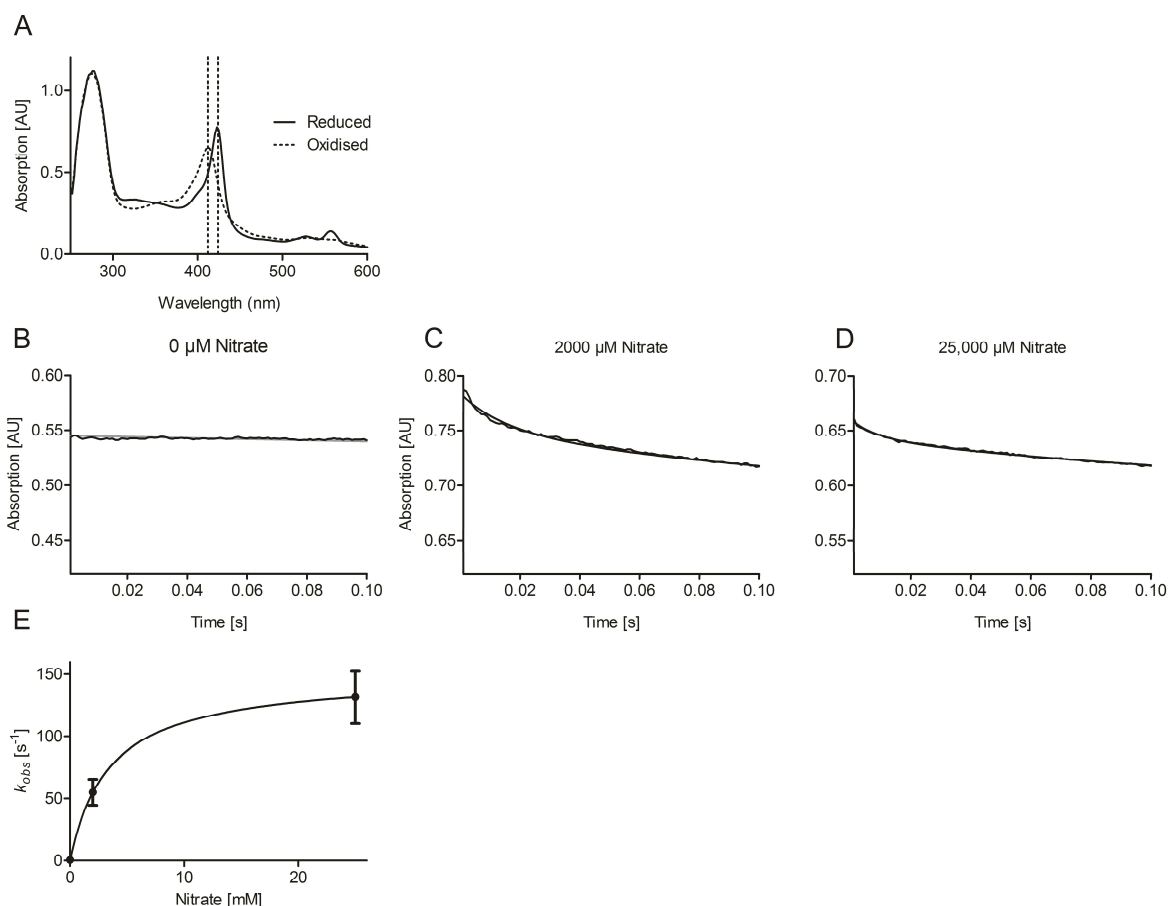


Figure 21: Pre-steady-state kinetic measurements of nitrate reduction by NR1. **A:** Spectrum of NR1-Mo-heme+At cytochrome *b* reductase, pre-reduced with NADH measured on the stopped flow before (0 sec) and after (10 sec) addition of 2 mM nitrate. Dotted lines indicate 412 nm and 424 nm **B – D:** A series of stopped flow 423 nm traces measured with the nitrate concentration indicated and with triple exponential curves fit to the 10 sec measurement (Traces shown to 0.1 sec) **H:** The kinetic constants k_{obs} for the first phase of the re-oxidation of the heme as shown in plots B, C and D, were plotted and a hyperbolic curve fit performed. Because only two concentrations of nitrate were measured, K_D and k_{ox} are preliminary.

2.6 Nitrite reducing activity of recombinant NR

2.6.1 Establishing a procedure for benzyl viologen nitrite activity determination (BV:nitrite)

When testing nitrite instead of nitrate with MV for activity measurement, it was observed that MV non-enzymatically reduced nitrite (Fig. 22A), while with nitrate no reduction was observed in the absence of enzyme (Fig. 22B). Therefore, an alternative was sought for steady-state kinetic measurement of nitrite reduction. It was observed that reduced benzyl viologen was stable in the presence of nitrite (Fig. 22C) but unstable in the presence of nitrate (Fig. 22D). It would appear that the differing redox potentials of the two viologen dye derivatives are responsible for this effect (MV: -446

mV, BV: -359 mV) (Bird, 1981; Michaelis and Hill, 1933). The finding that reduced BV is stable in the presence of nitrite presented the opportunity to use nitrite as substrate and $BV^{red.}$ as an artificial electron donor to measure the steady state kinetics of nitrite reduction in a system very similar to the established MV:nitrate activity determination. According to your knowledge, such a method for monitoring steady-state nitrite reduction has not been described to date providing a novel experimental tool to characterize the nitrite reductase activity of NR1-Mo-heme and NR2-Mo-heme fragments.

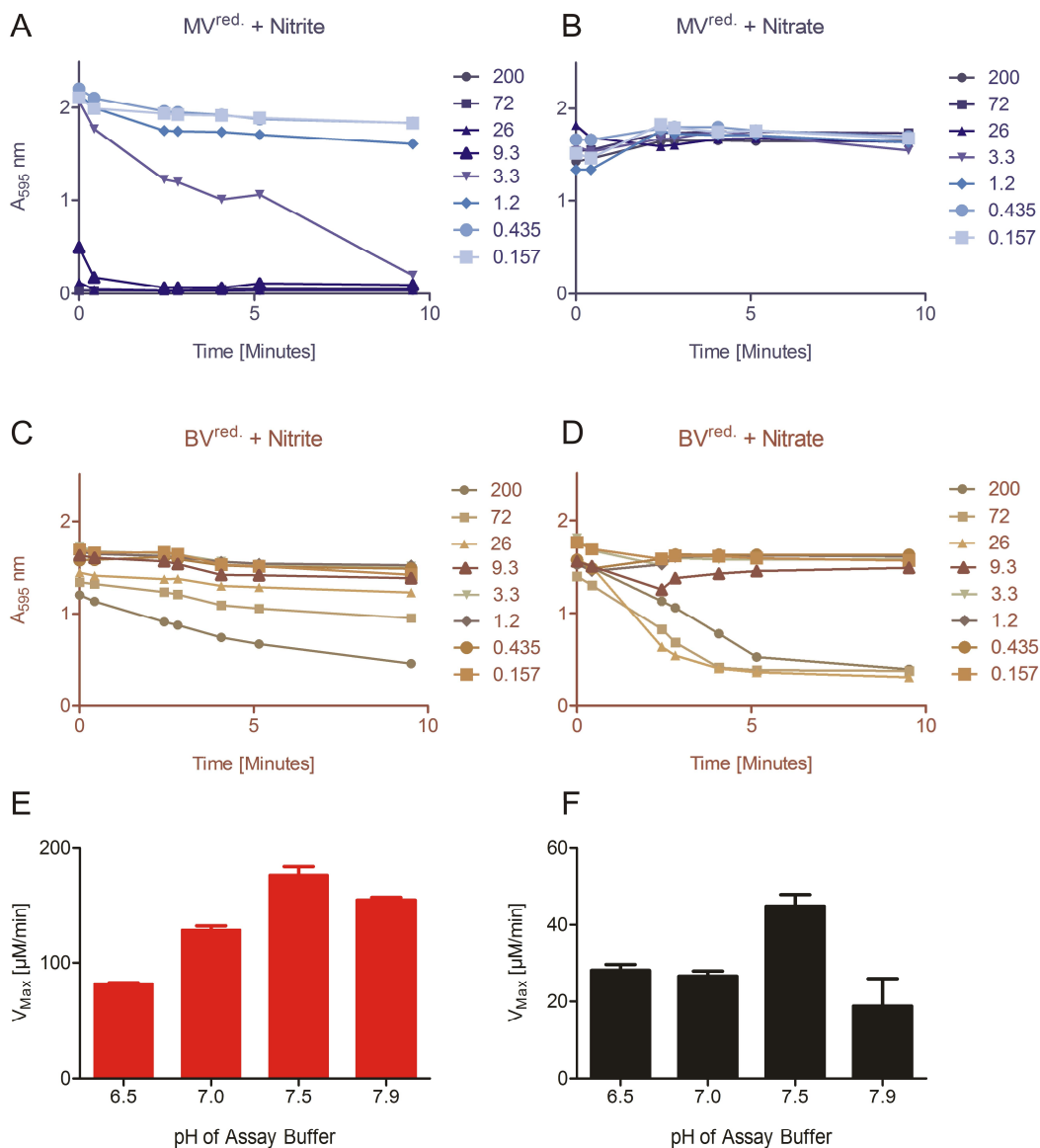


Figure 22: Stability of MV and BV in the presence of nitrate and nitrite. Determination of optimal pH for measuring BV:nitrite activity. A and B: Enzyme free mixture of buffer, reduced methyl viologen ($MV^{red.}$) and nitrite (A) or nitrate (B). **C and D:** Enzyme-free mixture of buffer, reduced benzyl viologen ($BV^{red.}$) and nitrite (C) or nitrate (D). **E and F:** BV:nitrite activity at four different buffer pH values (E) 0.5 μ M NR1-Mo-heme, (F) 0.5 μ M NR2-Mo-heme

Next, the optimal pH for nitrite reduction was determined using the BV:nitrite assay. A nitrite titration series was performed for the two isoforms at four different pH conditions (pH 6.5, 7.0, 7.5 and 7.9) in MOPS buffer. The V_{\max} was plotted for NR1-Mo-heme and NR2-Mo-heme (Fig. 22E, F). Both isoforms of NR showed optimal nitrite reduction at pH 7.5. NR1-Mo-heme was considerably more active (higher V_{\max}) than NR2-Mo-heme and in fact displayed high activity over a broad pH-range. This contrasts with the lack of nitrate reducing activity of NR1-Mo-heme at pH 7.9 (compare Fig. 18A).

2.6.2 NR-Mo-heme BV:nitrite activity

BV:nitrite activity of multiple protein batches was measured. In total 21 kinetic series with NR1-Mo-heme and 10 kinetic series with NR2-Mo-heme were recorded. One representative example for each isoform is shown in Fig. 23A. A summary of averaged kinetic parameters (K_M^{nitrite} and $k_{\text{cat}}^{\text{nitrite}}$) for all series were plotted (Fig. 23B, C) as well as summarized (Table 5). The mean \pm SEM K_M^{nitrite} was $36 \pm 3 \mu\text{M}$ for NR1-Mo-heme, and $14 \pm 3 \mu\text{M}$ for NR2-Mo-heme and was thus significantly lower for NR2-Mo-heme (unpaired t-test). The turnover number $k_{\text{cat}}^{\text{nitrite}}$ was greatly and significantly higher for NR1-Mo-heme ($20 \pm 5 \text{ s}^{-1}$ for NR1-Mo-heme and $1.8 \pm 0.3 \text{ s}^{-1}$ for NR2-Mo-heme). The catalytic efficiency for NR1-Mo-heme was $556 \text{ mM}^{-1} \text{ s}^{-1}$ and for NR2-Mo-heme was about 5 times lower at $129 \text{ mM}^{-1} \text{ s}^{-1}$. The higher catalytic efficiency of NR1-Mo-heme for nitrite can, for the most part be attributed to the $\sim 10\text{x}$ higher turnover number for the substrate nitrite compared with NR2-Mo-heme.

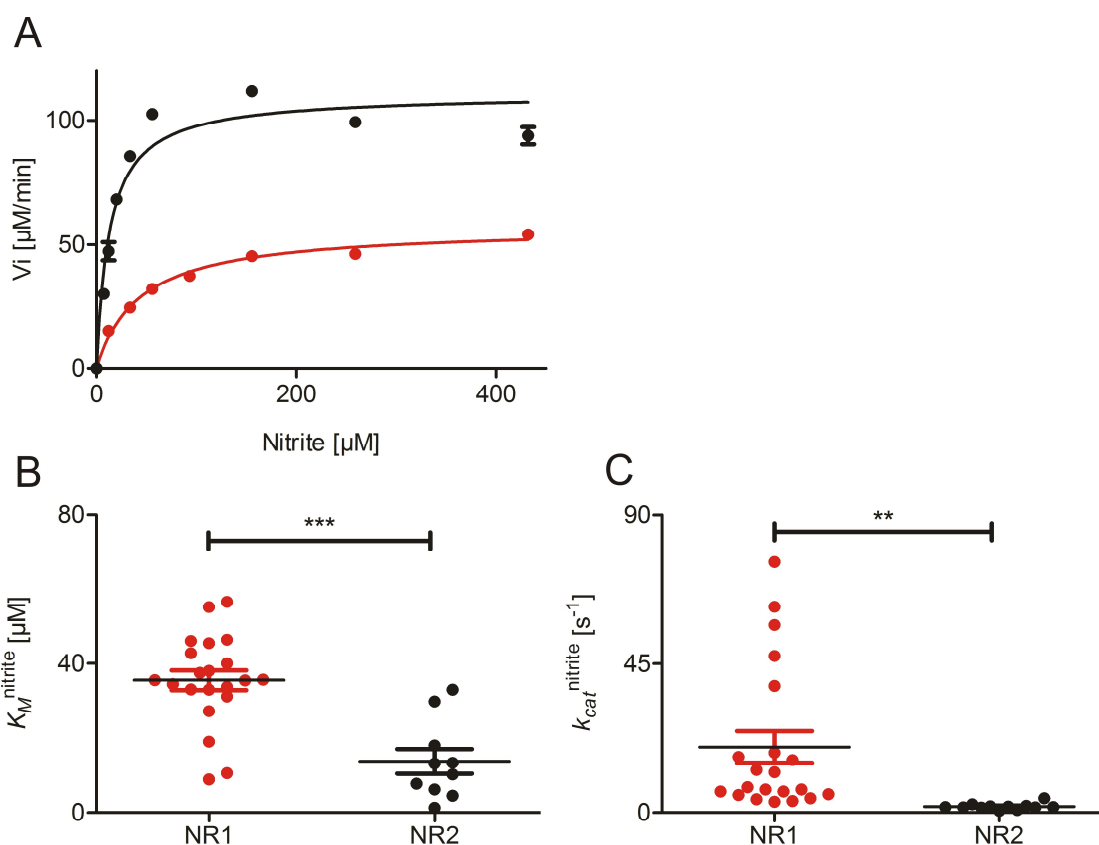


Figure 23: BV:nitrite steady-state activity measurement. **A:** 50 nM NR1-Mo-heme (red) and 1 μM NR2-Mo-heme in a representative Michaelis Menten titration series of BV:nitrite activity. **B and C:** Kinetic parameters for BV:nitrite activity, NR1-Mo-heme (red), NR2-Mo-heme (black). B: K_M , C: k_{cat} . The mean \pm SEM for 21 kinetic series (NR1-Mo-heme) or 10 kinetic series (NR2-Mo-heme) are shown. Statistical analysis via unpaired t-test (GraphPad Prism) *** $p < 0.0001$, ** $p < 0.01$. Figure modified from Mohn et al 2019.

Table 5: Michaelis Menten kinetic parameters of BV:nitrite activity for NR1-Mo-heme and NR2-Mo-heme.

	K_M^{nitrite} [μM]	$k_{\text{cat}}^{\text{nitrite}}$ [s^{-1}]	Catalytic efficiency [$k_{\text{cat}}/K_M \text{ s}^{-1}\text{mM}^{-1}$]
NR1-Mo-heme	36 ± 3	20 ± 5	556
NR2-Mo-heme	14 ± 3	1.8 ± 0.3	129

2.6.3 Nitrite reductase activity measured with an NO-Analyzer

A second and complementary methodology was used to confirm that NR1 and NR2 are indeed nitrite reductases *in vitro*. A NO analyzer was used for this purpose as it can specifically and quantitatively detect NO^{\bullet} . In preliminary experiments, it was seen that a mixture of benzyl viologen and dithionite did not remain in the pre-reduced (violet color) state with argon bubbling within the measurement chamber – even before the

addition of nitrite and enzyme. Therefore, it was not a suitable electron donor for nitrite reduction in this system. NADH, however was a suitable and stable electron donor and could be used following the previously described approach to re-constitute NR activity by co-incubating NR-Mo-heme with NR-FAD fragments in a 1:50 stoichiometry to reduce nitrite and to generate NO[•]. The NO[•] was quantified by the instrument using a chemiluminescent reaction with O₃.

Four different protein batches of NR1-Mo-heme and NR2-Mo-heme (re-constituted with the respective NR-FAD domains) were used for nitrite concentration titration series on the NO-analyzer. Substrate concentration dependent NO[•] production was observed for all lots; however the amount of NO[•] produced varied from lot to lot. Lot-to-lot variability in nitrite reduction activity had also been observed in the BV:nitrite activity determination (Fig. 23C) and it is thought that protein stability during purification (especially for NR1-Mo-heme) is an important and poorly controllable parameter. An example of the nitrite-concentration dependent NO[•] generation for FAD-domain re-constituted-NR1 and -NR2 is shown (Fig. 24A, B).

It is important to note that the NO-analyzer quantifies NO[•] generated in a liquid phase, which is subsequently transferred to the gas phase where quantification of NO[•] (in pmol) takes place in comparison with a standard curve of NO[•]. Therefore the measurement does not determine NO[•]-concentrations within the enzyme reaction mix solution. In order to convert 'amount of NO[•]' to 'concentration of NO[•]', the area under the initial increasing part of the NO[•] production curves was taken (Fig. 24A, B) and it was assumed that the amount of NO[•] detected in the gas phase corresponded to the NO[•] concentration in solution per unit time corresponding to the initial slope of the reaction. This concentration/min of NO[•] was plotted against concentration of substrate to yield steady state kinetic curves (Fig. 24C, D).

A similar conversion of NO[•]-amount to NO[•]-concentration was used in the past (Planchet et al., 2005). However, based upon the concentrations of NO[•] calculated, which were unexpectedly low (similarly to that observed by (Planchet et al., 2005)) it would appear that the concentration of NO[•] is greatly under-estimated by this method. Planchet et al. estimated ten-fold under estimation of NO[•] concentration. In the current case the problem was compounded by the fact that the rate of enzyme activity was additionally limited by the separation between the NR-Mo-heme domain and the NR-FAD domain, which led to a sub-maximal internal electron transfer rate (section 2.5.2).

In summary, this method was very useful to deliver confirmation that both NR1 and NR2 could reduce nitrite and produced NO^{*}, however the results were not quantitative. Nevertheless the pseudo MM-parameters are listed in Table 6 for the two example protein batches shown in Fig. 24.

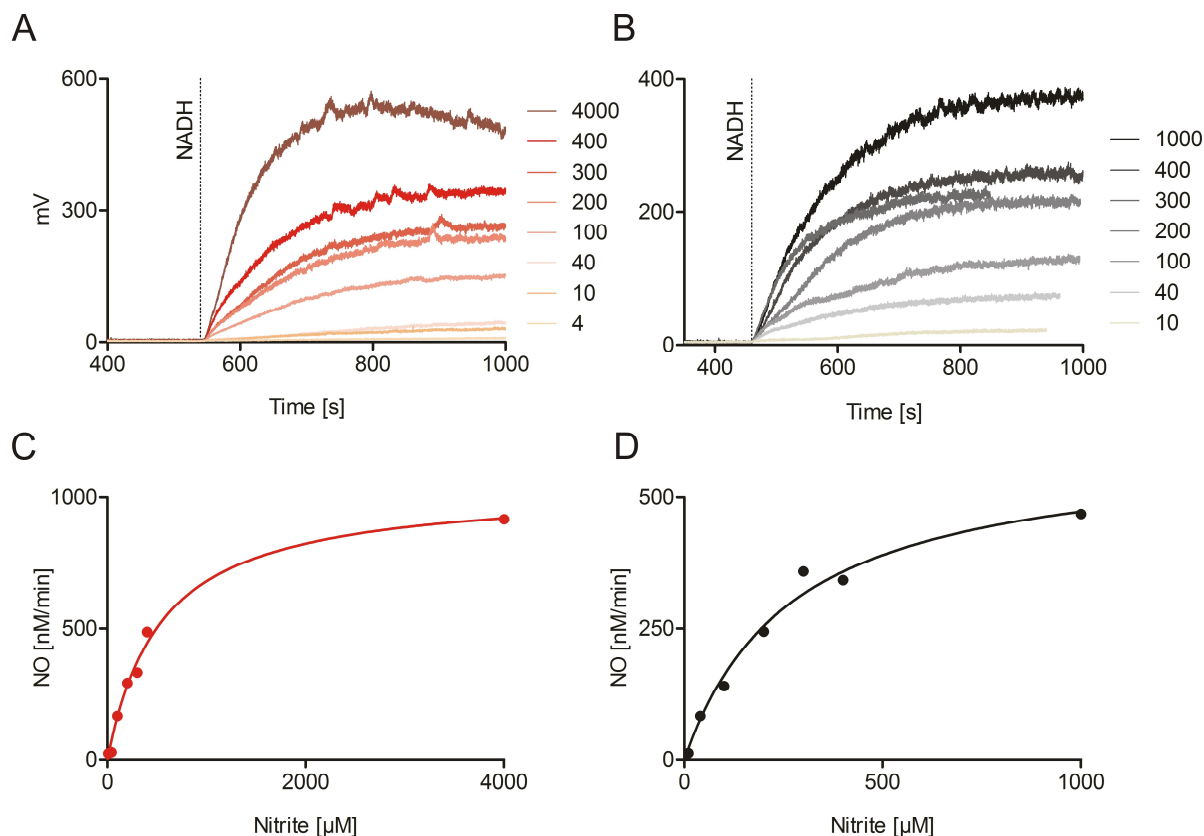


Figure 24: Substrate concentration dependent NO^{*} generation measured using the NO-analyzer. A: Nitrite dependent NO^{*} generation by NR1-Mo-heme + NR1-FAD (nitrite concentration is given by the numbers in μM). **B:** NO^{*} generation by NR2-Mo-heme + NR2-FAD at various concentrations of nitrite. **C and D:** Michaelis Menten curve fit to the NO^{*} generation kinetic observed in A and B. This figure is modified from Mohn et al 2019.

Table 6: Pseudo Michaelis Menten kinetic parameters of NR1-Mo-heme and NR2-Mo-heme determined using the NO-analyzer.

	$K_M^{\text{nitrite}} [\mu\text{M}]$	$k_{\text{cat}}^{\text{nitrite}} [\text{s}^{-1}]$	Catalytic efficiency $[k_{\text{cat}}/K_M \text{ s}^{-1}\text{mM}^{-1}]$
NR1-Mo-heme + NR1-FAD	538 ± 61.6	0.527	0.98
NR2-Mo-heme + NR2-FAD	273 ± 53.8	0.304	1.11

2.6.4 Interplay of nitrate and nitrite as substrates of NR

The nitric oxide analyzer provided the means to address two other questions relating to NR. Firstly, can nitrate serve as a substrate for NO[•] generation (by first being converted to nitrite and then to NO[•])? Secondly, what is the effect on nitrite reduction of having nitrate present in the reaction mixture, such as would be the case in the plant cell cytosol?

The first question was addressed for both isoforms of re-constituted NR enzyme and also for full-length NR2 enzyme. (Fig. 25A-E). In the complete absence of nitrite, nitrate was provided with saturating NADH concentration and NO[•] generation over time was recorded. In the samples containing the lower concentration of nitrite (400 μM), some NO[•] signal was observed, which increased over time. In contrast, the NO[•] trace for the 4 mM nitrate graphs remained at the baseline level. It would appear that conversion of nitrate to nitrite first occurred diminishing the nitrate concentrations before NO[•] can be generated. In the presence of high concentrations of nitrate (4 mM), nitrite reduction could not be observed.

To address the second question, a concentration of 400 μM nitrite was provided as this concentration of nitrite resulted in a strong production of NO[•] for re-constituted NR1 and NR2. By addition of increasing concentrations of nitrate (0 – 1 mM) at the same time as nitrite addition, the diminished amount of NO[•] produced was recorded compared to the sample without nitrate (Fig. 25 F, G). The areas under the curves, in the presence of nitrate were calculated and set as a percentage of the area recorded in absence of nitrate (100%) and were plotted (Fig. 25F). By fitting the data with a hyperbolic curve fit, it was possible to determine the concentration of nitrate resulting in half-maximal NO[•] generation (IC₅₀) to 12 ± 1.7 μM for re-constituted NR1 and 36 ± 2.7 μM for re-constituted NR2. Maximal inhibition for both isoforms was 97%.

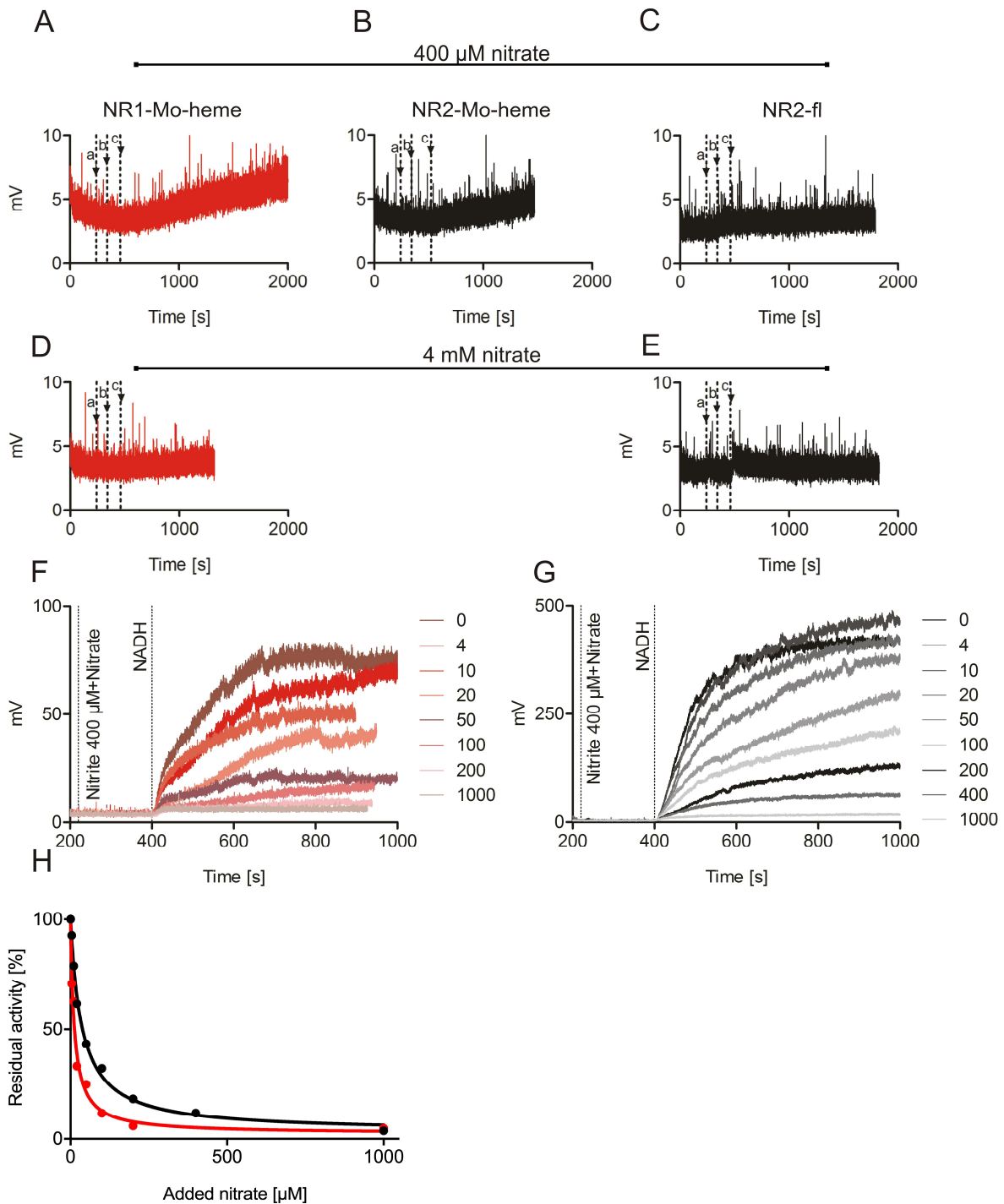


Figure 25: Interplay of nitrate and nitrite on NO generation. A and D: Re constituted NR1 (NR1-Mo-heme + NR1-FAD) supplied with nitrate (A: 400 μM, D: 4 mM) and NADH measured up to 33 minutes for NO release. **B:** Re-constituted NR2 (NR2-Mo-heme + NR2-FAD) supplied with 400 μM nitrate. **C and E:** Full-length NR2 supplied with nitrate (C: 400 μM, E: 4 mM). a. indicates addition of nitrate, b. addition of enzyme, c. addition of NADH **F and G:** Inhibition of NO[•] release by the addition of varying concentrations of nitrate (numbers in μM) simultaneously with 400 μM nitrite to re-constituted NR1 (F) and reconstituted NR2 (G). **H:** Calculated percent residual activity in the presence of nitrate, fitted with a hyperbolic curve using Graph Pad Prism to determine I_{Max} and IC₅₀.

2.6.5 Stoichiometry of NO[•] generation

Animal sulfite oxidase (SO) has a similar Moco and heme domain to NR and is also known to function as a nitrite reductase generating NO[•] (Wang et al., 2015). A feature of this NO[•] generation is that the pre-reduced enzyme Mo (IV) is only capable of producing one equivalent of NO[•], before it arrests in the partially oxidized Mo (V) state in the absence of any other electron acceptor. In order to understand the mechanism of NO[•] generation by NR, pre-reduced NR was used to reduce nitrite to NO[•]. By quantifying the amount of NO[•] released, the stoichiometry of NO[•] released per Moco was determined. For this purpose, NR2-Mo-heme fragment was used, rather than full-length enzyme and was directly reduced by addition of fresh dithionite solution. The excess of dithionite was subsequently removed by passing the protein through a PD-10 column. All protein handling was performed under the anaerobic bench and all solutions and instruments were made anaerobic.

A sample of the pre-reduced protein was placed in an anaerobic sealed cuvette and UV/visible spectrum was recorded (Fig. 26A unbroken trace). Likewise a control sample of NR2-Mo-heme that had assay buffer added instead of dithionite was recorded and showed an oxidized spectrum (Fig. 26A, dashed trace). Subsequently, four replicate samples of 400 pmol (heme-based concentration) pre-reduced NR2-Mo-heme, which was equivalent to 146 pmol Moco-containing protein (36.4% Form A saturation) were anaerobically injected into the NO-analyzer. A peak of NO[•] was generated and the area of the peak was determined (Fig. 26B). The negative control, oxidized sample did not produce a peak of NO[•] generation (Fig. 26C). The reproducibility of the area for the four reduced samples was high. An NO[•] standard curve (Appendix 3) was used to convert the area of the peaks to amount of NO[•] and on average 34.6 ± 1.5 pmol (Mean \pm SEM) NO[•] was generated per sample. If we assume that the mechanism of NO[•] generation by NR is similar to SO, then only the Mo (IV) state would be capable of donating an electron to nitrite for production of NO[•]. Considering that 400 pmol of fully reduced NR2-Mo-heme with 36.4% Moco saturation would contain a total of $(400 \text{ pmol} \times 2) \times 36.4\% = 291$ pmol electrons on Moco, then 145 pmol of those would be available for nitrite reduction. The result with 34.6 pmol NO[•] would mean that only about 25% of the reduced Moco actually produced NO[•].

A possible explanation for the low figure is that the enzyme was not fully reduced for the duration of the experiment. Immediately after the measurements, a UV/visible

spectrum was recorded for a 1:3 diluted sample of the pre-reduced enzyme and it was observed that it had lost its reduced state (Fig. 26A dotted trace). Pre-reduced NR-Mo-heme was extremely sensitive to re-oxidation, even under the strictest possible anaerobic conditions. Several repetitions of this experiment with variations on the method of pre-reduction were performed with similar results (data not shown).

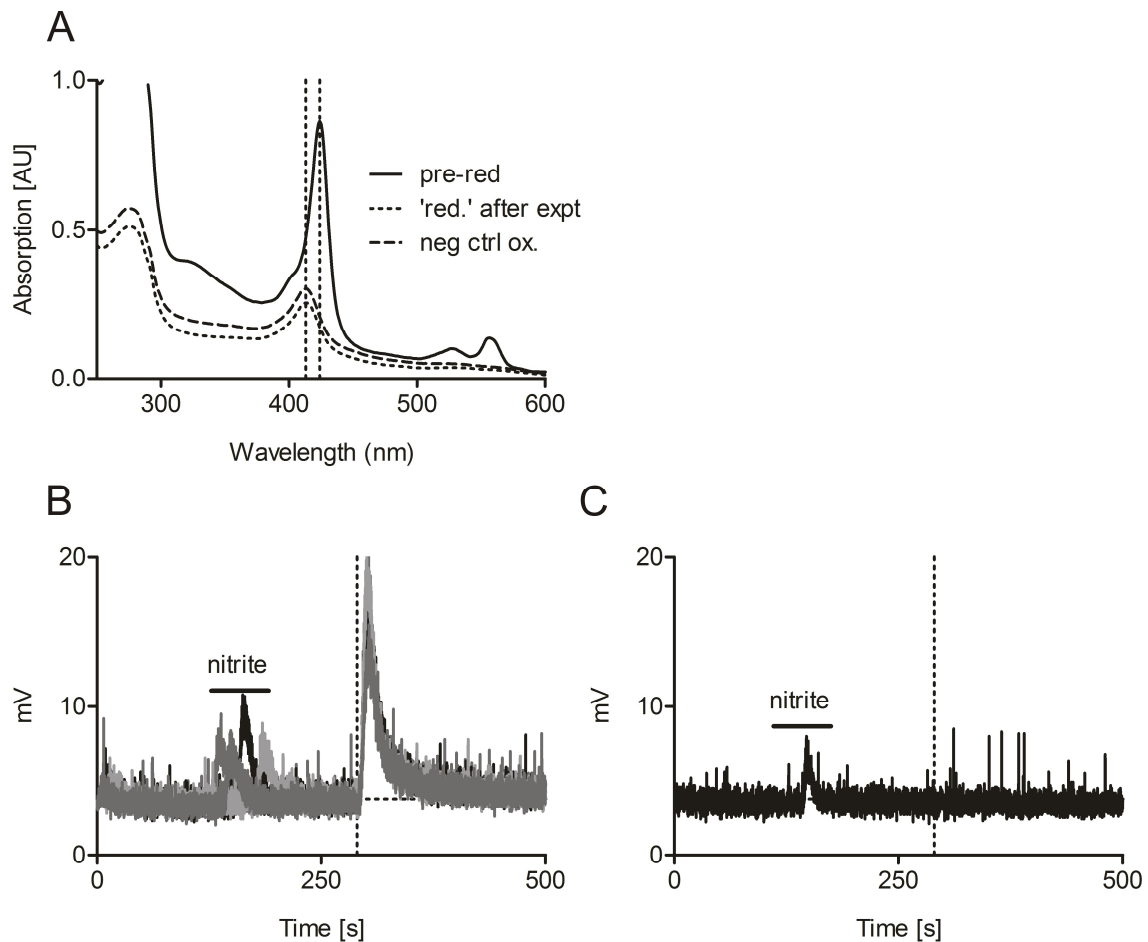


Figure 26 Stoichiometry of NO generation by pre-reduced NR2-Mo-heme. **A:** Spectrum confirming that the enzyme was pre-reduced immediately prior to the experiment (solid trace), 1:3 diluted enzyme after the experiment (dotted trace) showing that the enzyme was no longer reduced, The dashed trace shows a control sample of oxidized NR2-Mo-heme. **B:** Four replicate samples (overlaid) of 400 pmol pre-reduced NR2-Mo-heme with 400 μ M nitrite on the NO analyzer. The dotted line on the x-axis indicates the addition of enzyme. **C:** Oxidized NR2-Mo-heme control. Abbreviations: Pre-red, NR2-Mo-heme pre-reduced spectrum as measured at the outset of the experiment. 'red.' after expt, the pre-reduced NR2-Mo-heme spectrum immediately after (~30 min) measuring the four samples on the NO analyzer. Neg, ctrl ox., negative control sample of non-reduced enzyme

2.7 Regulation of NR by 14-3-3 proteins

2.7.1 Regulation of NR activity of NR1 and NR2

The method of regulation of nitrate reduction in NR2 by phosphorylation in the hinge 1 region and binding of 14-3-3 proteins to this phosphoserine and to an acidic N-terminal sequence is well characterized (Chi et al., 2015; Lambeck et al., 2012), while NR1 regulation by 14-3-3 proteins has not been studied to date. First, it was shown by mass spectrometry that NR1 can also be phosphorylated by the kinase CPK3 on a conserved serine in hinge 1 (pSer 537, Fig. 27A) (Mohn, 2016). Immunoblot analysis using hinge 1-phosphoserine specific antibodies (raised against the phosphorylated peptide of NR2-hinge 1) cross-reacted with the phosphorylated NR1 and could additionally confirm that it was phosphorylated (Fig. 27B). Following phosphorylation, it was next tested whether the MV:nitrate reduction activity of NR1-Mo-heme was affected by the phosphorylation. A set of kinetic series using phosphorylated or non-phosphorylated NR1-Mo-heme were compared and could confirm that no change in the kinetic parameters of K_M and k_{cat} were seen – as was known to also be the case for NR2 (Fig. 27C, D).

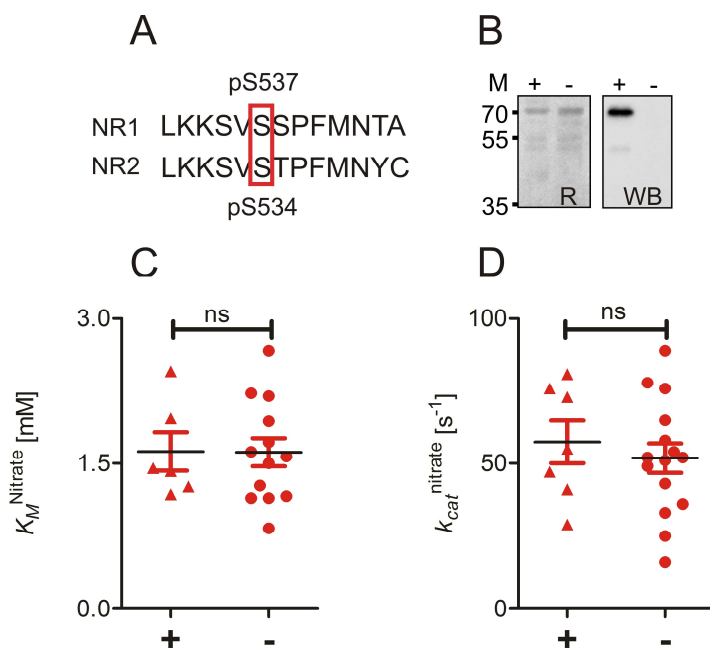


Figure 27: Phosphorylation of NR1-Mo-heme by CPK3 kinase and MV:nitrate activity measurement. A: immunoblot analysis of phosphorylated (+) vs non-phosphorylated (-) NR1-Mo-heme. R: ponceau red stained membrane, WB: anti phospho serine hinge 1 (of NR2) probed membrane. **B:** The phosphorylated conserved serine residue pSer 537 (highlighted by a red box) within the NR1-hinge 1 and compared with NR2-hinge 1. **C and D:** MV:nitrate activity series measured using multiple lots of phosphorylated and non-phosphorylated NR1-Mo-heme showed comparable kinetic parameters of K_M and k_{cat} . ns= non significant difference in an unpaired t-test.

Next, six *Arabidopsis* 14-3-3 isoforms were tested for inhibition of MV:nitrate activity of pNR1-Mo-heme (Fig. 28A). This system was seen in the past to closely model regulation in the full-length NR2 enzyme (Lambeck et al., 2012).

Inhibition of NR1-Mo-heme was seen for three isoforms, Chi, Omega Psi (Fig. 28, row B), and for the other three, Mu Epsilon Omicron, inhibition was not clearly present, (Fig. 28, row C). In each case the % inhibition was calculated as the residual activity in the presence of 14-3-3 compared to the activity of a control sample of pMoH1 without 14-3-3. For 14-3-3 isoform Chi, the results were pooled from three complete inhibition experiments. For Omega, the results of five inhibition experiments were pooled. For the other isoforms, triplicate measurements with a single batch of phosphorylated NR1-Mo-heme were performed. Likewise, inhibition experiments of pNR2-Mo-heme with three isoforms of 14-3-3 are plotted (Fig. 28, row D).

Overall, pNR1-Mo-heme was not well inhibited by the 14-3-3 isoforms tested (Table 7). Of the isoforms tested, isoform Omega was the best inhibitor ($IC_{50} = 62$ nM, $I_{Max} = 46\%$) with the quotient of I_{Max}/IC_{50} 0.75%/nM. The inhibitory parameters of 14-3-3 Omega were in fact similar to the values for p-NR2-Mo-heme measured here (Fig. 28D, Table 7) $IC_{50} = 68$ nM and $I_{Max} = 76\%$ yielding the quotient I_{Max}/IC_{50} 1.12%/nM and also comparable with the published values of K_i and I_{Max} for p-NR2-fl of 60 nM and 84% respectively (Lambeck et al., 2010). Maximal inhibition of NR2-Mo-heme was higher compared to NR1-Mo-heme.

Isoform 14-3-3 Mu has not been tested in the past for inhibition of pNR2-Mo-heme and could be shown here to be the best inhibitor tested with an inhibitory quotient of 4%/nM. In contrast, pNR1-Mo-heme was not consistently inhibited by 14-3-3 Mu. The non-linear regression curve delivered an ambiguous fit (Fig. 28C, Table 7).

In summary, 14-3-3 Omega inhibition of NR1 and NR2 appears similar, with a very similar IC_{50} of 62 and 68 nM respectively but with maximal inhibition level of about two-fold higher for NR2. 14-3-3 Mu is highly potent for inhibition of NR2-Mo-heme, but not for NR1-Mo-heme. Compared with the other tested (and/or published) isoforms for inhibition of NR2, Chi and Psi can far more poorly inhibit NR1-Mo-heme based on the IC_{50} which is about ten-fold higher for NR1-Mo-heme.

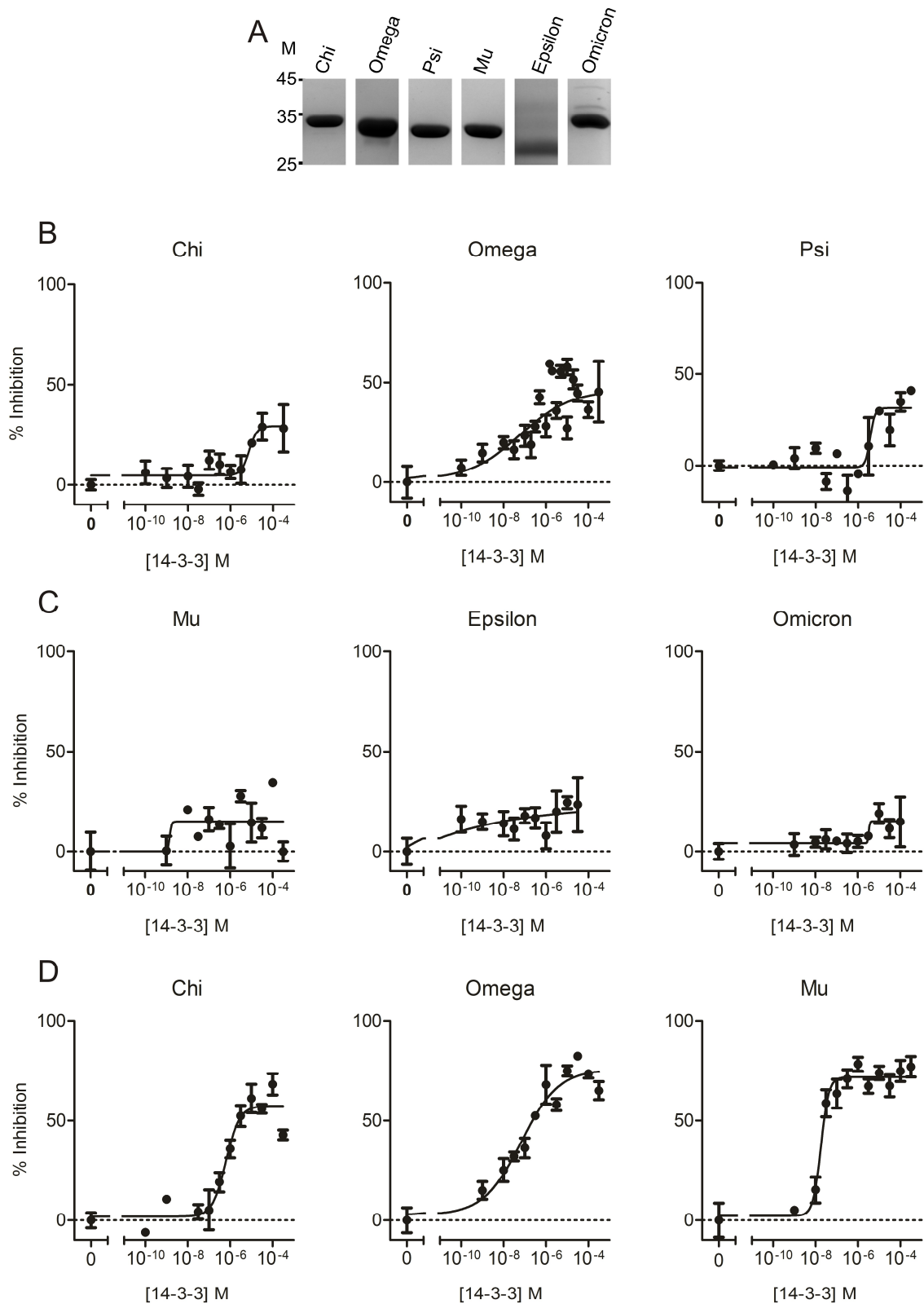


Figure 28: Inhibition of MV:NR activity by 14-3-3 isoforms. **A:** Coomassie blue stained SDS-PAGE of 6 isoforms of 14-3-3 used in inhibition experiments. **B, C** and **D:** Log of concentration of 14-3-3 [M] plotted against % MV:nitrate activity inhibition, compared with uninhibited phosphorylated NR-Mo-heme (0% inhibition). Data is fitted with the 'Log (inhibitor) vs response, variable slope' curve in GraphPad Prism. Rows B and C show pNR1-Mo-heme and six 14-3-3 isoforms (individually labeled). Row D shows phosphorylated NR2-Mo-heme with three 14-3-3 isoforms.

Table 7: NR1-Mo-heme and NR2-Mo-heme, 14-3-3 inhibition-kinetic parameters summarized (Fig. 28 and Lambeck et al., 2010). I_{Max} indicates the maximal inhibition level and IC_{50} , the concentration of inhibitor required to reach 50% inhibition. The quotient I_{Max}/IC_{50} gives an indication of the inhibitory efficiency of each 14-3-3 isoform. R^2 indicates goodness of fit of the non-linear regression to the data (Fig. 28). For NR1-Mo-heme and 14-3-3 -Mu and -Omicron, and -Epsilon the data could not be fit (n.d., not determined)

Phosphorylated NR1-Mo-heme					
	IC_{50} [nM]	I_{Max} [%]	R^2 [%]	I_{Max}/IC_{50} [%/nM]	Source
Chi (χ)	7478	29.24	31.39	0.004	This work
Omega (ω)	62	46.39	50.04	0.748	This work
Psi (ψ)	3742	31.53	62.11	0.008	This work
Mu (μ)	-	-	n.d.	-	This work
Epsilon (ϵ)	-	-	n.d.	-	This work
Omicron (\omicron)	-	-	n.d.	-	This work
Phosphorylated NR2-Mo-heme					
Chi (χ)	634	57.29	86.94	0.090	This work
Omega (ω)	68	75.87	88.61	1.116	This work
Psi (ψ)	310	70	-	0.225	Lambeck, 2010
Mu (μ)	18	71.92	91.37	3.995	This work
Epsilon (ϵ)	-	-	no inhibition	-	Lambeck, 2010

2.7.2 Regulation of nitrite reductase activity of NR1 and NR2

There are some indications in the literature that the post-translational regulation mechanism of NR proteins in the reduction of nitrite may also involve 14-3-3 proteins (Lea et al., 2004; Lillo et al., 2004; Rockel et al., 2002). In order to test this mode of regulation *in vitro*, the BV:nitrite determination method was used.

First, phosphorylated and non-phosphorylated NR1-Mo-heme and NR2-Mo-heme were compared for their BV:nitrite activity in a titration series of nitrite (Fig. 29A, B). Similarly to the MV:nitrate activity of phosphorylated NR enzyme, no difference in nitrite

reduction activity was observed. Next, the phosphorylated NR-Mo-heme was incubated with increasing concentrations of 14-3-3 isoform Omega, as this had been seen to inhibit NR1 and NR2 in nitrate reduction (Fig. 29C, D). No inhibitory effect was seen, which could be explained in two possible ways. Firstly, there may really be no inhibition of nitrite reduction by 14-3-3 isoform Omega, which is considered unlikely knowing the mechanism of nitrate reduction inhibition, which arrests domain movement and electron transfer between heme and Moco. Secondly, the artificial electron donor BV perhaps does not require the heme domain and rather delivers electrons directly to the Moco domain.

To investigate the latter possibility, two experiments were performed. Heme-free NR2-Mo-heme H600A mutant (Lambeck et al., 2012), which lacked one heme-coordinating histidine of NR2 and thus contained very low amounts of heme cofactor and in addition, the Mo-domain fragment of NR1 and NR2 (section 2.2.3) were used for BV:nitrite activity measurement (Fig. 29E, F). In all cases nitrite reduction activity was observed, confirming that BV donates electrons directly to the Moco domain and does not require the heme. This contrasts with MV, which donates electrons through the heme domain to the Moco (Lambeck et al., 2012). Therefore, 14-3-3 mediated regulation of nitrite reduction cannot be tested using the BV:nitrite method.

The kinetic parameters for nitrite reduction using the Mo-domain fragments of NR1 and NR2 and Heme-free H600A NR2-Mo-heme are summarized in Table 8. Compared with the kinetic parameters for BV:nitrite activity of the NR-Mo-heme fragments, the turnover numbers using the Mo-domain fragments were found to be higher; compare 140 s^{-1} for NR1-Mo with $20 \pm 5 \text{ s}^{-1}$ for NR1-Mo-heme and 6.0 s^{-1} for NR2-Mo with $1.8 \pm 0.3 \text{ s}^{-1}$ for NR2-Mo-heme. It is likely that even though BV donates electrons directly to the Moco-domain bypassing the heme that the heme cofactor would interfere in this process. In the absence of the heme domain both NR1 and NR2 had higher k_{cat} values.

Of the two isoforms, it could be confirmed that NR1 is the more efficient enzyme for nitrite reduction with a 22-fold higher catalytic efficiency (Table 8). Heme-free (H600A) mutant NR2-Mo-heme protein had a k_{cat} similar to heme-containing NR2-Mo-heme (compare Table 5 and Table 8). The K_M^{nitrite} for NR2-Mo and Heme-free NR2-Mo-heme was about twice the BV:nitrite K_M value determined for NR2-Mo-heme (on average), however it was within the range of variations for individual measurements (Fig. 23B).

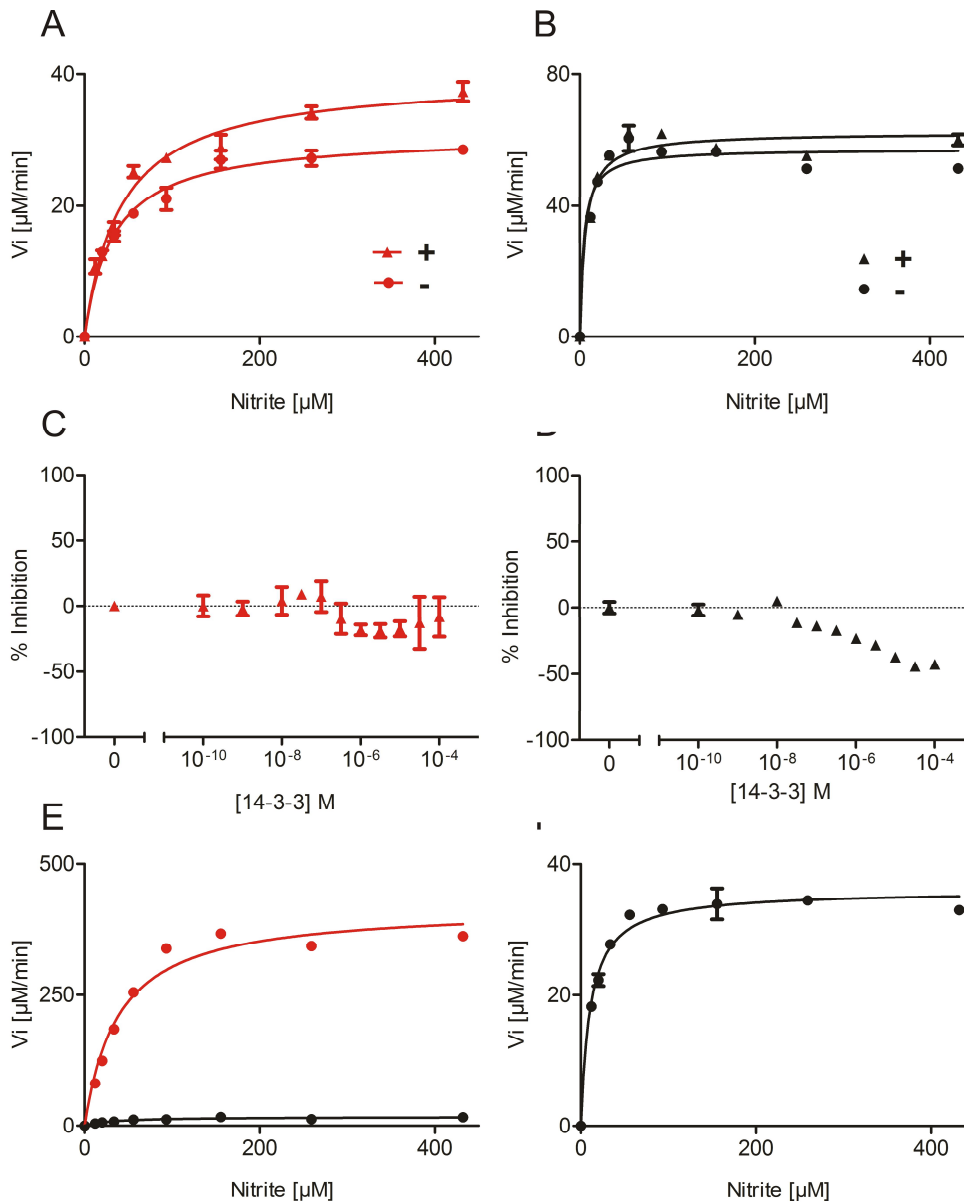


Figure 29: Test of 14-3-3 inhibition of BV:nitrite activity. **A, B:** Phosphorylated (+) and non-phosphorylated (-) NR1-Mo-heme (red) and NR2-Mo-heme (black) were compared for activity. **C, D:** phosphorylated NR1-Mo-heme (red) and NR2-Mo-heme (black) incubated with multiple concentrations of 14-3-3 Omega. Inhibition was not observed. **E:** 50 nM NR1-Mo domain (red) or 50 nM NR2-Mo-domain (black) BV:nitrite activity. **F:** 0.5 μM NR2-Mo-heme H600A (heme-free) used for BV:nitrite activity determination.

Table 8: Kinetic parameters for NR1- and NR2-Mo-domain and NR2-H600A heme free mutant.

	K_M^{nitrite} [μM]	$k_{\text{cat}}^{\text{nitrite}}$ [s^{-1}]	Catalytic efficiency [$k_{\text{cat}}/K_M \text{ s}^{-1}\text{mM}^{-1}$]
NR1-Mo	38.4 ± 4.0	140	3645
NR2-Mo	35.6 ± 5.6	6.0	168
NR2-Mo-heme (H600A)	36 ± 0.6	1.2	33

2.8 Structure model of NR

Many attempts to determine the crystal structure of NR have so far remained unfruitful. It is widely accepted that the flexible N-terminal domain as well as the two flexible linkers hinge 1 and hinge 2 allow for a broad range of conformations that make crystallization difficult. In this work, an attempt was made to crystallize NR1-Mo-heme but the crystals obtained were from a contaminated protein *E. coli* catalase (pdb entry 1p81).

An alternative to traditional crystallization is to perform cryo-electron microscopy (cryo-EM) in order to obtain the molecular structure of a protein. In cooperation with Professor Elmar Behrmann at University of Cologne/ Caesar Bonn cryo-EM was therefore performed for full-length NR2. The thawed protein was subjected to SEC immediately before cryo-EM (Fig. 30A). The concentration of the NR2 after SEC was determined to be 0.696 mg/mL by absorption at 280 nm and the ϵ_{280} 161,660 M⁻¹cm⁻¹. Moco saturation was determined to be 27%.

In the first screening step, the required dilution of protein to give, distinguishable particles by 2% uranyl acetate negative staining on copper-carbon grids was determined to be 0.01 µg/mL. Using this concentration, higher grade copper/carbon grids were prepared and imaged by cryo-EM (images prepared and evaluated by Christoph Klatt, Cesar, Bonn). An example image is shown (Fig. 30B, C).

Using the image analysis software 'Iterative stable alignment and clustering' ISAC (Yang et al., 2012), the light-colored particles were identified and sorted into groups consisting of at least 50-100 similar particles (representing a view of a certain NR conformation). In total 64,000 particles were imaged and 40,000 of those could be grouped into classes. After manual sorting of the classes and removal of non-particles, 11,000 particles remained that were in class groups. This data was then input into the software Viper (Penczek and Asturias, 2014) and an initial 3D model for NR2 was generated (Fig. 30D, E space filling views). For comparison a model of NR2-Mo-domain was generated using the software Swiss Model (Waterhouse et al., 2018) based on the high level of identity (45%) between *P. angusta* and *AtNR2* Moco-domains (Fig. 30D, E ribbon views). The cryo-EM model of NR2 is smaller than the model based on *P.angusta* Moco domain (Fischer et al., 2005), even though the full-

length protein would certainly be much larger by comprising the additional heme and FAD domains (Fig. 2, Fig. 3).

In the cryo-EM model, the dimeric state of NR2 can be recognized, as well as modular lobes, probably representing the domains. It would appear that, only the central portion of the protein is represented by the cryo-EM model (i.e. the Moco and dimerization domain), and that because of the flexible linkers attaching the heme and FAD/NADH domains, a defined structure model for these parts was not found. However, there is a 'detached' lobe of electron density that probably represents the core of either the heme- or the FAD-domain. Further attempts at cryo-EM are to be performed with pNR2 in a complex with 14-3-3 in order to stabilize the conformation of the protein.

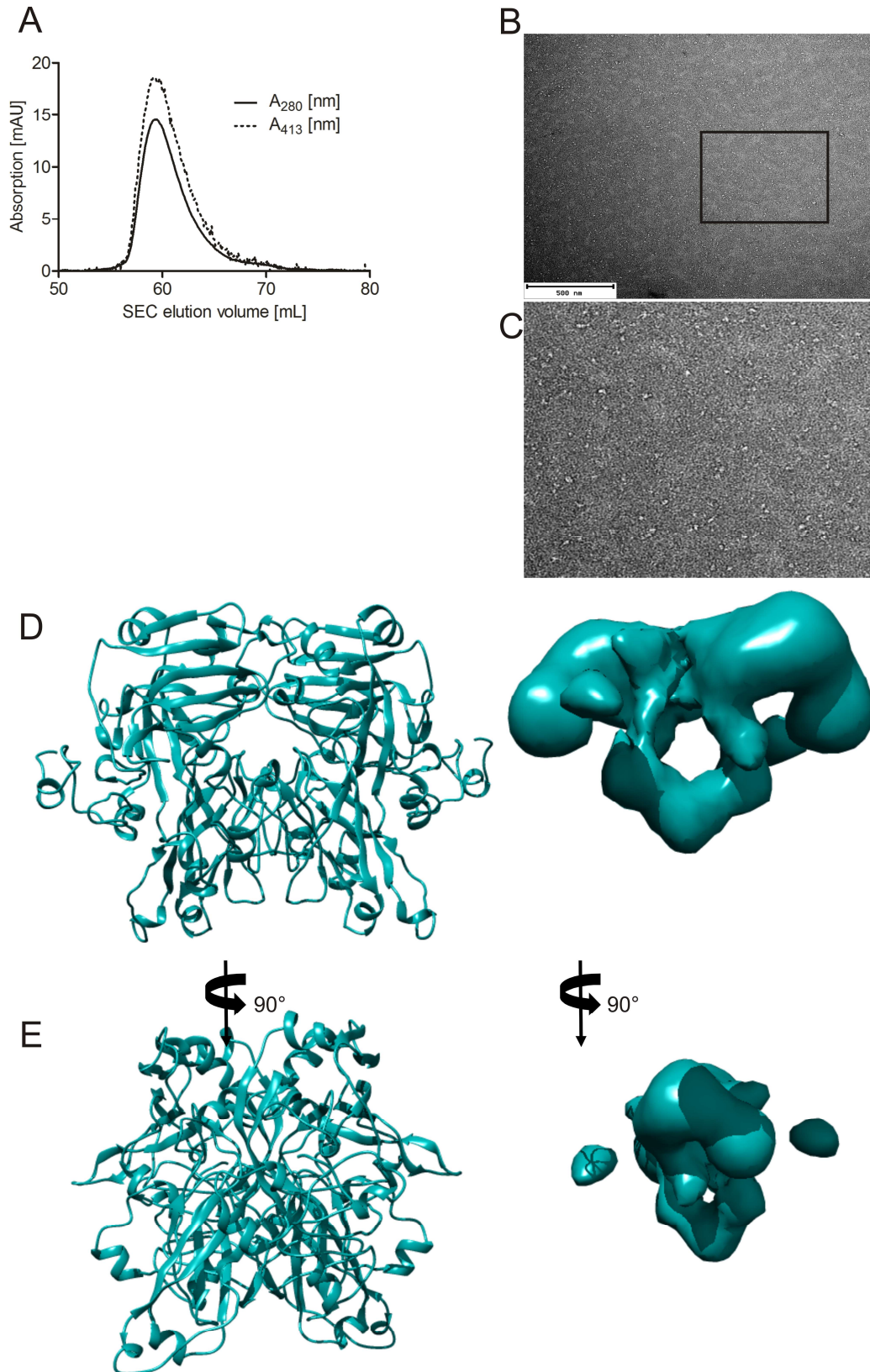


Figure 30: Cryo-EM for determination of molecular structure of NR2. **A:** SEC traces of pure NR2-fl immediately before cryo-EM showing absorption at 280 nm and 413 nm. **B and C:** Example image and zoomed part of image of uranyl acetate negatively stained copper-carbon grid with NR2 seen as light-coloured particles (unstained areas). **D:** Model of NR2 generated using Swiss Model based on *Pichia angusta* NR-Mo-domain (ribbon view) (PDB 2bih) shown next to space filling model of NR2 generated using Viper software from cryo-EM data. **E:** Both models turned 90° on the y-axis. Images D and E were generated using Chimera (Pettersen et al., 2004). Note: The orientation of the cryo-EM model relative to the calculated model is speculative.

3 Discussion

The discovery of a second physiological function for NR, that of NO[•] generation in addition to the canonical role in nitrate assimilation, led to the question whether multiple isoforms of NR in a given plant species might play different roles in these two functions. This question has not been addressed before using a fully defined *in vitro* system with recombinant purified NR protein of two isoforms, from a single plant species as is described in this work. Some studies have been performed, comparing the NR isoforms in soybean plants (Dean and Harper, 1986, 1988; Harper, 1981; Jolly et al., 1976; Klepper, 1979; Klepper, 1990), however the use of plant extracts for purification of protein, can lead to artefacts caused by impurities in the extract.

For the work described in this thesis, the plant species *A. thaliana* was chosen, as it is a frequently studied model plant system in which, the genome has been completely sequenced (The *Arabidopsis* Genome, 2000). This knowledge allows one to be certain that *Arabidopsis* contains 'only' two NR genes in contrast with several other plant species that are known to contain three or four genes encoding for potential NR enzymes (section 1.6.5). In addition, mutant plants of *Arabidopsis* are available with knock-outs of almost all genes (individually), facilitating many studies of individual gene functions on the whole plant level, thus providing some background information for the studies that were performed here using purified protein. Finally, some previous studies exist using recombinantly expressed *AtNR2* that could serve as a reference for the nitrate reduction activity and regulation of this isoform (Chi et al., 2015; Lambeck et al., 2010; Lambeck et al., 2012).

3.1 Recombinant NR expression

The primary aim of this project, was to obtain recombinant pure protein of isoform 1 and isoform 2 of *A. thaliana* NR and to compare the two enzymes in their two functional roles in nitrate and nitrite reduction. Although recombinant expression of full-length *AtNR2* has been reported in the past in the host *P. pastoris* (Su et al., 1996), it has been described as being difficult to achieve (Campbell, 1996). It is likely, that the incorporation of three cofactors (Moco, heme and FAD) into NR during biogenesis and folding, has a critical impact the stability of the protein. Incorrectly folded proteins can cause aggregation and are targeted for degradation in the host cells (Wu et al., 2012).

Interestingly Su et al., 1996 reported expression of several mutant variants of NR, each with a single serine residue mutated to an alanine or aspartate and although these varied by only a single point mutation, five of fourteen mutant proteins could not be expressed in the host strain GS115 (Su et al., 1996). The authors attributed this to a high protease sensitivity of the mutated proteins. It demonstrated, however, the variability of expression result caused by a single amino acid residue substitution in an otherwise identical recombinant protein expression system. This finding is interesting in light of the difficulties encountered in this work in expressing full-length NR1 in comparison to NR2 even though the two proteins are 78% identical on the primary sequence level.

In a subsequent publication (Su et al., 1997), the *AtNR2* cDNA was modified with an N-terminal His tag and affinity purified. A low level of recovery was reported at 180 µg of pure NR from 500 mL of *Pichia* shake-flask culture. The Moco-saturation of the protein was not recorded. The result described in this work for expression of NR2-fl compares favorably with Su et al., 1997 as 0.5 mg of Moco saturated NR2-fl was obtained per liter culture volume (results 2.1.5). Unfortunately, however, the yield of recombinantly expressed and purified NR1-fl was much lower with 11.5 µg/L (results 2.1.4).

In future, it may be beneficial to switch the expression of both NR1 and NR2 in *Pichia* to a fermenter system, which was reported for NR2 (Skipper et al., 2001). The authors report expression of up to 20 mg/L of full-length NR2 and the purification of 2 mg protein/100 g wet cells. Moco saturation was on average 18% for four batches of protein (Skipper et al., 2001). The Moco saturation of the NR2-preparations in this work ranged from 23-35%, and were thus somewhat higher.

While many variations of shake-flask culture for the expression of NR1-fl were attempted in this work, fermenter culture was not yet tried and clearly offers a promising way forward. It is widely accepted with the *Pichia* expression system, that the original attainment of expression at any level is the most important step and subsequent optimization of the expression protocol usually leads to yield improvement (Cregg et al., 2009; Looser et al., 2015). Fermenter culture has the advantages of much higher cell density in a smaller volume – thus offering a scale-up in cell bulk harvested – but also provides optimized culture conditions by continuous supply of fresh nutrients, methanol and oxygen to the expressing cells (Cereghino et al., 2002). Production of

up to 350 – 450 g/L wet cells can be achieved according to the Invitrogen ‘*Pichia* fermentation process guidelines’, which would be about 10-fold higher than cell-bulk harvested from shake flask culture.

At the beginning, the natural gene sequence of *AtNR1* was suboptimal for expression in yeast (see Appendix 1). Codon optimization of the gene sequence however, did not lead to greatly improved NR1 expression levels (results 2.1.2 – 2.1.4). This result was disappointing based on the successes that have been described using codon optimized gene sequences for recombinant protein expression (Kwon et al., 2016; Sjöhamn et al., 2011). There was however, some evidence that the codon optimized sequence resulted in less truncated/degraded protein, compared with protein expressed from the natural DNA sequence (compare Fig. 8 and Fig. 12). It was also seen in the comparison of two different yeast host strains, that *Pichia* GS115 appeared to express the recombinant protein at a higher level compared with KM71 (compare Fig. 9 and Fig. 10). Therefore combining these improvements with fermenter culture should lead to improvement of NR1 expression in future.

3.2 Functional domain fragments of NR

In the absence of a successful expression and purification protocol for the production of NR1-fl, functional domain fragments of NR were used for various studies of partial activities of NR. In addition a novel re-constitution of full-length NR activity using the Mo-heme domain fragment and the FAD-domain fragment was established. Therefore, NR1-Mo-heme was expressed in the *E. coli* strain TP1004, which similar to the earlier developed TP1000 strain, contains a mutation in the *mobA* operon and therefore cannot produce the bacterial-dinucleotide form of the Moco and instead overproduces the eukaryotic mono-nucleotide Moco (Palmer et al., 1996). This strain has proven useful in the past for producing eukaryotic Moco proteins such as sulfite oxidase (Wang et al., 2015).

Interestingly, in this system it can be seen that like in *Pichia*, the NR2-Mo-heme fragment is more abundantly expressed compared with NR1-Mo-heme. The expression protocol had to be optimized for NR1-Mo-heme (Mohn, 2016) but even the optimized protocol, resulted in far lower recoveries of the desired protein. Recovery of NR1-Mo-heme was only ~30 µg per liter of *E. coli* culture whereas it was 33-fold higher for NR2-Mo-heme, at about ~1 mg per liter. This could partially be explained by the

shorter culture duration (20 h) for NR1-Mo-heme, which allowed less time for cell biomass accumulation, and for lower average levels of Moco-incorporation. However, it also appeared to be an intrinsic property of the NR1-Mo-heme protein that it was far less stable than NR2-Mo-heme. It was severely degraded in *E. coli* cultures following longer times of expression culture or at higher temperatures (data not shown). Even using the optimized expression protocol, it was required to perform SEC to separate the degraded fragments, which was obviously detrimental to recovery. Although NR2-Mo-heme was also subject to degradation, the degraded fragments tended to form homo-dimers with a large size difference compared to non-degraded dimers, making separation by SEC more feasible.

Our results are not surprising, given that instability of the NR – in particular proteolytic cleavage in the hinge1 region – has frequently been reported in the literature (Mertens et al., 2000; Su et al., 1996). Early studies took advantage of this proteolytic instability to isolate the domain fragments of NR and to prove that they were linearly arranged in the primary polypeptide chain and to establish that the domain fragments retained the respective partial activities of full-length enzyme (described in 1.6.3) (Kubo et al., 1988; Shiraishi et al., 1991; Solomonson et al., 1987). In particular it was established that a conserved trypsin cleavage site in the hinge 1 and a V8-protease (from *Staphylococcus aureus*) site in the hinge 2 were naturally present (Shiraishi et al., 1991).

In one study, the ‘Mo-reductase’ (MoR) fragment of spinach and corn NR was expressed (Mertens et al., 2000) consisting of the FAD and heme domains (with the intervening hinge 2). Additionally, the so called MoR+ fragment was expressed which contained the FAD, heme, hinge 1 and dimerization region of NR (Fig. 2). The MoR+ fragment was especially labile in the hinge 1 region (Mertens et al., 2000). The results presented in this work are in good agreement with this finding, since it can be seen in the SEC profile that the smaller – later eluting fractions of NR1-Mo-heme have a lower heme absorption relative to the total protein absorption at $A_{280\text{nm}}$ suggesting that the heme domain has been cleaved. Adding protease inhibitor did not prevent this hinge 1 cut – probably because it had already taken place during growth and expression in the *E. coli*. It also cannot prevent the dimeric interaction between a full-length NR1-Mo-heme and a degraded fragment, which resulted in an additional SEC peak relative to NR2-Mo-heme (Peak at ~75 mL in Fig. 14C) and which was excluded from further analysis.

To summarize, NR1-Mo-heme could be reliably produced albeit in small amounts and at a low concentration, however, by expressing and comparing multiple (n=23) batches of this protein fragment, a large body of activity data could be generated for comparison with NR2-Mo-heme.

3.2.1 Nitrate reduction activity of NR-Mo-heme fragments

The first important finding in this work, was that NR1 is an active NR protein. Similarly to NR2-Mo-heme NR1-Mo-heme displayed MV:nitrate activity and allowed establishment for the first time of the steady-state kinetic parameters of nitrate reduction for NR1-Mo-heme, which, in the direct comparison with the catalytic efficiency of NR2-Mo-heme was about six-fold less efficient. This means that only part of the lower NR activity observed in shoot extract of *nia2* mutant *Arabidopsis* plants (only 10% of wild type level) (Wilkinson and Crawford, 1991) may be attributed to lower expression of *NIA1* in shoots compared to *NIA2* in shoots (Fig. 4). These observations in the plant can now also be explained by the fact NR1 has a lower intrinsic catalytic efficiency compared to NR2. In addition, it can be seen that the lower catalytic efficiency can, for the most part, be attributed to the larger K_M^{nitrate} of NR1, since the $k_{\text{cat}}^{\text{nitrate}}$ for the two isoforms does not differ much (NR1-Mo-heme $51 \pm 4 \text{ s}^{-1}$ vs NR2-Mo-heme $69 \pm 9 \text{ s}^{-1}$). This would suggest that of the two isoforms, NR2-Mo-heme has a higher affinity for nitrate and fosters the hypothesis that some differing residues in the substrate recruitment funnel between the two proteins might cause the differing affinities.

The NR1 and NR2 structures were therefore modeled using SWISS-MODEL (Waterhouse et al., 2018) based on the crystal structure of *Pichia angusta* NR Moco (Fischer et al., 2005) and visualized using PyMOL (DeLano, 2002) (Fig. 28). It can be seen, however, that the residues of the funnel were highly conserved between NR1 and NR2 and therefore the models overlay almost perfectly. The only difference that can be seen, is adjacent to the entrance of the substrate binding funnel: here an isoleucine is present in NR1, while the corresponding residue in NR2 is a lysine. This lysine residue can be seen in Fig. 31 protruding from the surface with its positively charged side-chain. This additional positive charge may play a role in binding to the negatively charged substrate nitrate and thus might account for the higher affinity of NR2 for this substrate. Although other, as yet unknown structural differences between NR1 and NR2 are possible, this residue offers a possible explanation for the observed

difference in nitrate affinity of NR1 and NR2. Site directed mutagenesis might be used to probe this proposal in future studies.

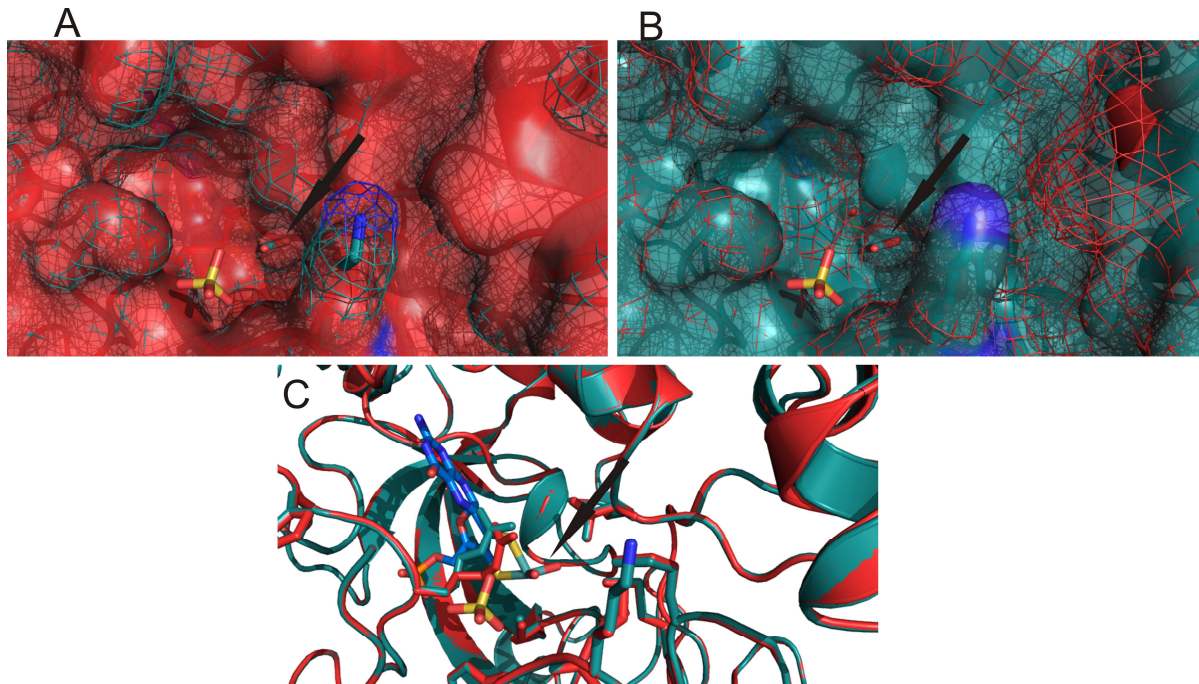


Figure 31: Substrate binding funnel of NR1 and NR2 compared in models based on *Pichia angusta* NR Moco crystal structure PDB 2bih (Fischer et al., 2005) generated using Swiss-Model (Waterhouse et al., 2018). Three identical views of the substrate recruitment funnel of NR1 and NR2. A black arrow points into the active site at the Moco. Model of NR1 (red), model of NR2 (teal). Moco and sulfate derived from the crystal structure of *Pichia* NR are shown in ball and stick with blue – nitrogen, red – oxygen, yellow – sulfur. **A:** NR1 model is shown in surface view and NR2 mesh view. **B:** NR2 is shown in surface view with NR1 mesh view. **C:** NR1 and NR2 models shown as cartoon depiction.

3.2.2 Nitrite reduction activity of NR-Mo-heme fragments

The comparison of NR1-Mo-heme and NR2-Mo-heme nitrite reductase activities was of critical importance in this study. At the beginning, an *in vitro* method for measuring steady-state kinetic parameters of nitrite \rightarrow NO[•] conversion was not available. The Griess test is a standard method for concentration determination of nitrite in solution but was very labor intensive to apply it to measurement of nitrite consumption by NR1-Mo-heme and NR2-Mo-heme. Results obtained in initial tests of this method were inconclusive (data not shown).

A continuous steady-state kinetic measurement offers a more convenient system to trace nitrite consumption. It was observed that the dye benzyl viologen, which is related to methyl viologen – differing only by the substituent of the pyridyl ring system (Fig. 32)

– displays the properties required for such a measurement. Like MV, it has a redox couple with vastly differing absorption at 595 nm between the BV^{2+} state (uncolored) and the single electron reduced $BV^{+\bullet}$ reduced state (high absorption at 595 nm) (Fig. 32). Most importantly however, $BV^{+\bullet}$ is stable in the presence of nitrite (Fig. 22C) – especially at the measurement buffer pH and the concentration of nitrite that was required (pH 7.5, 0-500 μ M nitrite). To protect the dithionite-reduced $BV^{+\bullet}$ radical, the experiments (analogous to the measurements with MV) had to be performed under anaerobic conditions. Using the BV:nitrite method, the consumption of reduced electron donor could be continuously followed stoichiometrically with nitrite consumption. To our knowledge, this method represents the first continuous measurement system for nitrite reduction reported and it may be useful for measuring the nitrite \rightarrow NO^{\bullet} activity of other Moco enzymes in future.

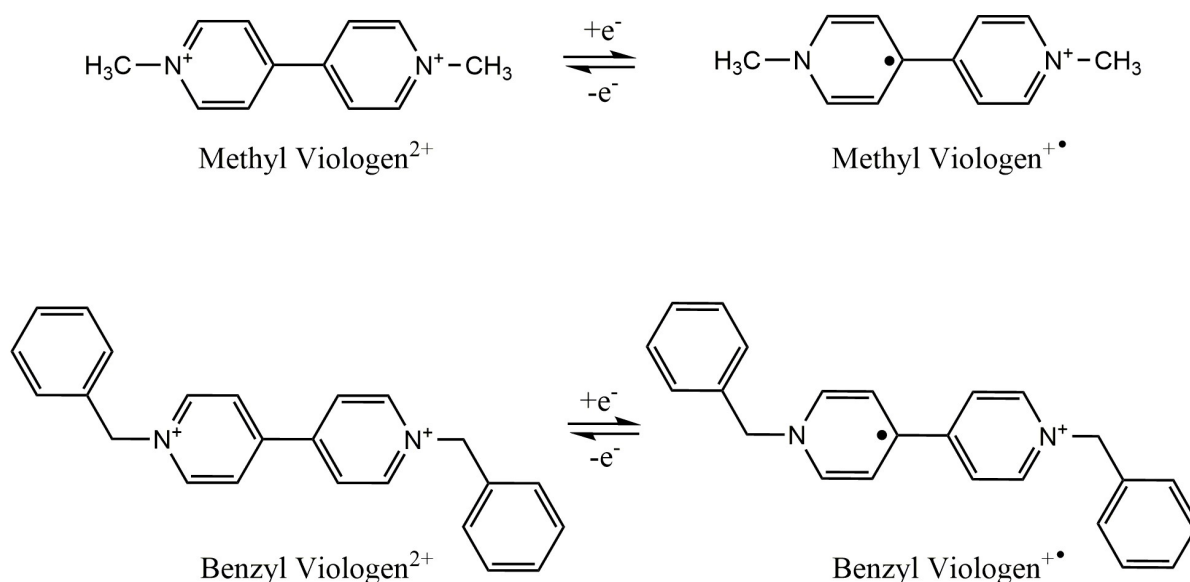


Figure 32: Chemical structures of Methyl viologen (MV) and benzyl viologen (BV) each shown with its single electron reduced radical

In the past, only NO^{\bullet} -evolution by whole plants, or by NR purified from plant extracts (Planchet et al., 2005; Rockel et al., 2002), or NO^{\bullet} visualization by fluorescent dyes in wild-type or *nia1/nia2* mutant plants has been performed (Bright et al., 2006; Lozano-Juste and Leon, 2010; Xie et al., 2013). In addition a measurement of nitrite consumption using MV has been described in the literature, which, given the non-enzymatic reactivity of reduced MV with nitrite (Fig. 22A), appears unsuitable to differentiate between enzymatic and non-enzymatic nitrite concentration dependent activity (Dean and Harper, 1988).

To establish the method for determination of BV:nitrite activity the first step was to determine the pH optimum for nitrite reduction by NR1-Mo-heme and NR2-Mo-heme. Interestingly, the optimum here was at pH 7.5 for both enzyme isoforms (Fig. 22E, F). It had been seen in the determination of MV:nitrate activity was highest at pH 7.0. This result is consistent with the nitrate reduction-pH optima for many characterized NR's of species such as spinach (Barber and Notton, 1990) and *Arabidopsis* (this work, (Su et al., 1997)), however it is, on the other hand, not a very large difference between the pH optima for the two reactions. In fact, pH optima for purified corn and spinach NR (nitrate reduction) have also been reported at pH 7.5 (Campbell and Smarrelli, 1978). It may be that the profile of the pH optima-curves is an addition important factor. NR2-Mo-heme displayed a broad optimum for nitrate reduction centering at pH 7.0 (Lambeck, 2009), while its optimum for nitrite reduction was narrow, at pH 7.5 (Fig. 22F). In contrast, NR1-Mo-heme had a narrow optimum for nitrate reduction at pH 7.0 but a broad optimum for nitrite reduction centering at pH 7.5 (Figs 18A and 22E). For NR1, high activity for nitrite reduction was seen at pH 7.9 contrasting with hardly any nitrate reduction activity at the same pH. Modulations of NR activity correlating with pH changes have been reported (Kaiser and Brendle-Behnisch, 1991; Kaiser et al., 2002). For example it has been shown that treatment of leaf discs with alkaline pH lowers NR activity (Kaiser and Brendlebehnisch, 1995).

Therefore, it would appear that a slight shift to a more alkaline pH may play a role in tuning NR activity toward nitrite reduction, perhaps more by NR1? This is however, not consistent with observations of increased NO emissions from plants under conditions in which a more acidic pH would be observed in the cytosol, for example under anoxia (Felle, 2005) in which case increased NO production was reported (Planchet et al., 2005; Rockel et al., 2002). However, spatially localized pH changes within the cytosol are possible (Pittman, 2012) and may represent the pH changes required to modulate NR activity. Other enzymes are known to be modulated by pH changes in the cytosol. This is the case for example for the enzyme phosphoenol pyruvate carboxylase that is activated by phosphorylation under conditions of increased pH in the cytosol (Giglioli-Guivarc'h et al., 1996). The plant cytosolic pH is maintained homeostatically at pH 7.2 – pH 7.5 (Pittman, 2012) – and thus spans the range that would be required for efficient nitrate or nitrite reduction.

By measuring its BV:nitrite activity, it could be established that NR1-Mo-heme has an approximately four-fold higher catalytic efficiency for nitrite reduction compared to NR2-Mo-heme (Table 5). Taken together with the catalytic efficiency for nitrate reduction for both isoforms and the pH-profiles observed seems to point toward NR1-Mo-heme being a nitrite rather than a nitrate reductase enzyme.

The nitrite reductase activity of the isolated NR1 and NR2 Mo-domains was also measured in this study and proved that BV donates its electrons directly to the Moco domain in contrast to MV which donates them to the heme domain (Fig. 2, results section 2.7.2 (Lambeck et al., 2012)). Interestingly, the turnover number for nitrite with this method was much larger than the $k_{cat}^{nitrite}$ determined for the NR-Mo-heme fragments (compare Table 5 and Table 8), however NR1 had a higher k_{cat} than NR2 in both cases. The higher turnover number for the Mo-domains implies that the presence of the heme domain interferes in electron donation by BV to Moco. It is known that the heme domain undergoes movement relative to the Moco domain in the course of catalytic turnover (Barbier and Campbell, 2005; Feng et al., 2002), and therefore there is likely a docking site on the Moco domain at which the heme interacts in order to deliver electrons. BV most likely delivers electrons at this same site and is thus in competition with the heme domain when it is present in the Mo-heme protein fragment. A similar increased $k_{cat}^{nitrite}$ is observed for human SO when the Moco domain is compared with the full-length (Moco and heme domain) protein (Bender, 2017). The SO system is not completely comparable however, because the Moco domain of SO accepts electrons from the heme and thus competes with nitrite for reducing equivalents. In NR, the heme donates electrons to Moco.

Importantly, the $K_M^{nitrite}$ determined for both NR isoforms (BV:nitrite method) is very low at 36 μM (NR1-Mo-heme) and 14 μM (NR2-Mo-heme) and is within a range that is physiologically relevant within the plant cell cytosol. Rockel et al, 2002, determined a $K_M^{nitrite}$ of 100 μM using their commercial purified maize NR (which would be a pool of three maize NR isoforms). They measured cytosolic nitrite concentrations at about 10 μM and thus concluded that nitrite reduction could only occur in cases in which a spike in nitrite concentration occurs (Rockel et al., 2002). Yamasaki and Sakihama used a similar purified maize NR and estimated the $K_M^{nitrite}$ at about 300 μM (Yamasaki and Sakihama, 2000). The $K_M^{nitrite}$ values measured in this work help to explain the observed nitrite to NO^* reduction that occurs in a large number of physiological settings,

and the basal NO[•] release by many/all plant species that has been reported (Wildt et al., 1997). Up to now it has been difficult to reconcile the observed NR/nitrite dependent-NO[•] release by plants in the context of the K_M^{nitrite} values reported and cytosolic nitrite concentration. The parameters determined here fit much better to a scheme in which NR can function as NO synthase.

3.2.3 A comparison of NR isoforms from *Arabidopsis* and Soybean

In light of the large K_M^{nitrate} of *AtNR1* it is interesting to compare *AtNR1* with soybean cNR1. Some differences and some similarities can be seen: Both have a high K_M^{nitrate} and both may be considered to be constitutively expressed (Cheng et al., 1991; Robin et al., 1985) although *AtNR1* is additionally highly nitrate inducible (Konishi and Yanagisawa, 2011a). Soybean cNR1 prefers the substrate NADPH while *AtNR1* can only function using NADH (Mohn et al. 2019). For nitrate reduction, cNR1 has a pH optimum of 6.5 compared to 7.0 for *AtNR1*.

For nitrite reduction, cNR1 has an optimal pH of 6.75 (Dean and Harper, 1988) and a K_M^{nitrite} of 0.49 mM (ten-fold lower than the K_M^{nitrate}). *AtNR1* has an optimal pH of 7.5 and K_M^{nitrite} (BV:nitrite method) of 36 μM (~60- fold lower than the K_M^{nitrate}).

Finally, mutant soybean plants that lack cNR1 cannot evolve NO[•] (Dean and Harper, 1988). There is also strong evidence that links *AtNR1* to NO[•] generation. For example, the guard cells of *nia1* plants can no longer close in response to ABA signaling or transfer from light into darkness (Bright et al., 2006; Ribeiro et al., 2009; Wilson et al., 2008) which are both responses to NO[•] signaling. The kinetic parameters for nitrite reduction that have been found in this work prove that due to its intrinsic catalytic properties, NR1 is the key enzyme producing NO in *Arabidopsis*.

3.3 Reconstitution of full-length NR activity

In the absence of full-length NR (isoform 1), full-length NR activity was reconstituted with domain fragments. For this, the NR-Mo-heme domain fragments were combined with the respective NR-FAD fragments in an attempt to re-establish the natural electron transport chain of the enzyme. Expression of the FAD domains of NR from *A. thaliana* has not been reported before. By using a protocol similar to that described for corn or spinach NR-FAD, both isoforms of *AtNR-FAD* could be successfully expressed and purified (Hyde and Campbell, 1990; Quinn et al., 1996) (Fig. 15).

It has been reported in the past that both the hinge 1 between the Moco- and heme-domain (Lambeck et al., 2012) and also the hinge 2 between the heme and FAD domain is essential for electron transport within NR (Skipper et al., 2001). In contrast to this, Pollock et al., 2002 could show that activity of NR was re-constituted from the three separately expressed domains of spinach NR *in vitro* implying that neither hinge is required (Pollock et al., 2002).

The system of re-constitution employed in this work, used an NR fragment with the hinge 1 intact (Mo-heme domain) but with the hinge 2 disrupted. Electron transfer through the NR could be successfully shown using the physiological electron donor NADH to reduce nitrate (Fig. 19). Pollock et al. determined a k_{cat} for NADH:nitrate reduction of 0.2 s^{-1} using a 1:1:1 stoichiometry of the three cofactor containing domains. At a stoichiometry of 1:1 for the measurements made here (as shown in Fig. 19A) only very little activity was recorded, which did not allow for determination of kinetic parameters. Therefore, the FAD-fragment was added in excess such that NR activity could be quantified, hereby it was seen that activity was dependent on the concentration of FAD added fragment.

By increasing the concentrations of NR1-FAD and NR2-FAD to the maximal levels tested (1:100 and 1:200 respectively), quite high k_{cat} values of 18 s^{-1} (NR1) and 23 s^{-1} (NR2) were determined. However, these values did not approach the respective k_{cat} MV:nitrate activity. However, for NR2 it was not that far from the published value of k_{cat} for NR2-fl of 33 s^{-1} (Lambeck et al., 2010). This suggests that fully-active NR could be re-constituted if sufficiently high FAD-domain concentration were supplied, however this was not possible for practical reasons. Also, the requirement for such high FAD-domain concentrations is almost certainly because the natural, efficient intramolecular electron transport from the FAD-domain to the heme-domain is disrupted, and is replaced by an intermolecular electron transfer. Without the continuous polypeptide chain of NR, the interaction between the two domains is transient and – since the heme can only take one electron at a time – requires two interactions with a reduced FAD before reduction of a single nitrate can occur. The K_M^{nitrate} for the re-constituted enzymes in the subsequently determined steady-state kinetic tests was far lower than the K_M -values for MV:nitrate activity. Slow, intermolecular electron transfer makes it appear that the affinity for substrate is higher.

Full-length NR activity could be re-constituted from the domain fragments and provided a valuable tool for further characterizations that will be discussed in the coming sections. It could be conclusively shown that the intact hinge 2 is not absolutely required for NR activity. Finally, it was shown that with sufficiently high concentrations of FAD-fragment, NR activity of the re-constituted enzyme could approach the activity of full-length enzyme.

3.4 Pre-steady-state kinetics

The re-constituted NR activity offered convenient means to measure the pre-steady state kinetics of heme re-oxidation by nitrate in NR. For this measurement it was an advantage that reduction of the Mo-heme fragment was slowed by the separation from the FAD fragment as this enabled the use of a slight excess of NADH in the reaction mixture that could buffer against contaminating oxygen in the anaerobic system. Contaminating oxygen is a problem for protein that is pre-reduced by, for example dithionite, as an excess of dithionite cannot remain in the enzyme solution or it would interfere with the subsequent re-oxidation by substrate. In contrast, the excess of NADH in the reaction mixture does not interfere with the rapid substrate dependent re-oxidation, but does maintain the enzyme in a fully reduced state for the duration of the experiment.

NADH- and FAD-domain-dependent reduction of NR2-Mo-heme was successfully utilized to determine the pre-steady state parameters for NR2 (section 2.5.3), confirming previously published kinetic parameters (Lambeck et al., 2012). In contrast the comparable analysis of NR1 was only partially successful due to a low concentration of available NR1-Mo-heme. In a preliminary experiment with NR1-Mo-heme it was confirmed that nitrate can re-oxidize the heme and the k_{obs} at a saturating concentration of nitrate (25 mM) was $131 \pm 21 \text{ s}^{-1}$ (section 2.5.3). Assuming that this value is close to the maximal re-oxidation rate k_{ox} , it can be compared with the k_{ox} determined for NR2-Mo-heme of $253 \pm 15 \text{ s}^{-1}$. NR2 is the faster isoform in this comparison, which is well in agreement with the k_{cat} values determined for the two isoforms (MV:nitrate activity). Further measurements are required to accurately determine the k_{ox} and the $K_D^{nitrate}$ for NR1.

This use of re-constituted NR activity for pre-reduction of NR1 and NR2 may also be applicable to determine the rapid kinetic parameters of nitrite reduction. Preliminary

studies with nitrite have been performed for NR2, however, the expected lower turnover rate based on the k_{cat} suggests that the re-reduction rate by excess NADH and FAD fragment may not be negligible any more. Also, competition with contaminating oxygen for re-oxidation of the heme may have caused problems in data interpretation. Based on the higher $k_{cat}^{nitrite}$ for NR1-Mo-heme when the activity is determined using BV:nitrite, the measurement of pre-steady state kinetic parameters may be more successful for this enzyme isoform. Higher concentrations of recombinantly expressed protein are required to conduct these studies.

3.5 Nitrite reduction activity with the nitric oxide analyzer

The nitric oxide analyzer was a useful tool for the detection and quantification of the product of NR-dependent nitrite reduction, confirming the results of the BV:nitrite activity measurement. The specific detection of NO[•], that was nitrite concentration dependent, confirmed that both NR1 and NR2 are nitrite reductase enzymes (Fig. 24). The results were analyzed according to Michaelis-Menten kinetics, showing that the parameters determined (Table 6) differed greatly (~ten-fold) from those determined with the BV:nitrite method (compare Table 5). How can a discrepancy of this scale be explained?

The quantification of NO[•] that was used here was compared to a reference standard curve for NO[•] generation that was prepared as described (MacArthur et al., 2007) by injection of nitrite of known concentration into an acidic tri-iodide solution. Generated NO[•] was stoichiometric with the amount of nitrite injected and resulted in a sharp peak in the NO analyzer, the area of which corresponded with the amount of NO[•] released by the reaction. What is observed in the enzymatic generation of NO[•] by NR is however of a very different nature (Fig. 24A, B). An initial sharp rise in NO[•] signal is seen, followed by a steady production that can be followed over a long period of time (up to 1 h has been recorded). It is questionable whether a comparison of the sharply defined area of the nitrite standards in the standard curve (Appendix 3) can be transferred to such a continuous generation system.

It was assumed that the amount of NO[•] released to the gas phase for the initial phase of the enzyme-dependent reaction reflected the time dependent change in concentration of NO[•] in the reaction solution. However, different initial rates of NO[•] generation would result in different concentrations of NO[•] in solution. It would be

expected that carriage of NO[•] to the gas phase would be more efficient at higher NO[•] concentrations than at lower ones. A direct measurement of NO[•] in solution using for example, an NO[•]-specific probe might help to clarify this situation (Yamasaki et al., 1999). Finally, NO[•] generation using the NO-analyzer was performed with re-constituted NR-activity. As already seen the NADH:nitrate activity determination, the reconstituted enzymes showed a reduced inter-molecular electron transfer rate. This would be an additional factor that contributed to slowed NO[•] production over time than that, which one would expect when using full-length enzyme.

The other two questions addressed using the NO-analyzer were independent of the absolute quantification of NO[•] and thus yielded more robust results. These were, whether nitrite reduction can proceed with nitrate as a substrate, and how the enzyme behaves in the presence of the two substrates simultaneously.

When re-constituted NR1 or NR2 or full-length NR2 were supplied with 400 μM nitrate as substrate, a weak but gradual increase in NO[•] release over time was recorded. Using 4 mM nitrate the NO[•] signal stayed at baseline. This observation, on the one hand confirms previous findings (Rockel et al., 2002; Yamasaki et al., 1999) that NO[•] generation with nitrate as a substrate is possible. On the other hand, the finding, that with the higher concentration of nitrate no NO[•] release was observed implies that the excess of nitrate hinders reduction of nitrite. Given that the cytosolic nitrate concentrations are typically 2 – 5 mM (Cookson et al., 2005; Miller and Smith, 2008) how can nitrite reduction by NR in the physiological situation proceed at all?

There is no doubt that NR is an important source of NO[•] in the plant in many situations such as controlling the induction of flowering (Seligman et al., 2008) stomatal closure (Desikan et al., 2002) defense response to pathogens (Shi and Li, 2008) and drought responses (Wu et al., 2017). The currently assumed model is that an 'activity switch' of NR from nitrate to nitrite reduction takes place in situations in, which nitrite concentration sharply increases in the cytosol (Maia and Moura, 2015; Planchet et al., 2005; Rockel et al., 2002).

The parameters for nitrate inhibition of nitrite reduction determined in this work, make it difficult to understand how nitrite reduction can take place in the cytosol. The half-maximal inhibition of nitrite reduction required only micromolar concentrations of nitrate. Several arguments may help to explain this paradox. Firstly, generation of only trace amounts of NO[•] are probably sufficient for plant signaling requirements and

therefore even 3% residual activity under physiological nitrate concentrations may suffice. Consistently, the fact that nitrite reductase activity quantitatively represents only about 1% of NR activity has been measured (Rockel et al., 2002). Secondly, probably very localized and transient nitrate depletion and concomitant nitrite accumulation may favor nitrite reduction. This is in line with observations showing NO[•] release upon transition from light to darkness or by anoxic conditions (Planchet et al., 2005; Rockel et al., 2002). Thirdly, the local pH environment may play an important role too. A clear pH optimum has been determined here for nitrite reduction at pH 7.5 and nitrate reduction at pH 7.0 and a possible role of cytosolic pH fluctuations in tuning NR activity has been discussed (section 3.2.2). Finally, NR regulation mechanisms in terms of tissue specific expression (Fig. 4), and differential regulation by 14-3-3 proteins provide a basis for explaining the observed NO[•] emission even in the presence of nitrate in plant cells.

There is another mechanism that might explain the observed NR-dependent NO[•] production that might be independent of the presence of nitrate in the cell (Chamizo-Ampudia et al., 2016). This pathway has so far only been described for *Chlamydomonas reinhardtii*, a unicellular eukaryotic algal species, however since the components required are also expressed in higher plants, it is possible that it also functions in these species. The mechanism involves a complex formed between NR and a second Moco-dependent enzyme ARC, which has been renamed by the authors in that study 'NO Forming Nitrite Reductase', NOFNiR. In *Chlamydomonas* NOFNiR accepts electrons from the diaphorase activity (FAD domain) of NR and reduces nitrite to NO (Chamizo-Ampudia et al., 2016). The reaction is reported to be independent of the presence of nitrate in the reaction solution (10 mM nitrite was supplied and 1 mM nitrate). The K_M^{nitrite} determined for the NR/NOFNiR enzyme complex in *Chlamydomonas* was 655 μM .

Similarly, human ARC enzymes have been shown to form a complex electron donor proteins cytochrome *b5* and cytochrome *b5* reductase and to reduce nitrite to NO[•]. The K_M for human mARC isoform 1 was 600 μM and for isoform mARC2 was 300 μM (Sparacino-Watkins et al., 2014). So far, a physiological function for ARC proteins has not been assigned. It is possible that NO-producing activity is the primary physiological function of this Moco enzyme, however, if a similar K_M^{nitrite} were to be observed in

higher plants, it would be unlikely to represent a physiological function since such a high nitrite concentration is not observed in higher plants.

3.6 Stoichiometry of NO[•] generation by NR

Next, we asked the question, how many turnovers of nitrite reduction can be performed by pre-reduced NR enzyme? This question was prompted by the observation for SO, that only the fully reduced Mo (IV) of Moco is capable of reducing nitrite to NO[•] (Wang et al., 2015). SO then arrests in the partially reduced Mo (V) state. Unfortunately, a satisfactory answer for NR could not be found in this work. The extreme sensitivity of the pre-reduced NR enzyme, probably to contaminating oxygen, made it impossible to accurately measure the stoichiometry of the reaction. The measured amount of 36 pmol of NO[•] released from 146 pmol of cofactor saturated NR-Mo-heme fragment reflected NO[•] production by only about 25% of the enzyme molecules. Most likely, the enzyme was no longer fully reduced at the measurement time point.

It could be speculated that the situation in full-length NR should be different to SO and that for the fully reduced (full-length) enzyme, at minimum four molecules of nitrite should be reduced to NO before the enzyme would arrest in the Mo (V) state. The electron flow in NR is as follows: NADH → FAD → heme → Moco. Several studies report on the full reduction of the heme cofactor before the FAD cofactor is fully reduced (proving the 'downhill' flow of electrons) (Campbell, 2001; Lambeck, 2009; Ratnam et al., 1996). Since the redox potential of the Moco is more positive than that of the heme, it would also become fully reduced before the heme and FAD cofactors (Skipper et al., 2001). During nitrite turnover, therefore, all electrons upstream of the Moco (on the FAD and the heme) would be passed to the Moco before the Moco would/could arrest in the Mo (V) state. Experimental confirmation of such a proposal is still missing and requires a different experimental approach. Dithionite pre-reduced NR was not stable for the duration of the measurement, probably due to contaminating oxygen.

3.7 14-3-3-mediated inhibition of NR1 and NR2

Phosphorylation of the conserved hinge 1 serine residue in NR1 without effect on nitrate reduction activity, could be firmly established. Subsequently, inhibition by three out of six 14-3-3 proteins could also be measured (Fig. 28). Three isoforms of 14-3-3

(Chi, Omega and Mu) were directly compared for inhibition of the two isoforms of NR, and in each case the maximal inhibition for NR2 was higher than for NR1 (Table 7).

In the case of 14-3-3 Mu, NR1 was not (or barely) inhibited, while NR2 was inhibited up to 72%. This seems to point to NR-isoform specific regulation. On the other hand, inhibition of NR2 by 14-3-3 Mu is in itself interesting, because 14-3-3 Mu is a member of the epsilon family of 14-3-3's. In the past, due to the absence of inhibition of NR2 by 14-3-3 family member epsilon (which was now also seen not to inhibit NR1), it was suggested that epsilon family members may not play a role in NR regulation (Lambeck et al., 2010). This can now definitely be seen not to be generally true. In fact, the inhibition by Mu was the most potent inhibitor of NR2 measured here or previously (Lambeck et al., 2010). According to SUBA4 (Subcellular Localization Database for *Arabidopsis* proteins 4) *At*14-3-3 Mu locates to the chloroplast stroma, nucleus, plasma membrane and cytoplasm (Hooper et al., 2017). NR2 and NR1 are located in the cytosol (Ritenour et al., 1967) although a localization of NR2 to the plasma membrane and vacuole is also reported (SUBA4) (Hooper et al., 2017). An interaction between NR2 and 14-3-3 Mu would therefore be possible *in vivo*. Isoform 14-3-3 Omega that was seen in this work to inhibit both NR1 and NR2 is localized to the plasma membrane and vacuole and thus is only localized in a similar compartment with NR2. Further studies are needed to determine whether *in vitro* interaction/ inhibition results for NR1 or NR2 in combination with various 14-3-3 isoforms are physiologically relevant.

For the two other 14-3-3 isoforms for which the NR1-Mo-heme inhibition was determined (Chi and Psi), the IC_{50} was about one order of magnitude larger than the inhibitory concentration required for NR2 (Table 7). Finally, it could be speculated that the lower levels of inhibition of NR1 compared with NR2 may be linked to the different conformations of the N-terminus of the NR proteins. It was found in this work that the secondary structure of the N-terminus of NR1 must be different from that of NR2 since the NR1 with an N-terminal His tag inserted between residues 2 and 3 of the protein expressed in *Pichia* did not bind to the Ni-NTA affinity column (Fig. 11), while in NR2, the N-terminal tag was accessible. It is also known (based on studies using NR2) that the N-terminus plays an important role in mediating inhibition of NR upon binding to 14-3-3s (Chi et al., 2015). Perhaps a differently folded N-terminus of NR1 precludes the second interaction with 14-3-3's and thus results in lower inhibition.

The question of whether 14-3-3 proteins may also regulate nitrite reduction *in vitro* could, unfortunately, not be studied using the BV:nitrite system, because reduced BV clearly donated its electrons to the Moco domain. As a result, nitrite reduction could not be inhibited by 14-3-3 proteins. Further direct *in vitro* studies of the 14-3-3 inhibition of nitrite reduction will either require full-length enzyme, or could be determined using re-constituted NR and the NO-analyzer.

Clearly, an inhibition of nitrite reduction would also be expected upon phosphorylation and interaction with 14-3-3 since the mechanism of 14-3-3-based inhibition is to arrest the domain movements between heme and Moco and to rigidly hold NR in a conformation not conducive to electron transfer between the domains (Lambeck et al., 2012). Indirect evidence already points to this mode of inhibition of nitrite reduction. In tobacco cells, mutation of the conserved pSer of the hinge 1, preventing interaction with 14-3-3 proteins, resulted in increased NO release by the cells (Lea et al., 2004). In crude NR extracts provided with Mg²⁺, ATP and protein phosphatase inhibitor (conditions that favor 14-3-3 binding and inhibition of NR activity), NO generation was also inhibited (Rockel et al., 2002). By inhibiting electron transfer from heme to Moco, 14-3-3 proteins would inhibit both nitrate and nitrite reduction taking place at the Moco since both reactions are dependent on reducing equivalents coming from the heme.

3.8 Structure model of NR

The structure model for NR obtained by cryo-EM in this work was too small to encompass the full size of the NR dimer. A central core could however be recognized in the model, that probably represented the Moco and dimerization domains, with the suggestion that other domains wrap around this core (Fig 30). It is likely that the Moco and dimerization region form a fairly rigid structure – since this domain has been successfully crystallized in the past (Fischer et al., 2005) – whereas the other domains due to their flexible linkers relative to Moco did not produce reproducible density in the cryo-EM images.

Model refinement and generation of a 3D-structure with the grids produced in this work was not pursued exhaustively for the following reasons: The size of the preliminary model generated was too small to represent the entire NR protein and also the NR2 dimer is rather small anyway for cryo-EM with its ~200 kDa size.

There are some reasons therefore, that complexation of pNR2 with 14-3-3 would be advantageous for cryo-EM studies. Firstly, the complex would offer an increased size to allow for better visualization. Secondly, by complexing pNR2 with 14-3-3, the flexibility and number of possible conformations of the protein would be reduced, making model fitting easier. Finally, an additional tool is to be applied, simultaneously to the strategy of complex formation: One of the proteins is to be expressed with a His tag (the 14-3-3). The second protein, NR is to be cloned with a removable His-tag using a PreScission protease cut site. Gold NTA particles can then be used that bind to the His tag to more easily identify 14-3-3:pNR complexes and aid in data interpretation (Ackerson et al., 2010). By applying these strategies going forward, cryo-EM offers some promising possibilities for determining the structure of NR.

4 Conclusion and outlook

Isoform specific steady state and pre-steady state catalytic parameters of NR1 and NR2 from *A. thaliana* could be established in this work. These were a lower K_M^{nitrate} for NR2 contrasting with a high K_M^{nitrate} for NR1. Both NR1 and NR2 had pH optima for nitrate reduction at pH 7.0. On the other hand, the K_M^{nitrite} for both isoforms of NR were in the low micromolar range, however, the $k_{\text{cat}}^{\text{nitrite}}$ was ~ 10-fold higher for NR1 than for NR2. The pH optima for nitrite reduction by both isoforms were pH 7.5.

Evidence was also seen for 14-3-3-isoform specific differences in the regulation of NR1 and NR2 in nitrate reduction. The most prominent difference was the very high inhibition of NR2 by 14-3-3 Mu and the absence of inhibition by the same isoform, of NR1. In addition, the inhibition I_{Max} for NR1 was generally lower and with a higher IC_{50} compared to NR2. The isoform that inhibited NR1 most effectively was 14-3-3 omega, with an IC_{50} comparable to NR2.

Going forward it would be very interesting to determine the inhibitory parameters for further 14-3-3 isoforms, and also to determine the inhibitory parameters for the 14-3-3 isoforms in nitrite reduction. The intracellular localization of individual 14-3-3 proteins and correlations with NR localization would also help to build a picture of the complex post translational regulation of NR activity. Taken together with the genome-wide transcription patterns for *NIA1* and *NIA2* (Fig. 4) showing higher *NIA1* transcription only in reproductive tissue and evidence from *nia* mutant plants emphasizing a role for NR1 in NO[•] signalling provide compelling evidence that NR1 is indeed a dedicated NO[•] generating enzyme while NR2 is more tuned to the basic and essential metabolic function of nitrate assimilation.

However, the fact that both isoforms can compensate for the absent isoform in single mutant plants, and the herein measured nitrate and nitrite reduction capacity of both isoforms underscores functional redundancy that is probably beneficial for plant survival. A question that should be addressed going forward is, how an NR from a plant species with only one NR isoform (e.g. spinach) can integrate nitrate assimilation with NO[•] signalling if other plants such as *Arabidopsis* have evolved two isoforms with divergent functions to manage these two roles.

The re-constitution of full-length NR-activity that was established in this work proved to be a very useful tool for studies in which the native NADH electron donor was a superior

choice or option for activity measurements – such as in NO[•] detection and in pre-steady state kinetic measurements.

Despite this progress, many challenges remain in clarifying a picture for isoform specific roles for NR1 and NR2. Firstly, a molecular structure of NR would be a major breakthrough in the field of nitrate metabolism and a structure comparing NR1 with NR2 would provide a structural basis for understanding the observed kinetic differences. The model of NR1 and NR2 shown here with a positively charged lysine residue adjacent to the substrate binding funnel of NR2 suggesting that this may be a cause of the increased affinity of NR2 for the substrate nitrate should be further verified by structure guided mutagenesis (Fig. 31). For obtaining the molecular structures of NR1 and NR2 the promising method of cryo-EM was explored in this work resulting in a first low resolution structure model of NR2. Future studies should use the known domain structures of NR or homologous domains to refine the data and to determine the different conformations that NR may adopt.

5 Materials and Methods

5.1 DNA cloning

Manipulations of DNA coding sequence for example, in order to transfer the DNA from one plasmid to another were performed using polymerase chain reaction (PCR) to amplify the required sequence and using primers to introduce the desired restriction enzyme cut sites to match the multiple cloning site (MCS) of the new target plasmid. PCR primers used in this work are listed in Appendix 2, along with an annotation describing the purpose and the restriction enzymes used. PCR reactions were performed as follows: 20 – 50 ng template DNA, 20 pmol each of forward and reverse primer, 12.5 µL 2 x REDTaq® ReadyMix™ PCR Reaction Mix (Sigma) and 0.5 µL Pwo polymerase (Sigma) were mixed in a final reaction volume of 25 µL and subjected to thermal cycling (Px2 ThermoCycler / Thermo Scientific) (95°C 3min, (95°C 30 sec, T_A (see primer list) 30 sec, 72°C 1min/1000 bp) 30 x cycles then 72°C 10 min, 10°C storage).

- pJET Cloning

Thermo Scientific CloneJET PCR cloning kit was used as described by the manufacturer (blunt end protocol) to secure intermediate PCR DNA fragments into the pJET1.2 blunt plasmid as required. Transformed into *E. coli* XL-2 blue or Turbo strain

- Transformation of chemically competent *E. coli*

Chemically competent cells were thawed on ice. The plasmid for transformation or a ligation mixture was pipetted onto the cells and mixed gently followed by incubation on ice for 30 min. Next, heat shock was applied for 60 s at 42°C, before returning to ice for 5 min. 700 µL of LB without antibiotic was added to the cells and cultured at 37°C with shaking for 1 h. The cells were then plated on LB-agar containing selection antibiotic as required

- Agarose gel electrophoresis

Separation of DNA fragments was performed using 1% Agarose gels prepared in 1x TAE buffer containing 0.5 µg/mL ethidium bromide. Gels were run at 100 V for 20-30 min in TAE running buffer. DNA bands were visualized using a UV transilluminator.

- Extraction of DNA from agarose gels

DNA was extracted from agarose gels using the Omega Bio-tek E.N.Z.A® gel extraction kit according to the manufacturer instructions

- Plasmid preparation

Plasmid preps were prepared in 5 mL portions of liquid LB medium (+ appropriate antibiotic) in 15 mL sterile glass vials with a single *E. coli* colony used to inoculate the prep. Plasmid DNA was extracted using the Omega Bio-tek E.N.Z.A® Plasmid DNA mini-kit I according to the manufacturer instructions. DNA concentration was determined using a Nanodrop instrument. DNA was stored at -20°C

- Restriction enzyme digestion

ThermoScientific Fast Digest restriction enzymes were used in combination with the manufacturers' digestion buffer according to the manufacturer recommendations except that in some cases longer incubation times were used, (1 h to 16 h) (but considering the star activity time given by the manufacturer). Heat inactivation of the respective enzyme was according to the manufacturer recommendations.

- DNA ligation

Sticky end DNA fragments were mixed typically using 20 ng digested sticky-end plasmid and a ratio of plasmid to insert of ~1:5 in a total volume of 8.5 µL in PCR tubes and heated to 45°C for 15 min followed by cooling on ice. 1 µL of 10x T4 Ligase buffer (Thermo Scientific) was added followed by 5 units (0.5 µL) of T4 DNA ligase enzyme. The reaction was incubated for 1 h at 22°C and the complete reaction mix was used for transformation of an appropriate *E. coli* strain.

- Colony PCR

Transformed *E. coli* colonies were picked using a sterile tip and transferred to 10 µL of PCR mix in a PCR tube and followed by transfer of the tip to inoculate a 5 mL LB culture. PCR mix consisted of 5 µL of 2x REDTaq® Ready Mix™ PCR, (Sigma-Aldrich, Munich Germany) appropriate forward and reverse primers for detecting the plasmid insert (frequently T7for and T7terminator were used) and water. PCR reaction as described above.

- DNA sequencing

DNA sequencing was performed by GATC Biotech (Cologne)/ Eurofins Genomics (Ebersberg) using the Sanger Sequencing LightRun service

5.2 Yeast methods

Instructions for preparing YPD, Low salt LB, YPDS/Zeocin, Breaking buffer BMGY, BMMY, BMMH and the recipes for all appropriate stock solutions were taken from the Invitrogen manual 'EasySelect™ Pichia Expression Kit For Expression of Recombinant Proteins Using pPICZ and pPICZ α in *P. pastoris* Cat. no. K1740-01, Rev. Date 18 June 2010, Manual part no. 25-0172'. All liquid growth media were supplemented with 100 μ L per liter of antifoam Y-30 and for some experiments 100 μ g/mL ampicillin to prevent bacterial contamination.

- Transformation

pPICZ containing the NR insert of interest (3 – 5 μ g) was linearized using MssI/PmeI in preparation for transformation of yeast. After thermal inactivation, the DNA was purified using the Omega Bio-tek E.N.Z.A® gel extraction kit according to the manufacturer instructions for PCR reaction clean-up, with elution of the purified DNA in 20 μ L of ddH₂O. Two different transformation protocols were used:

1. PEG 1000 transformation protocol

Empty *P. pastoris* KM71 or GS115 were scratched from glycerol stocks and plated on YPD agar. A single colony from a fresh agar plate was used to inoculate 5 mL YPD, grown overnight at 30°C, then used to inoculate a 100 mL culture with 0.1 – 0.2 OD₆₀₀. The culture was grown at 30°C and 250 rpm in a shaking incubator until the OD₆₀₀ had reached 0.6 – 1. Cells were pelleted by centrifugation 1000 rpm at RT, 5 min then washed one time with 40 mL filter sterilized RT Buffer A (1 M Sorbitol, 10 mM Bicine-NaOH pH 8.35 (Sigma), 3% v/v ethylene glycol (Merck)) and resuspended in 4 mL buffer A. Portions of 200 μ L cells were aliquoted into cryogenic vials, 11 μ L fresh DMSO was added, gently vortexed, then frozen slowly to -80°C before being used for transformation.

Digested DNA (containing insert of interest, or empty plasmid, or DNA-free water blank) was pipetted onto an aliquot of frozen cells. followed by 1 mL of Buffer B (40% PEG 1000 (Roth) 0.2 M bicine pH 8.35), cells were incubated for 1 h at 30°C in a water bath with mixing ever 15 min. Heat shock was performed for 10 min at 42°C, followed by addition of 2 mL YPD and incubation for 1 h at 30°C. Then the cells were centrifuged 5 min at 3000 x g at RT and the supernatant discarded. The cells were resuspended in 1 mL of Buffer C (0.15 M NaCl, 10 mM bicine pH8.35) centrifuged 3000 x g 5 min

then resuspended in 100 to 150 μL Buffer C. The entire volume was then plated in YPDS agar plates containing 100 $\mu\text{g}/\text{mL}$ zeocin. Plates were incubated at 30°C for 2 – 4 days to allow transformed colonies to grow.

2. Electroporation transformation protocol

Empty *Pichia* KM71 or GS115 were grown up from glycerol stocks as described, but using a 300 mL culture volume for the final growth phase from 0.2 OD to 1.5 OD₆₀₀. Cells were harvested by centrifugation at 4°C, washed twice with 300 mL ice cold sterile water, then washed once with 50 mL ice cold 1 M sorbitol before resuspending in ~300 μL of 1 M sorbitol. 80 μL of electro competent cells were transferred to an ice cold electroporation cuvette (Molecular BioProducts, #5520) containing 20 μL linearized pPICZ:NR DNA. The cells were pulsed 0.5 millisecond at 2 kV in a BioRad Mini electroporation device (Biorad, Munich) before being returned to ice. 1mL liquid YPDS was added to the cuvette and it was then transferred to 30°C incubator for 2 h, with occasional inversion to mix. Cells transformed by electroporation were typically selected-for using a gradient of zeocin concentration (100 $\mu\text{g}/\text{mL}$, 500 $\mu\text{g}/\text{mL}$ and 1000 $\mu\text{g}/\text{mL}$), therefore the mix of transformed cells was divided between three YPDS agar/zeocin plates, spread and allowed to dry before incubation at 30°C for 2 – 4 days. Transformed colonies growing on higher zeocin concentrations were chosen for expression testing.

- Clone selection

Transformed colonies were picked and used to inoculate BMGY liquid cultures, as well as fresh YPD/zeocin agar to conserve the clone. Test expressions/clone comparisons were typically performed using 15 mL BMGY in 50 mL polypropylene tubes, or using 50 mL BMGY in 250 mL wide neck Erlenmeyer flasks. Picked colonies were grown overnight, 30 °C, 250 rpm to 2 – 6 OD, then 700 μL of culture was removed for preparation of glycerol stocks and 100 μL was removed for colony PCR (described below). The remaining culture was harvested and re-suspended in 5 mL or 10 mL of BMMY containing 1% methanol for induction of protein expression. Induction culture duration was as described in the results section. For culture duration beyond 24 h, fresh methanol was added from a 20% stock solution to a final concentration in the culture of 0.5% every 24 h.

- Test culture harvest and lysis

The entire test expression culture was harvested for lysis by spheroblasting, or in later experiments, 1 mL of expression culture was harvested for lysis using glass beads and vortexing.

1. Lysis by spheroblasting

For spheroblasting the cells were resuspended in 10 – 20 mL spheroblasting buffer (1.4 M Sorbitol, 50 mM Potassium phosphate (KPO₄) pH 7.5, 0.3% β-Mercaptoethanol) then centrifuged 3000 x g 5 min at RT. The supernatant was discarded and the approximate weight of the cell pellet was determined. The cells were resuspended in 6 mL spheroblasting buffer per gram cells and 0.5 mg of Zymolase (US Biological Life Sciences, Z10000) was added per gram cells. The cells were incubated at 37°C with gentle shaking 65 rpm and a 10 µL sample was removed every 5 - 10 min to test for % spheroblasting by mixing with 990 µL 1% SDS in water. % Spheroblasting is defined as:

$$100 - \frac{[\text{OD}_{800} \text{ at time } x] - 100}{\text{OD}_{800} \text{ at } 0 \text{ min}}$$

Once 80% had been reached, the tube was filled up with fresh ice cold spheroblasting buffer and centrifuged 1000 x g for 5 min at 4°C before being resuspended in ice cold NR lysis buffer (50 mM KPO₄ pH 7.5, 200 mM NaCl, 10% glucose, 15 mM glutathione, COMPLETE without EDTA). Spheroblasts were lysed by sonification at 30% amplitude for 30 sec – 1 min then cell debris was removed by centrifugation 21,000 x g for 10 min at 4°C. Total protein concentration was determined by the method of Bradford as described by the manufacturer (Carl Roth, Roti®-quant) performing a fresh standard curve of BSA for each day of measurement. Samples of raw lysate were separated by SDS-PAGE and analysed for NR protein expression by Coomassie blue staining or anti NR-immunoblotting (as described below).

2. Lysis by glass beads and vortexing

1 mL samples of induced *Pichia* clone cultures were removed at various timepoints during culture centrifuged to remove supernatant then stored at -80°C until lysis. Cells were thawed on ice and 200 µL ice cold breaking buffer was added (50 mM sodium phosphate (NaOH) pH 7.4, 1 mM EDTA, 5% glycerol, COMPLETE protease inhibitor).

An equal volume of ice cold glass beads (0.5 mm, Sigma) was added (volume estimated by displacement), then the cells were vortexed for eight cycles of 30 sec vortexing 30 sec incubation on ice. The lysed cells were centrifuged 10 min at 21,000 x g and the cleared supernatant removed to a fresh tube. Protein concentration determination and SDS gel analysis as standard.

- Preparation of glycerol stocks

700 µL of a fresh, rapidly growing *Pichia* culture was placed in a cryogenic vial and mixed with an equal volume of 50% glycerol, vortexed for 10 sec then frozen slowly and stored at -80°C

- Colony PCR for analysis of yeast transformants

100 µL of rapidly growing liquid culture was taken, centrifuged 3000 x g 5 min RT, then resuspended in 100 µL lysis solution (200 mM lithium acetate, 1% SDS) and incubated at 70°C for 15 min in a heating block. 300 µL 96% ethanol was added and mixed by vortexing to precipitate DNA. The DNA was then pelleted by centrifugation 15,000 x g for 3 min. The pellet was re-suspended in 100 µL TE buffer (10 mM Tris/HCl pH 8.0, 1 mM EDTA), centrifuged again at 15,000 x g for 1 min to remove cell debris. 1 µL of the supernatant was used for PCR. Depending on the insert of interest an appropriate pair of forward and reverse primer were chosen to amplify the insert or a segment thereof in comparison to DNA from yeast cells transformed with empty plasmid.

5.3 Full-length NR expression in *Pichia* and affinity purification

Constructs for protein expression in *Pichia* are listed in Table 1. Transformation and clone selection was as described.

Large scale yeast expression was performed as follows: a positive clone expressing the protein of interest was streaked onto fresh YPD agar and grown 24 - 48 h at 30°C then used to inoculate a 20 ml liquid BMGY culture in a 200 mL flask, which was grown for 8 h 200 rpm, 30 °C. The culture volume was increased to 250 mL BMGY in a 1 L flask, then culture was continued overnight. This culture was then used to inoculate 6 x 500 mL BMGY in 5 L flasks and culture continued until an OD 600 of about 2 – 6 was reached (Typically 24 h). The cultures were harvested 3000 x g 10 min at RT, then re-suspended in the same volume of RT BMMY containing 1% methanol for induction. After the appropriate induction period the cells were again harvested 3000 x g, 10 min

at RT and the weight of cell pellet determined. For lysis by spheroblasting, cells were re-suspended in spheroblasting buffer as described for small-scale lysis, for lysis by Bead Beater (BioSpec Products), the cells were re-suspended in 10 mL/gram of NR lysis buffer (50 mM KPO₄ pH 7.5, 200 mM NaCl, 10% glucose, 20 mM Imidazole, 15 mM glutathione, COMPLETE without EDTA) then stored at -80°C until lysis.

Lysis by Bead Beater was at 4°C as follows: The chamber of the bead beater was half filled with 0.5 mm glass beads and pre-cooled on ice. The cell suspension containing 10 – 80 g of cells was added (~200 mL) adjusting the fill volume to the brim with lysis buffer as required. The chamber was mounted on the bead beater and the ice-water cooling jacket was filled. The instrument was run with 10 cycles of 30 sec interspersed by 1 min cooling periods. The lysed supernatant was decanted, the beads were washed with lysis buffer and added to the lysate.

Lysis by spheroblasting was essentially the same at the large scale as described for the small scale (above): Sonification time was extended to 5 min total with 10 x 30 sec intervals.

Lysis by Constant systems Cell disruptor was by two passages of the *Pichia* suspension through the instrument at 2.5 bar followed by sonication 1 - 3 min 50% amplitude as required to reduce viscosity.

Affinity purification was as follows: Raw lysate was centrifuged at 48,000 x g in a Beckmann JA20/J21 XP centrifuge and the cleared supernatant was pooled in a Schott flask. Ni-NTA Immobilized metal affinity chromatography IMAC was performed in-batch for 30 min as the manufacturer describes (HisPur NiNTA, Thermo Fischer Scientific). After pouring the resin into a column, it was washed using lysis buffer, followed by elution using buffer of the same composition but with a higher imidazole concentration (250 mM). Eluted protein was concentrated using an Amicon centrifuge concentrator MW CO 50 000 (Merck, Darmstadt) and buffer exchanged over a PD-10 column (GE Healthcare) into NR-storage buffer (20 mM Tris/HCl pH 7.5, 200 mM NaCl, 10 mM MgAc, 0.05% Tween 20). Protein was shock frozen in liquid nitrogen and a portion was later thawed in order to determine protein concentration and Molybdenum cofactor (Moco) saturation. Protein concentration was determined via absorption at 413 nm and using the extinction coefficient $\epsilon_{413}=120,000 \text{ M}^{-1} \text{ cm}^{-1}$ Moco cofactor saturation was determined by oxidation to Form A and quantitation via HPLC compared to a Form A standard as described (Schwarz et al., 1997).

5.4 Recombinant protein expression in *E. coli*

- *AtNR2*-Mo-heme

pQE80 plasmid containing *AtNR2*-MoHeme DNA was expressed in TP1004 *E. coli* (kindly provided by Tracy Palmer, Newcastle University) using a protocol modified from that previously described (Lambeck et al., 2012). Briefly, transformed *E. coli* were cultured in LB medium supplemented with ampicillin (100 µg/mL), kanamycin (25 µg/mL), sodium molybdate (1 mM), magnesium chloride (2 mM) and iron (III) chloride (10 µM) in shake flasks at 37°C to an OD₆₀₀ of 0.2 – 0.4 and then induced by the addition of 50 µM isopropyl-β-D-thiogalactoside (IPTG). The culture temperature was reduced to 18°C and culture was continued for 70 h then harvested by centrifugation. All subsequent steps were performed at 4°C and all buffers for IMAC were supplemented with Roche COMPLETE EDTA-free protease inhibitor. Cells were re-suspended in 10 mL lysis buffer per gram wet cells (50 mM potassium phosphate pH 7.0, 200 mM NaCl) and then frozen at -80°C. After thawing the cell suspension, lysis was performed using treatment with lysozyme (11 mg/liter *E. coli* culture) and 20 min incubation at RT followed by sonication (Branson Digital Sonifier) and an Emulsiflex C5 (Avestin). The raw lysate was supplemented with 10 µM Hemin (from a 1 mM stock in 20 mM sodium hydroxide) (Krainer et al., 2015). Nickel IMAC was performed in-batch as described for FL NR expressed in *Pichia* except that an additional wash with lysis buffer containing 5 mM imidazole was performed to remove unspecifically bound proteins. Elution was with lysis buffer containing 200 mM imidazole. Deeply red heme-protein containing fractions were pooled. Size exclusion chromatography (SEC) was performed using a Superdex 200 120 mL column into NR-storage buffer (20 mM Tris/HCl pH 7.5, 200 mM NaCl, 10 mM MgAc, 0.05% Tween 20) and the protein peak eluting at about 60 mL was pooled and shock frozen in liquid nitrogen for storage at -80°C. Protein concentration determination and cofactor saturation as described for FL NR.

- *AtNR1*-Mo-heme

AtNR1-MoHeme expression from the pQE80 plasmid (kindly provided by K. Schrader) was similar but with the following changes: Growth phase and expression of the transformed cells was at 25°C. Induction was at OD₆₀₀=0.4 with 100 µM IPTG for a duration of 20 h. The pH of the lysis, wash and elution buffers was adjusted to pH 7.5

Wash of the IMAC column was with lysis buffer containing 20 mM imidazole in order to remove degraded NR1-Mo-heme protein and unspecifically bound proteins. Elution was with lysis buffer containing 250 mM 1imidazole. SEC was performed as for NR2-Mo-heme, however the elution profile differed significantly from the NR2-Mo-heme and the pool containing non-degraded NR1-Mo-heme was pooled (results 2.2.1). Concentration and cofactor saturation determination as for MoHeme 2.

- *At*NR-Mo domains

The DNA sequence for NR1-Mo (residues 1 – 488) was PCR amplified out of the full-length-DNA sequence (in pQE80) with restriction enzyme cut sites KpnI inserted in the forward primer Appendix 2 and a stop codon plus a Sall cut site in the reverse primer. The digested DNA was then re-inserted into pQE80 plasmid for expression. pQE80 plasmid containing NR2-Mo was kindly provided by K. Schrader. Expression and purification for the two Mo-domains was the same using *E. coli* TP1004 and LB supplemented with ampicillin (100 µg/mL), kanamycin (25 µg/mL) and sodium molybdate (1 mM). For initial growth phase the culture was incubated at 37°C to an OD₆₀₀ of 0.2 – 0.4 and then, after reducing the temp to 30°C, induced by the addition of 20 µM IPTG. Harvest followed after 30 h, after which the cells were suspended (1 g/10 mL) in lysis buffer (50 mM K-phosphate pH 7.5, 200 mM NaCl, 10 mM DTT, 1 mM sodium molybdate, 10 mM imidazole, COMPLETE-without EDTA). After freeze-thaw, the cells were lysed using an Emulsiflex and His-tagged protein, affinity purified using IMAC as described for NR2-Mo-heme. Wash of the column was with lysis buffer and elution buffer was supplemented with 250 mM imidazole. Protein containing fractions of IMAC-elution were pooled and further purified using SEC (as described for NR2-Mo-heme). The protein peak (with A280 and A380 nm absorption) that eluted between 60 and 70 mL was pooled, concentrated using an Amicon centrifuge concentrator MW CO 50 000, then frozen in liquid nitrogen. Protein concentration determination was estimated by the A280 and the calculated ϵ_{280} 108,330 M⁻¹ cm⁻¹, however because of impurities in the pooled protein, the actual concentration was taken as the concentration of Form A/ concentration of Moco saturated protein.

- *At*NR-FAD domains

The FAD-domain DNA of NR1 and NR2 were PCR amplified out of the respective full-length NR DNA sequences and had restriction enzyme cut sites (BamHI and HindIII

for NR FAD 1, and PstI and HindIII for NR FAD2) introduced at the 5' and 3' ends in order to clone them into the pQE80L plasmid. Plasmid was amplified in *E. coli* Turbo and then used to transform expression strain *E. coli* BL-21 Rosetta (Novagen). The culture and expression conditions were the same for both FAD-fragments. Transformed cells were cultured at 37°C to an OD₆₀₀ of 0.4 and then induced by the addition of 400 µM IPTG. Induction was for 4 h at 37°C. Cells were resuspended 1 g in 10 mL using lysis buffer (50 mM potassium phosphate pH 7.0, 300 mM NaCl, 5 mM imidazole, Roche Complete EDTA-free inhibitor mixture). Wash of the IMAC was performed using lysis buffer supplemented with 20 mM imidazole and elution buffer contained 250 mM imidazole. After elution, buffer exchange was performed using PD-10 columns (GE Healthcare) and NR Storage buffer. Protein was shock frozen in liquid nitrogen. Concentration determination was based on the FAD-cofactor specific absorption at 450 nm and using an extinction coefficient ϵ_{450} 11,300 M⁻¹ cm⁻¹.

- *At14-3-3* expressions

Plasmid pET15b containing the DNA sequence of *At14-3-3* epsilon was kindly provided by K. Schrader and was transformed into *E. coli* BL-21 Rosetta (Novagen) for protein expression. Culture was performed in LB medium supplemented with ampicillin (100 µg/mL). Expression was induced by addition of 100 µM IPTG at OD₆₀₀ = 0.6, at which point the culture temperature was reduced to 20°C. Cells were harvested after 23 h, centrifuged and re-suspended in lysis buffer (100 mM KPO₄ pH 7.5, 300 mM NaCl, 20 mM imidazole, Sigma protease inhibitor without EDTA). Ni-NTA affinity purification via the 6xHis tag in the recombinant protein was performed as described above. Elution buffer contained 300 mM imidazole. SEC was performed for further purification using buffer (50 mM Bis/Tris Ac pH7.0, 50 mM KCl, 5 mM MgAc, 1mM CaCl₂) with the protein peak eluting between 85 mL and 100 mL pooled. Protein concentration was determined using the calculated ϵ_{280} 27,515 M⁻¹ cm⁻¹.

pET15b containing *At14-3-3* Omega was likewise kindly provided by K. Schrader and transformed into *E. coli* BL-21 Rosetta (Novagen) for protein expression. Culture was in LB medium supplemented with ampicillin (100 µg/mL). Expression was induced by addition of 250 µM IPTG at OD₆₀₀ = 0.6, then expression culture was continued for 6 h at 37°C. Cells were harvested, lysed and Ni-NTA performed as described above. Lysis and elution buffers were as described for 14-3-3 epsilon. SEC was not required, after IMAC, the 14-3-3 Omega was buffer exchanged into storage buffer (50 mM

Bis/Tris Ac pH7.0, 50 mM KCl, 5 mM MgAc, 1mM CaCl₂) before freezing in liquid nitrogen. Protein concentration determination as for 14-3-3 epsilon.

Other 14-3-3 isoform proteins used in this work were provided.

- Size standard calibration on the Äkta using the Superdex 200 16/60 column

A protein size standard-mix was prepared using the Kit 28-4038-42 'High Molecular Weight' from GE Healthcare. For 500 µL of mix the following proteins and volumes were used: 125 µL Thyroglobulin, 7.5 µL Ferritin, 100 µL Aldolase, 75 µL Covalbumin, 100 µL Ovalbumin and filled up to 500 µL using 100 mM Tris/HCl pH 7.2. The entire volume was injected into a 1 mL sample loop and applied to the buffer-equilibrated column. The elution volumes for the protein peaks were plotted against the log₁₀ of the respective molecular weight to yield a standard curve. Unknown protein sizes separated on the same column using the same buffer could be determined by comparison with the standard curve.

5.5 Other biochemical techniques

- SDS-PAGE and Immunoblotting

Protein samples were separated by 10% or 12% SDS PAGE as described (Laemmli, 1970). Samples were run for approx. 75 min 200 V (maximum 35 mA per gel). Gels were cooled to 8°C while running using a water flow cooling system (Fisher Brand). 5xSample loading buffer consisted of Bromphenol Blue 0.05%, 250 mM Tris pH 6.8, 10% SDS, 30% Glycerol, 5% β-Mercaptoethanol. Proteins were visualized in the gel via Coomassie Blue G250 staining (Lawrence and Besir, 2009). Proteins for immunoblotting were transferred after PAGE to a PVDF membrane using a semi-dry blotter (Towbin et al., 1979) using transfer buffer consisting of 25 mM Tris, 192 mM glycine, 10% methanol. Membranes were blocked with 5% fat-free milk powder solution in TBST buffer (Tris buffered saline 0.05% Tween 20) - alternatively for Ni-NTA conjugate staining blocking was in 3% BSA as per manufacturer protocol. Membranes were probed as follows:

For NR proteins or fragments thereof: NR-specific rabbit polyclonal antibodies (AS08 310, Agrisera) diluted 1:10,000 in 1% Milk-TBST and using 1:5000 diluted secondary goat anti rabbit HRP coupled antibody (Thermo Fischer Scientific).

For detection of phosphorylated NR: polyclonal rabbit anti NR phospho-hinge antibody (Eurogentec) described in (Lambeck et al., 2012) was used 1:25,000 followed by 1:5000 diluted secondary goat anti rabbit HRP coupled antibody (Thermo Fischer Scientific).

For any His-tagged proteins: Ni-NTA-HRP staining conjugate (Qiagen, Hilden) according to the manufacturer's instructions.

Blots were developed using ECL solution (Thermo Fischer) and visualized using a GelDoc instrument (BioRad, Munich). Coomassie stained gels were photographed using the same instrument.

5.6 Enzyme activity measurements

All steady-state enzyme kinetic measurements were performed in an anaerobic chamber (Coy Laboratory Products, USA) at 22 – 25°C. Plastic ware, chemicals and solutions were brought into the chamber several days before use to ensure that they were completely anaerobic. All enzyme kinetic samples were run parallel to a sample containing all reaction components except the enzyme to ensure that activities measured were enzyme specific. This blank measurement was subtracted from the respective measurement with enzyme.

- NADH:nitrate activity determination

The NADH:nitrate activity determination using full-length or re-constituted NR was performed using 25 nM (NR1-fl), 100 nM (NR2-fl) or 100 nM NR-Mo-heme plus 50 nM – 10 or 20 μ M NR-FAD protein fragments for reconstitution of activity. Proteins were diluted using activity measurement buffer (50 mM MOPS pH 7.0, 50 mM KCl, 5 mM MgAc, 1 mM CaCl₂) in Greiner 96-well plates. The final volume in the well was 120 μ L resulting in a layer thickness of 0.7082 cm. NADH was supplied at a final saturating NADH concentration of 220 μ M (based on its absorption spectrum and $\epsilon_{340} = 6220 \text{ M}^{-1} \text{ cm}^{-1}$). For the measurement of the stoichiometry of NR-FAD fragment to NR-Mo-heme fragment, a saturating nitrate concentration of 2 mM was provided. For steady-state kinetic studies a range of nitrate concentrations from 0 – 10 mM were used. For steady state measurements with the re-constituted NR-activity a 1:50 ratio of NR-Mo-heme (100 nM) to NR-FAD (5 μ M) was used. All measurements were performed in triplicate. Multiple NR-Mo-heme protein batches were tested. The reaction was started

by addition of NADH and nitrate (pre-mixed). The reduction in absorption at 340 nm was followed using a Tecan Sunrise 96 well plate reader with one mole of NADH consumption equivalent to one mole of nitrate reduced. The initial slopes of A_{340} nm consumption were analysed using the Tecan Magellan software to generate the initial velocities (v_i). Triplicate values were used to determine mean and standard error of the mean (SEM) and then plotted and fitted in GraphPad Prism 5 using the 'Michaelis Menten' curve fit to yield k_{cat} and K_M values.

- Methyl viologen:nitrate activity determination

The MV:nitrate activity determination was performed as described (Lambeck et al., 2012) but using a modified buffer (which was the same as the NADH:nitrate activity measurement buffer) (50 mM MOPS pH 7.0, 50 mM KCl, 5 mM MgAc, 1 mM CaCl₂). 25 nM cofactor saturated NR-Mo-heme protein was used in a final volume in the well of 120 μ L. The slope of A_{595} nm was monitored to record consumption of reduced methyl viologen with two moles of reduced MV consumed per one mole of nitrate reduced. Evaluation in GraphPad Prism as described for NADH:nitrate activity. Activity determinations were performed with multiple NR-Mo-heme purification batches on multiple days (n = 33 for NR1-Mo-heme and n = 13 for NR2-Mo-heme).

- Benzyl viologen:nitrite activity determination

The BV:nitrite activity determination was performed using NR-Mo-heme fragments similarly to the MV:nitrate activity determination. The pH optimum for nitrite reduction by NR1-Mo-heme and NR2-Mo-heme was shown to be pH 7.5 (Fig. 21) and therefore the buffer composition for nitrite reduction was: 50 mM MOPS pH 7.5, 50 mM KCl, 5 mM MgAc, 1 mM CaCl₂. A nitrite standard curve (0 – 435 μ M) was prepared fresh from anaerobic sodium nitrite solids for each day of measurement. In general, 50 nM NR1-Mo-heme and 500 nM NR2-Mo-heme protein were required to obtain good measurable initial slopes (unless otherwise indicated in the figure legends). Reduced BV being re-oxidised was followed by absorbance change A_{595} . One mole of BV consumption was equivalent to one mole of nitrite reduced. Activity determinations were performed for multiple NR-Mo-heme purification batches on multiple days (n=21 for NR1-Mo-heme and n=10 for NR2-Mo-heme). The mean K_M and $k_{cat} \pm$ SEM was determined using GraphPad Prism.

- 14-3-3 inhibition in the MV:nitrate or BV:nitrite activity determination methods

For inhibition studies, NR-Mo-heme protein fragments were phosphorylated using calcium dependent kinase 3 (CPK3) for 30 to 60min at RT in buffer (50 mM Bis-Tris/Ac pH 7.0, 50 mM KCl, 5 mM MgCl₂ and 1 mM CaCl₂.) in the presence of 400 μM ATP and 1/10th molar concentration of CPK3 (relative to the concentration of NR-Mo-heme fragment). Inhibition measurements with 14-3-3 were performed using the MV:nitrate or BV:nitrite activity determination measurements and a range of 14-3-3 concentrations from 0 to 316 μM on a log scale and a constant saturating concentration of 432 μM sodium nitrite or 15 mM potassium nitrate. pNR-Mo-heme and 14-3-3 were mixed and incubated for 5 - 15 min before kinetic activity measurement. Reaction velocities were calculated based on the initial slopes of red. MV or red. BV consumption then analysed using GraphPad Prism to yield I_{max} and IC₅₀ data.

- Measurement of NO[•] using the NO-analyzer

For nitric oxide quantification, an NO-analyzer (Sievers NOA 280i, GE Analytical Instruments) and pH 7.5 buffer was used (as for BV:nitrite activity determination). Antifoam Y-30 (Sigma) was supplemented at a rate of 500 μL/L of buffer. An oxygen-free, argon gas stream was bubbled through the glass reaction vessel containing the reaction components in a volume of 3 mL. Reaction components were mixed in the following order: buffer was first placed in the vessel and the vessel was closed. Subsequently, the argon flow rate was adjusted to be equivalent to the vacuum coming from the NO[•] analyzer after which the solution was allowed to bubble and become anaerobic. At timepoint T= 4 min, anaerobic sodium nitrite solution to yield final concentrations of 10 μM to 4 mM (or nitrite + nitrate for inhibition experiments) was added from a sealed vial using a Hamilton syringe, followed at T= 6 min by anaerobic protein mix (100 pmol NR-Mo-heme + 5000 pmol NR-FAD). The reaction was started at T= 8 minutes by addition of NADH solution (220 μM). Steady-state NO[•] release was recorded up to 20 min (or longer). For the evaluation, the areas under the steeply increasing start of the curve were determined (typically for 200 sec) and converted to pmol NO[•] by comparison with the NO[•] standard curve ((MacArthur et al., 2007) Appendix 3). It was assumed that the amount of NO[•] released from the solution in the reaction vessel correlated with the concentration of NO[•] in the solution. Therefore, by converting the amount of NO[•] released from the 3 mL (at a given concentration of substrate nitrite) to pMolar NO[•] per unit time, we could arrive at an estimate of (v_i) of

NO[•] generation and by plotting this against concentration of substrate could generate a Michaelis Menten-like plot from which a pseudo k_{cat} and K_M for nitrite could be determined.

The determination of the inhibition parameters for nitrate was performed by comparing the re-constituted NR-dependent NO[•] release from a 400 μ M nitrite solution (set to 100% activity) with the lowered NO[•] release from solutions containing 400 μ M nitrite mixed with 4 – 1000 μ M nitrate expressed as a percentage of uninhibited NO[•] release. Data were fitted in GraphPad Prism 7 to a [inhibitor] vs response curve to yield IC₅₀ and I_{max}.

For determination of the stoichiometry of NO[•] release from pre-reduced NR2-Mo-heme, one sample of NR2-Mo-heme was pre-reduced, under the anaerobic bench by addition of freshly prepared dithionite solution (~4 mg/mL) while a parallel sample had buffer instead of dithionite added (oxidised control). The samples were then passed through anaerobic-equilibrated PD-10 columns and the spectrum of the protein was then determined in anaerobic cuvettes, sealed before removal from the anaerobic bench in a Perkin Elmer Lambda 265 spectrophotometer (Langenfeld). After confirming that the protein was reduced (in the reduced sample), and determining the concentration based on the A_{424nm} and the ϵ_{424} 91,000 M⁻¹ cm⁻¹ (Skipper et al., 2001), replicate 400 pmol samples were loaded into multiple anaerobic Hamilton syringes and as rapidly as possible, injected into the NO-analyser containing buffer and 400 μ M nitrite solution. The area under the peak of NO[•] released was determined and converted to pmol NO[•] compared with the NO[•] standard curve (Appendix 3).

- Pre-Steady State Kinetics

Pre-steady state kinetics were measured using an Applied Photophysics Inc. SX-20MV stopped-flow instrument at 25 °C using the monochromator detector at 413 nm. pH 7.0 MOPS buffer was used (as for MV:nitrate activity determination). For reaction with nitrate, NR-Mo-heme and (0.5-fold) NR-FAD protein mix was prepared under the anaerobic bench and buffer exchanged into anaerobic buffer using PD-10 columns (GE Healthcare). NADH was added from a stock solution to yield a final concentration of about 0.1 μ M in excess (based on the 340 nm absorption of the protein-NADH mix). A spectrum of the protein was measured using a Perkin Elmer Lambda 265 spectrophotometer (Langenfeld) to ensure it was fully reduced (based on a shift in

heme absorption from 413 nm to 423 nm and the appearance of two typical Soret peaks at ~530 nm and 557 nm. The concentration based on heme for NR2-Mo-heme protein was about 3 μM . The anaerobic protein/NADH solution was loaded in a gas-tight syringe and mounted on the stopped flow instrument. Anaerobic buffer or substrate was loaded on the second port of the stopped flow instrument. Triplicate measurements were made with each substrate concentration and compared with a blank trace (buffer). Curve fitting was performed using the Pro Data Viewer software (Applied Photophysics). A single exponential curve with the formula $a \cdot \exp(-kx) + c$ was fit to the first increase in absorption at 413 nm to yield the k_{obs} for each respective substrate concentration. The k_{obs} were plotted using GraphPad Prism and fit using a 'Michaelis Menten' equation to yield k_{ox} and K_D .

6 References

- Ackerson, C.J., Powell, R.D., and Hainfeld, J.F. (2010). Site-Specific Biomolecule Labeling with Gold Clusters. *481*, 195-230.
- Alber, N.A., Sivanesan, H., and Vanlerberghe, G.C. (2017). The occurrence and control of nitric oxide generation by the plant mitochondrial electron transport chain. *Plant Cell Environ* *40*, 1074-1085.
- Arita, N., Cohen, M., Tokuda, G., and Yamasaki, H. (2006). Fluorometric Detection of Nitric Oxide with Diaminofluoresceins (DAFs): Applications and Limitations for Plant NO Research. pp. 269-280.
- Bachmann, M., Huber, J.L., Liao, P.C., Gage, D.A., and Huber, S.C. (1996a). The inhibitor protein of phosphorylated nitrate reductase from spinach (*Spinacia oleracea*) leaves is a 14-3-3 protein. *Febs Letters* *387*, 127-131.
- Bachmann, M., Shiraishi, N., Campbell, W.H., Yoo, B.C., Harmon, A.C., and Huber, S.C. (1996b). Identification of Ser-543 as the major regulatory phosphorylation site in spinach leaf nitrate reductase. *The Plant cell* *8*, 505-517.
- Barber, M.J., and Notton, B.A. (1990). Spinach Nitrate Reductase : Effects of Ionic Strength and pH on the Full and Partial Enzyme Activities. *Plant physiology* *93*, 537-540.
- Barbier, G.G., and Campbell, W.H. (2005). Viscosity effects on eukaryotic nitrate reductase activity. *The Journal of biological chemistry* *280*, 26049-26054.
- Barroso, J.B., Corpas, F.J., Carreras, A., Sandalio, L.M., Valderrama, R., Palma, J.M., Lupianez, J.A., and del Rio, L.A. (1999). Localization of nitric-oxide synthase in plant peroxisomes. *The Journal of biological chemistry* *274*, 36729-36733.
- Beevers, L., Flesher, D., and Hageman, R.H. (1964). STUDIES ON THE PYRIDINE NUCLEOTIDE SPECIFICITY OF NITRATE REDUCTASE IN HIGHER PLANTS AND ITS RELATIONSHIP TO SULFHYDRYL LEVEL. *Biochim Biophys Acta* *89*, 453-464.
- Beevers, L., and Hageman, R.H. (1983). Uptake and Reduction of Nitrate: Bacteria and Higher Plants. 351-375.
- Beligni, M.V., and Lamattina, L. (2000). Nitric oxide stimulates seed germination and de-etiolation, and inhibits hypocotyl elongation, three light-inducible responses in plants. *Planta* *210*, 215-221.
- Benamar, A., Rolletschek, H., Borisjuk, L., Avelange-Macherel, M.H., Curien, G., Mostefai, H.A., Andriantsitohaina, R., and Macherel, D. (2008). Nitrite-nitric oxide control of mitochondrial respiration at the frontier of anoxia. *Biochim Biophys Acta* *1777*, 1268-1275.
- Bender, D. (2017). PhD thesis: Molecular mechanism of sulfite oxidation and nitrite reduction in vertebrate sulfite oxidase. In PhD thesis (University of Cologne).
- Bender, D., and Schwarz, G. (2018). Nitrite-dependent nitric oxide synthesis by molybdenum enzymes. *FEBS Letters* *592*, 2126-2139.
- Bethke, P.C., Badger, M.R., and Jones, R.L. (2004). Apoplastic synthesis of nitric oxide by plant tissues. *The Plant cell* *16*, 332-341.
- Bethke, P.C., Libourel, I.G., Aoyama, N., Chung, Y.Y., Still, D.W., and Jones, R.L. (2007). The Arabidopsis aleurone layer responds to nitric oxide, gibberellin, and abscisic acid and is sufficient and necessary for seed dormancy. *Plant physiology* *143*, 1173-1188.
- Bird, K. (1981). Electrochemistry of the viologens.
- Bredt, D.S., and Snyder, S.H. (1990). Isolation of nitric oxide synthetase, a calmodulin-requiring enzyme. *Proceedings of the National Academy of Sciences of the United States of America* *87*, 682-685.

- Bright, J., Desikan, R., Hancock, J.T., Weir, I.S., and Neill, S.J. (2006). ABA-induced NO generation and stomatal closure in *Arabidopsis* are dependent on H₂O₂ synthesis. *The Plant journal : for cell and molecular biology* *45*, 113-122.
- Britto, D.T., Siddiqi, M.Y., Glass, A.D., and Kronzucker, H.J. (2001). Futile transmembrane NH₄(+) cycling: a cellular hypothesis to explain ammonium toxicity in plants. *Proceedings of the National Academy of Sciences of the United States of America* *98*, 4255-4258.
- Buchanan, B.B., Gruissem, W., and Jones, R.L. (2015). *Biochemistry and Molecular Biology of Plants*, 2 edn (Wiley Blackwell).
- Butt, Y.K., Lum, J.H., and Lo, S.C. (2003). Proteomic identification of plant proteins probed by mammalian nitric oxide synthase antibodies. *Planta* *216*, 762-771.
- Campbell, W.H. (1988). Nitrate Reductase and Its Role in Nitrate Assimilation in Plants. *Physiol Plantarum* *74*, 214-219.
- Campbell, W.H. (1996). Nitrate reductase biochemistry comes of age. *Plant physiology* *111*, 355-361.
- Campbell, W.H. (1999). NITRATE REDUCTASE STRUCTURE, FUNCTION AND REGULATION: Bridging the Gap between Biochemistry and Physiology. *Annu Rev Plant Physiol Plant Mol Biol* *50*, 277-303.
- Campbell, W.H. (2001). Structure and function of eukaryotic NAD(P)H:nitrate reductase. *CMLS, Cell. Mol. Life Sci.* *58*, 194-204.
- Campbell, W.H., and Remmler, J.L. (1986). Regulation of Corn Leaf Nitrate Reductase : I. Immunochemical Methods for Analysis of the Enzyme's Protein Component. *Plant physiology* *80*, 435-441.
- Campbell, W.H., and Smarrelli, J. (1978). Purification and Kinetics of Higher Plant NADH:Nitrate Reductase. *Plant physiology* *61*, 611-616.
- Canfield, D.E., Glazer, A.N., and Falkowski, P.G. (2010). The evolution and future of Earth's nitrogen cycle. *Science* *330*, 192-196.
- Castro Marín, I., Loeff, I., Bartetzko, L., Searle, I., Coupland, G., Stitt, M., and Osuna, D. (2011). Nitrate regulates floral induction in *Arabidopsis*, acting independently of light, gibberellin and autonomous pathways. *Planta* *233*, 539-552.
- Cereghino, G.P., Cereghino, J.L., Ilgen, C., and Cregg, J.M. (2002). Production of recombinant proteins in fermenter cultures of the yeast *Pichia pastoris*. *Curr Opin Biotechnol* *13*, 329-332.
- Chamizo-Ampudia, A., Sanz-Luque, E., Llamas, A., Ocana-Calahorra, F., Mariscal, V., Carreras, A., Barroso, J.B., Galvan, A., and Fernandez, E. (2016). A dual system formed by the ARC and NR molybdoenzymes mediates nitrite-dependent NO production in *Chlamydomonas*. *Plant Cell Environ* *39*, 2097-2107.
- Cheng, C.L., Acedo, G.N., Cristinsin, M., and Conkling, M.A. (1992). Sucrose mimics the light induction of *Arabidopsis* nitrate reductase gene transcription. *Proceedings of the National Academy of Sciences of the United States of America* *89*, 1861-1864.
- Cheng, C.L., Acedo, G.N., Dewdney, J., Goodman, H.M., and Conkling, M.A. (1991). Differential expression of the two *Arabidopsis* nitrate reductase genes. *Plant physiology* *96*, 275-279.
- Cheng, C.L., Dewdney, J., Nam, H.G., den Boer, B.G., and Goodman, H.M. (1988). A new locus (NIA 1) in *Arabidopsis thaliana* encoding nitrate reductase. *The EMBO journal* *7*, 3309-3314.
- Chi, J.C. (2012). Dissertation- Molecular mechanism of 14-3-3-mediated inhibition of Plant Nitrate Reductase.

- Chi, J.C., Roeper, J., Schwarz, G., and Fischer-Schrader, K. (2015). Dual binding of 14-3-3 protein regulates Arabidopsis nitrate reductase activity. *Journal of biological inorganic chemistry : JBIC : a publication of the Society of Biological Inorganic Chemistry* 20, 277-286.
- Childers, K.C., and Garcin, E.D. (2018). Structure/function of the soluble guanylyl cyclase catalytic domain. *Nitric oxide : biology and chemistry* 77, 53-64.
- Cookson, S.J., Williams, L.E., and Miller, A.J. (2005). Light-Dark Changes in Cytosolic Nitrate Pools Depend on Nitrate Reductase Activity in Arabidopsis Leaf Cells. *Plant physiology* 138, 1097-1105.
- Corpas, F.J., Barroso, J.B., Carreras, A., Quiros, M., Leon, A.M., Romero-Puertas, M.C., Esteban, F.J., Valderrama, R., Palma, J.M., Sandalio, L.M., *et al.* (2004). Cellular and subcellular localization of endogenous nitric oxide in young and senescent pea plants. *Plant physiology* 136, 2722-2733.
- Corpas, F.J., Palma, J.M., Del Rio, L.A., and Barroso, J.B. (2013). Protein tyrosine nitration in higher plants grown under natural and stress conditions. *Front Plant Sci* 4, 29.
- Correa-Aragunde, N., Graziano, M., Chevalier, C., and Lamattina, L. (2006). Nitric oxide modulates the expression of cell cycle regulatory genes during lateral root formation in tomato. *Journal of experimental botany* 57, 581-588.
- Crawford, N.M. (2005). Mechanisms for nitric oxide synthesis in plants. *Journal of experimental botany* 57, 471-478.
- Crawford, N.M., and Glass, A.D.M. (1998). Molecular and physiological aspects of nitrate uptake in plants. *Trends Plant Science* 3, 389-395.
- Cregg, J.M., Tolstorukov, I., Kusari, A., Sunga, J., Madden, K., and Chappell, T. (2009). Expression in the yeast *Pichia pastoris*. *Methods Enzymol* 463.
- Dailey, F.A., Kuo, T., and Warner, R.L. (1982). Pyridine nucleotide specificity of barley nitrate reductase. *Plant physiology* 69, 1196-1199.
- Dean, J.V., and Harper, J.E. (1986). Nitric Oxide and Nitrous Oxide Production by Soybean and Winged Bean during the *in vivo* Nitrate Reductase Assay. *Plant physiology* 82, 718-723.
- Dean, J.V., and Harper, J.E. (1988). The Conversion of Nitrite to Nitrogen Oxide(s) by the Constitutive NAD(P)H-Nitrate Reductase Enzyme from Soybean. *Plant physiology* 88, 389-395.
- Del Castello, F., Nejamkin, A., Cassia, R., Correa-Aragunde, N., Fernandez, B., Foresi, N., Lombardo, C., Ramirez, L., and Lamattina, L. (2019). The era of nitric oxide in plant biology: Twenty years tying up loose ends. *Nitric Oxide*.
- DeLano, W. (2002). The PyMOL Molecular Graphics System (2002) DeLano Scientific, Palo Alto, CA, USA. <http://www.pymol.org>.
- DeLille, J.M., Sehnke, P.C., and Ferl, R.J. (2001). The arabidopsis 14-3-3 family of signaling regulators. *Plant physiology* 126, 35-38.
- Delledonne, M., Xia, Y., Dixon, R.A., and Lamb, C. (1998). Nitric oxide functions as a signal in plant disease resistance. *Nature* 394, 585-588.
- Deng, M.D., Moureaux, T., Leydecker, M.T., and Caboche, M. (1990). Nitrate-reductase expression is under the control of a circadian rhythm and is light inducible in *Nicotiana tabacum* leaves. *Planta* 180, 257-261.
- Desikan, R., Griffiths, R., Hancock, J., and Neill, S. (2002). A new role for an old enzyme: nitrate reductase-mediated nitric oxide generation is required for abscisic acid-induced stomatal closure in *Arabidopsis thaliana*. *Proceedings of the National Academy of Sciences of the United States of America* 99, 16314-16318.

- Erismann, J.W., Sutton, M.A., Galloway, J., Klimont, Z., and Winiwarter, W. (2008). How a century of ammonia synthesis changed the world. *Nature Geosci* 1, 636-639.
- Evans, H.J., and Nason, A. (1953). Pyridine Nucleotide-Nitrate Reductase from Extracts of Higher Plants. *Plant physiology* 28, 233-254.
- Felle, H.H. (2005). pH regulation in anoxic plants. *Annals of botany* 96, 519-532.
- Feng, C., Kedia, R.V., Hazzard, J.T., Hurley, J.K., Tollin, G., and Enemark, J.H. (2002). Effect of solution viscosity on intramolecular electron transfer in sulfite oxidase. *Biochemistry* 41, 5816-5821.
- Feng, J., Chen, L., and Zuo, J. (2019). Protein S-Nitrosylation in Plants: Current Progresses and Challenges. *J Integr Plant Biol*.
- Fischer, K., Barbier, G.G., Hecht, H.J., Mendel, R.R., Campbell, W.H., and Schwarz, G. (2005). Structural basis of eukaryotic nitrate reduction: crystal structures of the nitrate reductase active site. *The Plant cell* 17, 1167-1179.
- Focht, D., Croll, T.I., Pedersen, B.P., and Nissen, P. (2017). Improved Model of Proton Pump Crystal Structure Obtained by Interactive Molecular Dynamics Flexible Fitting Expands the Mechanistic Model for Proton Translocation in P-Type ATPases. *Front Physiol* 8, 202.
- Forde, B., and Clarkson, D. (1999). Nitrate and Ammonium Nutrition of Plants: Physiological and Molecular Perspectives, Vol 30.
- Forde, B., and Zhang, H.M. (1998). ... response: Nitrate and root branching. *Trends in plant science* 3, 204-205.
- Fredes, I., Moreno, S., Díaz, F.P., and Gutiérrez, R.A. (2019). Nitrate signaling and the control of Arabidopsis growth and development. *Current opinion in plant biology* 47, 112-118.
- Fuhrmann, M., Hausherr, A., Ferbitz, L., Schödl, T., Heitzer, M., and Hegemann, P. (2004). Monitoring dynamic expression of nuclear genes in *Chlamydomonas reinhardtii* by using a synthetic luciferase reporter gene. *Plant Molecular Biology* 55, 869-881.
- Garcia-Mata, C., Gay, R., Sokolovski, S., Hills, A., Lamattina, L., and Blatt, M.R. (2003). Nitric oxide regulates K⁺ and Cl⁻ channels in guard cells through a subset of abscisic acid-evoked signaling pathways. *Proceedings of the National Academy of Sciences of the United States of America* 100, 11116-11121.
- Giglioli-Guivarc'h, N., Pierre, J.N., Vidal, J., and Brown, S. (1996). Flow cytometric analysis of cytosolic pH of mesophyll cell protoplasts from the crabgrass *Digitaria sanguinalis*. *Cytometry* 23, 241-249.
- Gross, F., Durner, J., and Gaupels, F. (2013). Nitric oxide, antioxidants and prooxidants in plant defence responses. *Front Plant Sci* 4, 419.
- Guerra, D., Ballard, K., Truebridge, I., and Vierling, E. (2016). S-Nitrosation of Conserved Cysteines Modulates Activity and Stability of S-Nitrosogluthathione Reductase (GSNOR). *Biochemistry* 55, 2452-2464.
- Guo, F.-Q., Okamoto, M., and Crawford, N.M. (2003). Identification of a Plant Nitric Oxide Synthase Gene Involved in Hormonal Signaling. *Science* 302, 100-103.
- Hancock, J.T., and Neill, S.J. (2019). Nitric Oxide: Its Generation and Interactions with Other Reactive Signaling Compounds. *Plants (Basel)* 8.
- Hao, F., Zhao, S., Dong, H., Zhang, H., Sun, L., and Miao, C. (2010). Nia1 and Nia2 are involved in exogenous salicylic acid-induced nitric oxide generation and stomatal closure in Arabidopsis. *J Integr Plant Biol* 52, 298-307.
- Harper, J.E. (1981). Evolution of Nitrogen Oxide(s) during *In vivo* Nitrate Reductase Assay of Soybean Leaves. *Plant physiology* 68, 1488-1493.

Harrison, R. (2002). Structure and function of xanthine oxidoreductase: where are we now? *Free Radic Biol Med* 33, 774-797.

Hedfalk, K., Pettersson, N., Oberg, F., Hohmann, S., and Gordon, E. (2008). Production, characterization and crystallization of the Plasmodium falciparum aquaporin. *Protein expression and purification* 59, 69-78.

Hooper, C.M., Castleden, I.R., Tanz, S.K., Aryamanesh, N., and Millar, A.H. (2017). SUBA4: the interactive data analysis centre for Arabidopsis subcellular protein locations. *Nucleic Acids Res* 45, D1064-D1074.

Hruz, T., Laule, O., Szabo, G., Wessendorp, F., Bleuler, S., Oertle, L., Widmayer, P., Gruissem, W., and Zimmermann, P. (2008). Genevestigator v3: a reference expression database for the meta-analysis of transcriptomes. *Adv Bioinformatics* 2008, 420747.

Hyde, G.E., and Campbell, W.H. (1990). High-level expression in Escherichia coli of the catalytically active flavin domain of corn leaf NADH:nitrate reductase and its comparison to human NADH:cytochrome B5 reductase. *Biochem Biophys Res Commun* 168, 1285-1291.

Ignarro, L.J., Buga, G.M., Wood, K.S., Byrns, R.E., and Chaudhuri, G. (1987). Endothelium-derived relaxing factor produced and released from artery and vein is nitric oxide. *Proceedings of the National Academy of Sciences of the United States of America* 84, 9265-9269.

Jaspert, N., Throm, C., and Oecking, C. (2011). Arabidopsis 14-3-3 proteins: fascinating and less fascinating aspects. *Front Plant Sci* 2, 96.

Jih, P.J., Chen, Y.C., and Jeng, S.T. (2003). Involvement of hydrogen peroxide and nitric oxide in expression of the ipomoelin gene from sweet potato. *Plant physiology* 132, 381-389.

Jolly, S.O., Campbell, W., and Tolbert, N.E. (1976). NADPH- and NADH-nitrate reductases from soybean leaves. *Arch Biochem Biophys* 174, 431-439.

Jonassen, E.M., Sandsmark, B.A., and Lillo, C. (2009a). Unique status of NIA2 in nitrate assimilation: NIA2 expression is promoted by HY5/HYH and inhibited by PIF4. *Plant Signal Behav* 4, 1084-1086.

Jonassen, E.M., Sevin, D.C., and Lillo, C. (2009b). The bZIP transcription factors HY5 and HYH are positive regulators of the main nitrate reductase gene in Arabidopsis leaves, NIA2, but negative regulators of the nitrate uptake gene NRT1.1. *J Plant Physiol* 166, 2071-2076.

Kaiser, W.M., and Brendle-Behnisch, E. (1991). Rapid Modulation of Spinach Leaf Nitrate Reductase Activity by Photosynthesis : I. Modulation *in vivo* by CO₂ Availability. *Plant physiology* 96, 363-367.

Kaiser, W.M., and Brendlebehnisch, E. (1995). Acid-Base-Modulation of Nitrate Reductase in Leaf Tissues. *Planta* 196, 1-6.

Kaiser, W.M., and Huber, S.C. (2001). Post-translational regulation of nitrate reductase: mechanism, physiological relevance and environmental triggers. *Journal of experimental botany* 52, 1981-1989.

Kaiser, W.M., Weiner, H., Kandlbinder, A., Tsai, C.B., Rockel, P., Sonoda, M., and Planchet, E. (2002). Modulation of nitrate reductase: some new insights, an unusual case and a potentially important side reaction. *Journal of experimental botany* 53, 875-882.

Keicher, J., Jaspert, N., Weckermann, K., Möller, C., Throm, C., Kintzi, A., and Oecking, C. (2017). Arabidopsis 14-3-3 epsilon members contribute to polarity of PIN auxin carrier and auxin transport-related development. *eLife* 6, e24336.

Kisker, C., Schindelin, H., Pacheco, A., Wehbi, W.A., Garrett, R.M., Rajagopalan, K.V., Enemark, J.H., and Rees, D.C. (1997). Molecular Basis of Sulfite Oxidase Deficiency from the Structure of Sulfite Oxidase. *Cell* 91, 973-983.

Klepper, L. (1979). Nitric oxide (NO) and nitrogen dioxide (NO₂) emissions from herbicide-treated soybean plants. *Atmospheric Environment (1967)* 13, 537-542.

- Klepper, L. (1990). Comparison between NO(x) Evolution Mechanisms of Wild-Type and nr(1) Mutant Soybean Leaves. *Plant physiology* *93*, 26-32.
- Konishi, M., and Yanagisawa, S. (2011a). The regulatory region controlling the nitrate-responsive expression of a nitrate reductase gene, NIA1, in Arabidopsis. *Plant Cell Physiol* *52*, 824-836.
- Konishi, M., and Yanagisawa, S. (2011b). Roles of the transcriptional regulation mediated by the nitrate-responsive cis-element in higher plants. *Biochem Biophys Res Commun* *411*, 708-713.
- Krainer, F.W., Capone, S., Jäger, M., Vogl, T., Gerstmann, M., Glieder, A., Herwig, C., and Spadiut, O. (2015). Optimizing cofactor availability for the production of recombinant heme peroxidase in *Pichia pastoris*. *Microbial Cell Factories* *14*, 4.
- Krainer, F.W., Dietzsch, C., Hajek, T., Herwig, C., Spadiut, O., and Glieder, A. (2012). Recombinant protein expression in *Pichia pastoris* strains with an engineered methanol utilization pathway. *Microb Cell Fact* *11*.
- Kronzucker, H., Glass, A., Siddiqi, M.Y., and Kirk, G. (2000). Comparative kinetic analysis of ammonium and nitrate acquisition by tropical lowland rice: Implications for rice cultivation and yield potential, Vol 145.
- Krouk, G., Crawford, N.M., Coruzzi, G.M., and Tsay, Y.F. (2010). Nitrate signaling: adaptation to fluctuating environments. *Current opinion in plant biology* *13*, 266-273.
- Kubo, Y., Ogura, N., and Nakagawa, H. (1988). Limited proteolysis of the nitrate reductase from spinach leaves. *The Journal of biological chemistry* *263*, 19684-19689.
- Kwon, K.-C., Chan, H.-T., León, I.R., Williams-Carrier, R., Barkan, A., and Daniell, H. (2016). Codon Optimization to Enhance Expression Yields Insights into Chloroplast Translation. *Plant physiology* *172*, 62-77.
- Laemmli, U.K. (1970). Cleavage of structural proteins during the assembly of the head of bacteriophage T4. *Nature* *227*, 680-685.
- Lam, H.M., Coschigano, K.T., Oliveira, I.C., Melo-Oliveira, R., and Coruzzi, G.M. (1996). THE MOLECULAR-GENETICS OF NITROGEN ASSIMILATION INTO AMINO ACIDS IN HIGHER PLANTS. *Annu Rev Plant Physiol Plant Mol Biol* *47*, 569-593.
- Lamas, S., Marsden, P.A., Li, G.K., Tempst, P., and Michel, T. (1992). Endothelial nitric oxide synthase: molecular cloning and characterization of a distinct constitutive enzyme isoform. *Proceedings of the National Academy of Sciences of the United States of America* *89*, 6348-6352.
- Lambeck, I. (2009). Dissertation. Inhibition NR durch 14-3-3. In *Mathematisch Naturwissenschaftliche Fakultät (University of Cologne)*, p. 126.
- Lambeck, I., Chi, J.C., Krizowski, S., Mueller, S., Mehler, N., Teige, M., Fischer, K., and Schwarz, G. (2010). Kinetic analysis of 14-3-3-inhibited *Arabidopsis thaliana* nitrate reductase. *Biochemistry* *49*, 8177-8186.
- Lambeck, I.C., Fischer-Schrader, K., Niks, D., Roeper, J., Chi, J.C., Hille, R., and Schwarz, G. (2012). Molecular mechanism of 14-3-3 protein-mediated inhibition of plant nitrate reductase. *The Journal of biological chemistry* *287*, 4562-4571.
- Lawrence, A.M., and Besir, H.U. (2009). Staining of proteins in gels with Coomassie G-250 without organic solvent and acetic acid. *J Vis Exp*.
- Lea, U.S., Leydecker, M.T., Quillere, I., Meyer, C., and Lillo, C. (2006). Posttranslational regulation of nitrate reductase strongly affects the levels of free amino acids and nitrate, whereas transcriptional regulation has only minor influence. *Plant physiology* *140*, 1085-1094.

- Lea, U.S., ten Hoopen, F., Provan, F., Kaiser, W.M., Meyer, C., and Lillo, C. (2004). Mutation of the regulatory phosphorylation site of tobacco nitrate reductase results in high nitrite excretion and NO emission from leaf and root tissue. *Planta* *219*, 59-65.
- Lejay, L., Tillard, P., Lepetit, M., Olive, F., Filleur, S., Daniel-Vedele, F., and Gojon, A. (1999). Molecular and functional regulation of two NO₃⁻ uptake systems by N- and C-status of Arabidopsis plants. *The Plant journal : for cell and molecular biology* *18*, 509-519.
- Lillo, C., Lea, U.S., Leydecker, M.T., and Meyer, C. (2003). Mutation of the regulatory phosphorylation site of tobacco nitrate reductase results in constitutive activation of the enzyme *in vivo* and nitrite accumulation. *The Plant journal : for cell and molecular biology* *35*, 566-573.
- Lillo, C., Meyer, C., Provan, F., Oltedal, S., and Lea, U.S. (2004). Mechanism and importance of post-translational regulation of nitrate reductase. *Journal of experimental botany* *55*, 1275-1282.
- Lin, Y., and Cheng, C.L. (1997). A chlorate-resistant mutant defective in the regulation of nitrate reductase gene expression in Arabidopsis defines a new HY locus. *The Plant cell* *9*, 21-35.
- Lin, Y., Hwang, C.F., Brown, J.B., and Cheng, C.L. (1994). 5' proximal regions of Arabidopsis nitrate reductase genes direct nitrate-induced transcription in transgenic tobacco. *Plant physiology* *106*, 477-484.
- Looser, V., Bruhlmann, B., Bumbak, F., Stenger, C., Costa, M., Camattari, A., Fotiadis, D., and Kovar, K. (2015). Cultivation strategies to enhance productivity of *Pichia pastoris*: A review. *Biotechnology Advances* *33*, 1177-1193.
- Lozano-Juste, J., and Leon, J. (2010). Enhanced Abscisic Acid-Mediated Responses in *nia1nia2noa1-2* Triple Mutant Impaired in NIA/NR-and AtNOA1-Dependent Nitric Oxide Biosynthesis in Arabidopsis. *Plant physiology* *152*, 891-903.
- Lu, G., Campbell, W.H., Schneider, G., and Lindqvist, Y. (1994). Crystal structure of the FAD-containing fragment of corn nitrate reductase at 2.5Å resolution: relationship to other flavoprotein reductases. *Structure* *2*, 809-821.
- MacArthur, P.H., Shiva, S., and Gladwin, M.T. (2007). Measurement of circulating nitrite and S-nitrosothiols by reductive chemiluminescence. *J Chromatogr B Analyt Technol Biomed Life Sci* *851*, 93-105.
- Maia, L.B., and Moura, J.J. (2015). Nitrite reduction by molybdoenzymes: a new class of nitric oxide-forming nitrite reductases. *Journal of biological inorganic chemistry : JBIC : a publication of the Society of Biological Inorganic Chemistry* *20*, 403-433.
- Masclaux-Daubresse, C., Reisdorf-Cren, M., Pageau, K., Lelandais, M., Grandjean, O., Kronenberger, J., Valadier, M.-H., Feraud, M., Jouglet, T., and Suzuki, A. (2006). Glutamine Synthetase-Glutamate Synthase Pathway and Glutamate Dehydrogenase Play Distinct Roles in the Sink-Source Nitrogen Cycle in Tobacco. *Plant physiology* *140*, 444-456.
- Matasci, N., Hung, L.H., Yan, Z., Carpenter, E.J., Wickett, N.J., Mirarab, S., Nguyen, N., Warnow, T., Ayyampalayam, S., Barker, M., *et al.* (2014). Data access for the 1,000 Plants (1KP) project. *Gigascience* *3*, 17.
- Medici, A., and Krouk, G. (2014). The Primary Nitrate Response: a multifaceted signalling pathway. *Journal of experimental botany* *65*, 5567-5576.
- Mertens, J.A., Shiraishi, N., and Campbell, W.H. (2000). Recombinant Expression of Molybdenum Reductase Fragments of Plant Nitrate Reductase at High Levels in *Pichia pastoris*. *Plant physiology* *123*, 743-756.
- Michaelis, L., and Hill, E.S. (1933). THE VIOLAGEN INDICATORS. *The Journal of general physiology* *16*, 859-873.

- Michelet, B., and Boutry, M. (1995). The Plasma Membrane H⁺-ATPase (A Highly Regulated Enzyme with Multiple Physiological Functions). *Plant physiology* *108*, 1-6.
- Miller, A.J., Fan, X., Orsel, M., Smith, S.J., and Wells, D.M. (2007). Nitrate transport and signalling. *Journal of experimental botany* *58*, 2297-2306.
- Miller, A.J., and Smith, S.J. (2008). Cytosolic nitrate ion homeostasis: could it have a role in sensing nitrogen status? *Annals of botany* *101*, 485-489.
- Mlodzinska, E., Klobus, G., Christensen, M.D., and Fuglsang, A.T. (2015). The plasma membrane H⁽⁺⁾-ATPase *AHA2* contributes to the root architecture in response to different nitrogen supply. *Physiol Plant* *154*, 270-282.
- Modolo, L.V., Augusto, O., Almeida, I.M.G., Magalhaes, J.R., and Salgado, I. (2005). Nitrite as the major source of nitric oxide production by *Arabidopsis thaliana* in response to *Pseudomonas syringae*. *FEBS Letters* *579*, 3814-3820.
- Modolo, L.V., Augusto, O., Almeida, I.M.G., Pinto-Maglio, C.A.F., Oliveira, H.C., Seligman, K., and Salgado, I. (2006). Decreased arginine and nitrite levels in nitrate reductase-deficient *Arabidopsis thaliana* plants impair nitric oxide synthesis and the hypersensitive response to *Pseudomonas syringae*. *Plant Science* *171*, 34-40.
- Modolo, L.V., Cunha, F.Q., Braga, M.R., and Salgado, I. (2002). Nitric oxide synthase-mediated phytoalexin accumulation in soybean cotyledons in response to the *Diaporthe phaseolorum* f. sp. *meridionalis* elicitor. *Plant physiology* *130*, 1288-1297.
- Mohn, M.A. (2016). Recombinant expression and biochemical evaluation of higher-plant nitrate reductase. In Department of chemistry, Institute for biochemistry (University of Cologne), pp. 1-76.
- Moncada, S., Palmer, R.M., and Higgs, E.A. (1989). Biosynthesis of nitric oxide from L-arginine. A pathway for the regulation of cell function and communication. *Biochem Pharmacol* *38*, 1709-1715.
- Moore, B.W., and Perez, V.J. (1967). Specific acidic proteins of the nervous system.
- Neill, S., Barros, R., Bright, J., Desikan, R., Hancock, J., Harrison, J., Morris, P., Ribeiro, D., and Wilson, I. (2008). Nitric oxide, stomatal closure, and abiotic stress. *Journal of experimental botany* *59*, 165-176.
- Neill, S.J., Desikan, R., Clarke, A., and Hancock, J.T. (2002). Nitric oxide is a novel component of abscisic acid signaling in stomatal guard cells. *Plant physiology* *128*, 13-16.
- Obsil, T., and Obsilova, V. (2011). Structural basis of 14-3-3 protein functions. *Semin Cell Dev Biol* *22*, 663-672.
- Orozco-Cardenas, M.L., and Ryan, C.A. (2002). Nitric oxide negatively modulates wound signaling in tomato plants. *Plant physiology* *130*, 487-493.
- Palmer, T., Santini, C.L., Iobbi-Nivol, C., Eaves, D.J., Boxer, D.H., and Giordano, G. (1996). Involvement of the *narJ* and *mob* gene products in distinct steps in the biosynthesis of the molybdoenzyme nitrate reductase in *Escherichia coli*. *Mol Microbiol* *20*, 875-884.
- Parani, M., Rudrabhatla, S., Myers, R., Weirich, H., Smith, B., Leaman, D.W., and Goldman, S.L. (2004). Microarray analysis of nitric oxide responsive transcripts in *Arabidopsis*. *Plant Biotechnol J* *2*, 359-366.
- Parinov, S., Sevugan, M., Ye, D., Yang, W.C., Kumaran, M., and Sundaresan, V. (1999). Analysis of flanking sequences from dissociation insertion lines: a database for reverse genetics in *Arabidopsis*. *The Plant cell* *11*, 2263-2270.
- Penczek, P.A., and Asturias, F.J. (2014). Ab initio cryo-EM structure determination as a validation problem. In 2014 IEEE International Conference on Image Processing (ICIP), pp. 2090-2094.

- Pettersen, E.F., Goddard, T.D., Huang, C.C., Couch, G.S., Greenblatt, D.M., Meng, E.C., and Ferrin, T.E. (2004). UCSF Chimera--a visualization system for exploratory research and analysis. *Journal of computational chemistry* 25, 1605-1612.
- Pickenhahn, A. (2015). Structural characterization of 14-3-3 ω in complex with nitrate reductase. (University of Cologne).
- Pittman, J.K. (2012). Multiple Transport Pathways for Mediating Intracellular pH Homeostasis: The Contribution of H(+)/ion Exchangers. *Frontiers in plant science* 3, 11-11.
- Planchet, E. (2006). Nitric oxide production in plant. *Plant Signaling & Behavior* 1, 46-51.
- Planchet, E., Jagadis Gupta, K., Sonoda, M., and Kaiser, W.M. (2005). Nitric oxide emission from tobacco leaves and cell suspensions: rate limiting factors and evidence for the involvement of mitochondrial electron transport. *The Plant journal : for cell and molecular biology* 41, 732-743.
- Pollock, V.V., Conover, R.C., Johnson, M.K., and Barber, M.J. (2002). Bacterial expression of the molybdenum domain of assimilatory nitrate reductase: production of both the functional molybdenum-containing domain and the nonfunctional tungsten analog. *Arch Biochem Biophys* 403, 237-248.
- Prado, A.M., Porterfield, D.M., and Feijo, J.A. (2004). Nitric oxide is involved in growth regulation and re-orientation of pollen tubes. *Development* 131, 2707-2714.
- Provan, F., Aksland, L.-M., Meyer, C., and Lillo, C. (2000). Deletion of the Nitrate Reductase N-Terminal Domain Still Allows Binding of 14-3-3 Proteins but Affects Their Inhibitory Properties. *Plant physiology* 123, 757-764.
- Quinn, G.B., Trimboli, A.J., Prosser, I.M., and Barber, M.J. (1996). Spectroscopic and kinetic properties of a recombinant form of the flavin domain of spinach NADH:Nitrate reductase. *Archives of Biochemistry and Biophysics* 327, 151-160.
- Ratnam, K., Shiraishi, N., Campbell, W.H., and Hille, R. (1996). Spectroscopic and kinetic characterization of cytochrome c reductase domain of nitrate reductase. *Faseb Journal* 10, 2926-2926.
- Redinbaugh, M.G., and Campbell, W.H. (1985). Quaternary structure and composition of squash NADH:nitrate reductase. *The Journal of biological chemistry* 260, 3380-3385.
- Remmler, J.L., and Campbell, W.H. (1986). Regulation of Corn Leaf Nitrate Reductase : II. Synthesis and Turnover of the Enzyme's Activity and Protein. *Plant physiology* 80, 442-447.
- Ribeiro, D.M., Desikan, R., Bright, J.O., Confraria, A.N.A., Harrison, J., Hancock, J.T., Barros, R.S., Neill, S.J., and Wilson, I.D. (2009). Differential requirement for NO during ABA-induced stomatal closure in turgid and wilted leaves. *Plant, Cell & Environment* 32, 46-57.
- Ribeiro, E.A., Jr., Cunha, F.Q., Tamashiro, W.M., and Martins, I.S. (1999). Growth phase-dependent subcellular localization of nitric oxide synthase in maize cells. *FEBS Lett* 445, 283-286.
- Ritenour, G.L., Joy, K.W., Bunning, J., and Hageman, R.H. (1967). Intracellular Localization of Nitrate Reductase, Nitrite Reductase, and Glutamic Acid Dehydrogenase in Green Leaf Tissue. *Plant physiology* 42, 233.
- Robin, P., Streit, L., Campbell, W.H., and Harper, J.E. (1985). Immunochemical Characterization of Nitrate Reductase Forms from Wild-Type (cv Williams) and nr(1) Mutant Soybean. *Plant physiology* 77, 232-236.
- Rockel, P., Strube, F., Rockel, A., Wildt, J., and Kaiser, W.M. (2002). Regulation of nitric oxide (NO) production by plant nitrate reductase *in vivo* and *in vitro*. *Journal of experimental botany* 53, 103-110.

- Savidov, N.A., Tokarev, B.I., and Lips, S.H. (1997). Regulation of Mo-cofactor, NADH- and NAD(P)H-specific nitrate reductase activities in the wild type and two nar-mutant lines of barley (*Hordeum vulgare* L.). *Journal of experimental botany* *48*, 847-855.
- Schwarz, G., Boxer, D.H., and Mendel, R.R. (1997). Molybdenum cofactor biosynthesis. The plant protein Cnx1 binds molybdopterin with high affinity. *The Journal of biological chemistry* *272*, 26811-26814.
- Sehnke, P.C., Rosenquist, M., Alsterfjord, M., DeLille, J., Sommarin, M., Larsson, C., and Ferl, R.J. (2002). Evolution and isoform specificity of plant 14-3-3 proteins. *Plant Mol Biol* *50*, 1011-1018.
- Seligman, K., Saviani, E.E., Oliveira, H.C., Pinto-Maglio, C.A., and Salgado, I. (2008). Floral transition and nitric oxide emission during flower development in *Arabidopsis thaliana* is affected in nitrate reductase-deficient plants. *Plant Cell Physiol* *49*, 1112-1121.
- Shen, T.C. (1972). Nitrate reductase of rice seedlings and its induction by organic nitro-compounds. *Plant physiology* *49*, 546-549.
- Shi, F.M., and Li, Y.Z. (2008). *Verticillium dahliae* toxins-induced nitric oxide production in *Arabidopsis* is major dependent on nitrate reductase. *BMB Rep* *41*, 79-85.
- Shiraishi, N., Kubo, Y., Takeba, G., Kiyota, S., Sakano, K., and Nakagawa, H. (1991). Sequence-Analysis of Cloned Cdna and Proteolytic Fragments for Nitrate Reductase from *Spinacia-Oleracea* L. *Plant and Cell Physiology* *32*, 1031-1038.
- Sjöhamn, J., Conner, M.T., Bill, R.M., and Hedfalk, K. (2011). Improving recombinant eukaryotic membrane protein yields in *Pichia pastoris*: The importance of codon optimization and clone selection AU - Öberg, Fredrik. *Molecular Membrane Biology* *28*, 398-411.
- Skipper, L., Campbell, W.H., Mertens, J.A., and Lowe, D.J. (2001). Pre-steady-state kinetic analysis of recombinant *Arabidopsis* NADH:nitrate reductase: rate-limiting processes in catalysis. *The Journal of biological chemistry* *276*, 26995-27002.
- Smil, V. (2002). Nitrogen and food production: proteins for human diets. *Ambio* *31*, 126-131.
- Smil, V. (2011). Nitrogen Cycle and World Food Production. *World Agriculture* *2*, 9-13.
- Solomonson, L.P., and Barber, M.J. (1990). Assimilatory Nitrate Reductase: Functional Properties and Regulation. *Annu Rev Plant Phys* *41*, 225-253.
- Solomonson, L.P., McCreery, M.J., Kay, C.J., and Barber, M.J. (1987). Radiation inactivation analysis of assimilatory NADH:nitrate reductase. Apparent functional sizes of partial activities associated with intact and proteolytically modified enzyme. *The Journal of biological chemistry* *262*, 8934-8939.
- Sparacino-Watkins, C.E., Tejero, J., Sun, B., Gauthier, M.C., Thomas, J., Ragireddy, V., Merchant, B.A., Wang, J., Azarov, I., Basu, P., *et al.* (2014). Nitrite reductase and nitric-oxide synthase activity of the mitochondrial molybdopterin enzymes mARC1 and mARC2. *The Journal of biological chemistry* *289*, 10345-10358.
- Stitt, M. (1999). Nitrate regulation of metabolism and growth. *Current opinion in plant biology* *2*, 178-186.
- Streit, L., Nelson, R.S., and Harper, J.E. (1985). Nitrate Reductases from Wild-Type and nr(1)-Mutant Soybean (*Glycine max* [L.] Merr.) Leaves : I. Purification, Kinetics, and Physical Properties. *Plant physiology* *78*, 80-84.
- Su, W., Huber, S.C., and Crawford, N.M. (1996). Identification *in vitro* of a post-translational regulatory site in the hinge 1 region of *Arabidopsis* nitrate reductase. *The Plant cell* *8*, 519-527.
- Su, W., Mertens, J.A., Kanamaru, K., Campbell, W.H., and Crawford, N.M. (1997). Analysis of wild-type and mutant plant nitrate reductase expressed in the methylotrophic yeast *Pichia pastoris*. *Plant physiology* *115*, 1135-1143.

- Sudhamsu, J., Lee, G.I., Klessig, D.F., and Crane, B.R. (2008). The structure of YqeH. An AtNOS1/AtNOA1 ortholog that couples GTP hydrolysis to molecular recognition. *The Journal of biological chemistry* 283, 32968-32976.
- Sugden, C., Donaghy, P.G., Halford, N.G., and Hardie, D.G. (1999). Two SNF1-related protein kinases from spinach leaf phosphorylate and inactivate 3-hydroxy-3-methylglutaryl-coenzyme A reductase, nitrate reductase, and sucrose phosphate synthase *in vitro*. *Plant physiology* 120, 257-274.
- Taoka, K., Ohki, I., Tsuji, H., Furuita, K., Hayashi, K., Yanase, T., Yamaguchi, M., Nakashima, C., Purwestri, Y.A., Tamaki, S., *et al.* (2011). 14-3-3 proteins act as intracellular receptors for rice Hd3a florigen. *Nature* 476, 332-335.
- The Arabidopsis Genome, I. (2000). Analysis of the genome sequence of the flowering plant *Arabidopsis thaliana*. *Nature* 408, 796.
- Thomas, D.D. (2015). Breathing new life into nitric oxide signaling: A brief overview of the interplay between oxygen and nitric oxide. *Redox biology* 5, 225-233.
- Thomas, D.D., Liu, X., Kantrow, S.P., and Lancaster, J.R., Jr. (2001). The biological lifetime of nitric oxide: implications for the perivascular dynamics of NO and O₂. *Proceedings of the National Academy of Sciences of the United States of America* 98, 355-360.
- Tischner, R. (2000). Nitrate uptake and reduction in higher and lower plants. *Plant, Cell & Environment* 23, 1005-1024.
- Towbin, H., Staehelin, T., and Gordon, J. (1979). Electrophoretic transfer of proteins from polyacrylamide gels to nitrocellulose sheets: procedure and some applications. *Proceedings of the National Academy of Sciences of the United States of America* 76, 4350-4354.
- Trewavas, A. (1983). Nitrate as a Plant Hormone. *J Sci Food Agr* 34, 939-940.
- Vitousek, P.M., and Howarth, R.W. (1991). Nitrogen Limitation on Land and in the Sea - How Can It Occur. *Biogeochemistry* 13, 87-115.
- Vohwinkel, L. (2017). Kinetic characterization of the human mitochondrial amidoxime reducing component. In Institute for Biochemistry, Department of Chemistry (Cologne, University of Cologne).
- Wang, J., Krizowski, S., Fischer-Schrader, K., Niks, D., Tejero, J., Sparacino-Watkins, C., Wang, L., Ragireddy, V., Frizzell, S., Kelley, E.E., *et al.* (2015). Sulfite Oxidase Catalyzes Single-Electron Transfer at Molybdenum Domain to Reduce Nitrite to Nitric Oxide. *Antioxid Redox Signal* 23, 283-294.
- Wang, L., and Macko, S.A. (2011). Constrained preferences in nitrogen uptake across plant species and environments. *Plant Cell Environ* 34, 525-534.
- Wang, R., Guan, P., Chen, M., Xing, X., Zhang, Y., and Crawford, N.M. (2010). Multiple regulatory elements in the Arabidopsis NIA1 promoter act synergistically to form a nitrate enhancer. *Plant physiology* 154, 423-432.
- Wang, R., Okamoto, M., Xing, X., and Crawford, N.M. (2003). Microarray analysis of the nitrate response in Arabidopsis roots and shoots reveals over 1,000 rapidly responding genes and new linkages to glucose, trehalose-6-phosphate, iron, and sulfate metabolism. *Plant physiology* 132, 556-567.
- Wang, R., Tischner, R., Gutiérrez, R.A., Hoffman, M., Xing, X., Chen, M., Coruzzi, G., and Crawford, N.M. (2004). Genomic analysis of the nitrate response using a nitrate reductase-null mutant of Arabidopsis. *Plant physiology* 136, 2512-2522.
- Waterhouse, A., Bertoni, M., Bienert, S., Studer, G., Tauriello, G., Gumienny, R., Heer, F.T., de Beer, T.A.P., Rempfer, C., Bordoli, L., *et al.* (2018). SWISS-MODEL: homology modelling of protein structures and complexes. *Nucleic Acids Res* 46, W296-W303.

- Wildt, J., Kley, D., Rockel, A., Rockel, P., and Segschneider, H.J. (1997). Emission of NO from several higher plant species. *Journal of Geophysical Research: Atmospheres* *102*, 5919-5927.
- Wilkinson, J.Q., and Crawford, N.M. (1991). Identification of the Arabidopsis CHL3 gene as the nitrate reductase structural gene NIA2. *The Plant cell* *3*, 461-471.
- Wilkinson, J.Q., and Crawford, N.M. (1993). Identification and characterization of a chlorate-resistant mutant of Arabidopsis thaliana with mutations in both nitrate reductase structural genes NIA1 and NIA2. *Mol Gen Genet* *239*, 289-297.
- Wilson, I.D., Neill, S.J., and Hancock, J.T. (2008). Nitric oxide synthesis and signalling in plants. *Plant Cell Environ* *31*, 622-631.
- Wu, D., Chu, J., Hao, Y.-Y., Wang, Y.-H., Zhuang, Y.-P., and Zhang, S.-L. (2012). Incomplete protein disulphide bond conformation and decreased protein expression result from high cell growth during heterologous protein expression in Pichia pastoris. *Journal of Biotechnology* *157*, 107-112.
- Wu, S., Hu, C., Tan, Q., Xu, S., and Sun, X. (2017). Nitric Oxide Mediates Molybdenum-Induced Antioxidant Defense in Wheat under Drought Stress. *Frontiers in Plant Science* *8*.
- Wu, S., Lu, Q., Kriz, A.L., and Harper, J.E. (1995). Identification of cDNA clones corresponding to two inducible nitrate reductase genes in soybean: analysis in wild-type and nr1 mutant. *Plant Mol Biol* *29*, 491-506.
- Xie, Q.W., Cho, H.J., Calaycay, J., Mumford, R.A., Swiderek, K.M., Lee, T.D., Ding, A., Troso, T., and Nathan, C. (1992). Cloning and characterization of inducible nitric oxide synthase from mouse macrophages. *Science* *256*, 225-228.
- Xie, Y.J., Mao, Y., Lai, D.W., Zhang, W., Zheng, T.Q., and Shen, W.B. (2013). Roles of NIA/NR/NOA1-dependent nitric oxide production and HY1 expression in the modulation of Arabidopsis salt tolerance. *Journal of experimental botany* *64*, 3045-3060.
- Yamasaki, H. (2005). The NO world for plants: achieving balance in an open system. *Plant, Cell & Environment* *28*, 78-84.
- Yamasaki, H., and Sakihama, Y. (2000). Simultaneous production of nitric oxide and peroxynitrite by plant nitrate reductase: *in vitro* evidence for the NR-dependent formation of active nitrogen species. *Febs Letters* *468*, 89-92.
- Yamasaki, H., Sakihama, Y., and Takahashi, S. (1999). An alternative pathway for nitric oxide production in plants: new features of an old enzyme. *Trends in plant science* *4*, 128-129.
- Yanagisawa, S. (2014). Transcription factors involved in controlling the expression of nitrate reductase genes in higher plants. *Plant science : an international journal of experimental plant biology* *229*, 167-171.
- Yang, J., Giles, L.J., Ruppelt, C., Mendel, R.R., Bittner, F., and Kirk, M.L. (2015). Oxyl and hydroxyl radical transfer in mitochondrial amidoxime reducing component-catalyzed nitrite reduction. *J Am Chem Soc* *137*, 5276-5279.
- Yang, Z., Fang, J., Chittuluru, J., Asturias, F.J., and Penczek, P.A. (2012). Iterative stable alignment and clustering of 2D transmission electron microscope images. *Structure (London, England : 1993)* *20*, 237-247.
- Yu, X., Sukumaran, S., and Mrton, L. (1998). Differential expression of the arabidopsis nia1 and nia2 genes. cytokinin-induced nitrate reductase activity is correlated with increased nia1 transcription and mrna levels. *Plant physiology* *116*, 1091-1096.
- Zeidler, D., Zahringer, U., Gerber, I., Dubery, I., Hartung, T., Bors, W., Hutzler, P., and Durner, J. (2004). Innate immunity in Arabidopsis thaliana: lipopolysaccharides activate nitric oxide synthase

Marie Mohn

(NOS) and induce defense genes. *Proceedings of the National Academy of Sciences of the United States of America* *101*, 15811-15816.

Zemojtel, T., Frohlich, A., Palmieri, M.C., Kolanczyk, M., Mikula, I., Wyrwicz, L.S., Wanker, E.E., Mundlos, S., Vingron, M., Martasek, P., *et al.* (2006). Plant nitric oxide synthase: a never-ending story? *Trends in plant science* *11*, 524-525; author reply 526-528.

Appendix 1

Codon usage frequency for expression of AtNR1-fl in *P. pastoris*.



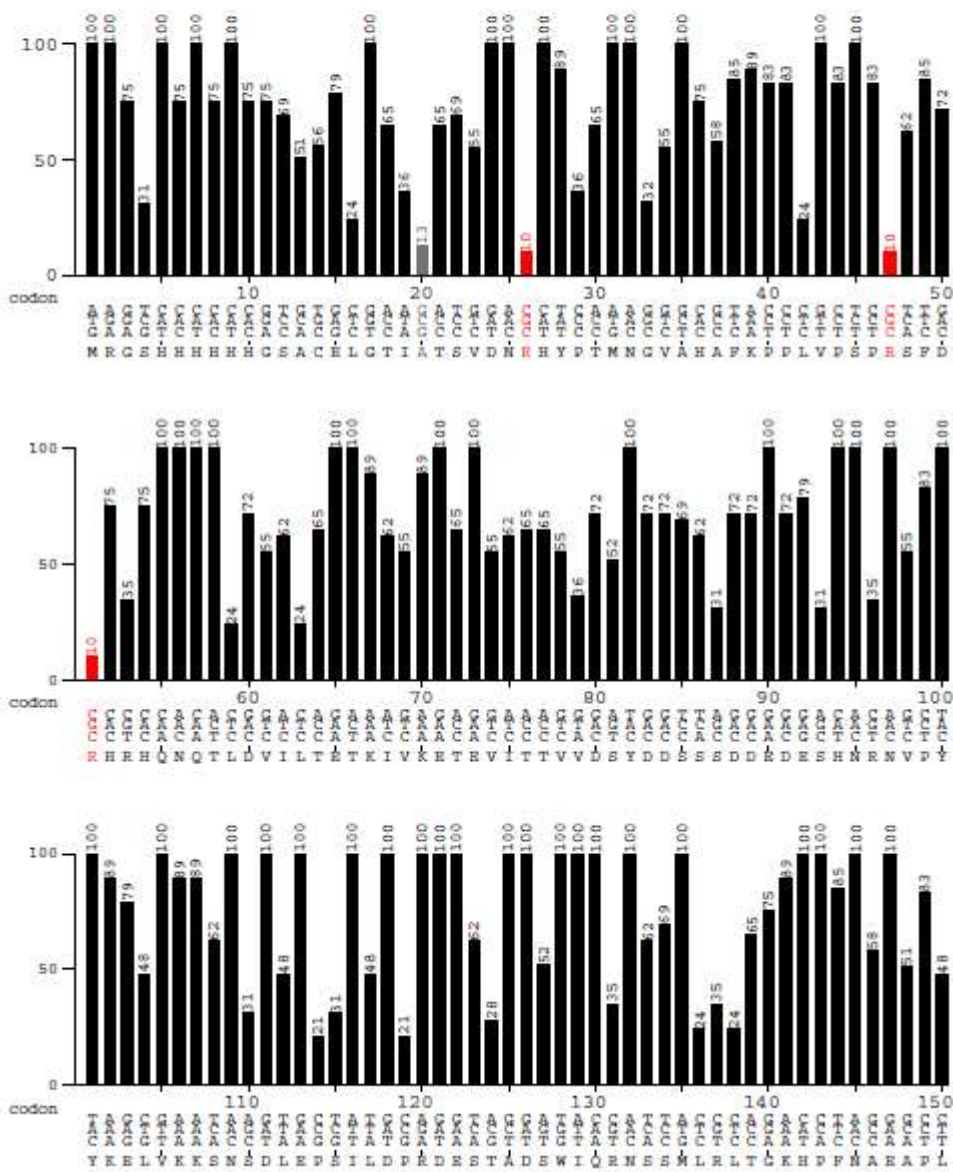
www.gcu.de

created: 31.01.2019

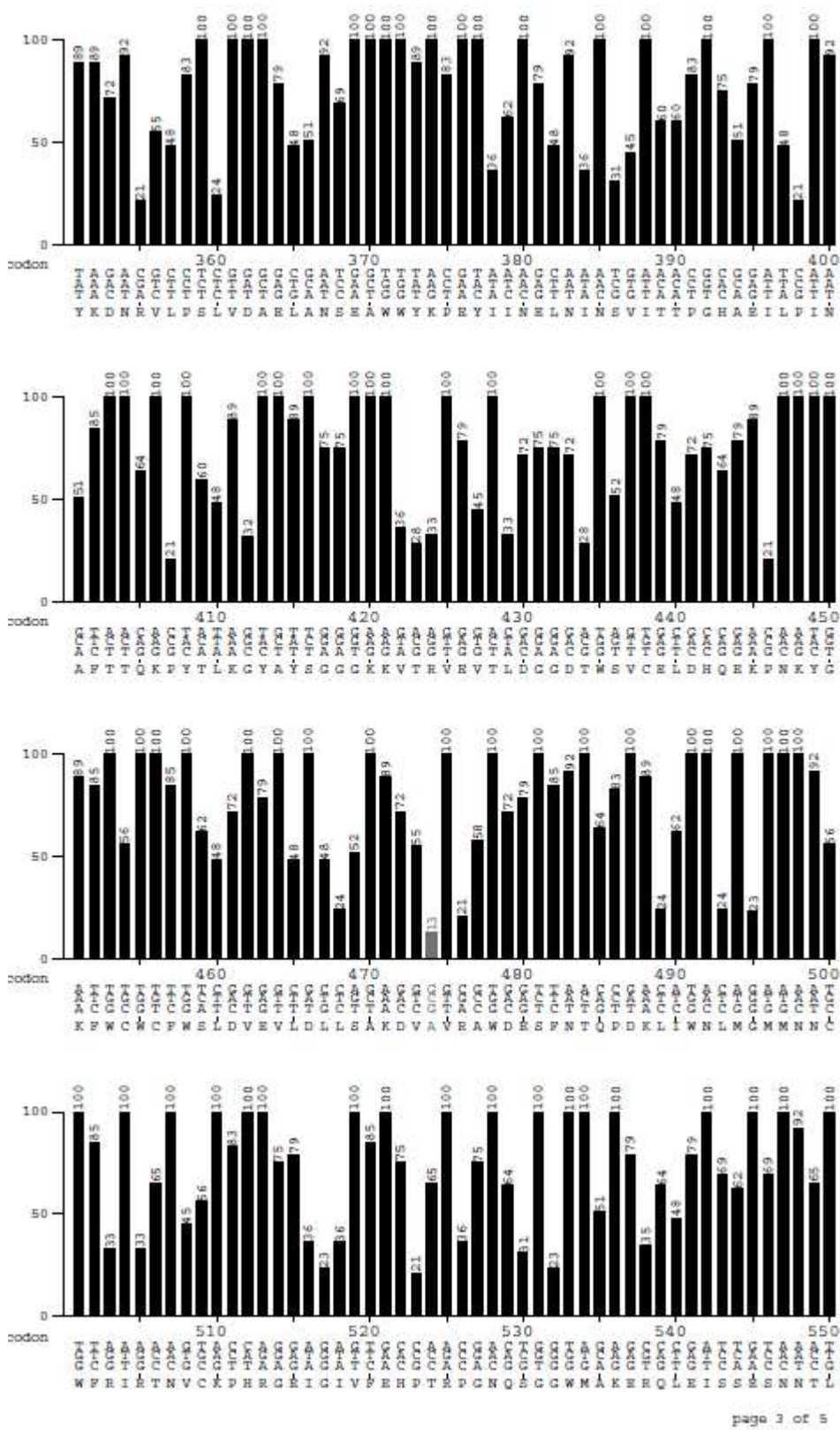
AtNR1-fl
sequence derived from Arabidopsis thaliana

Codontable:
Pichia pastoris

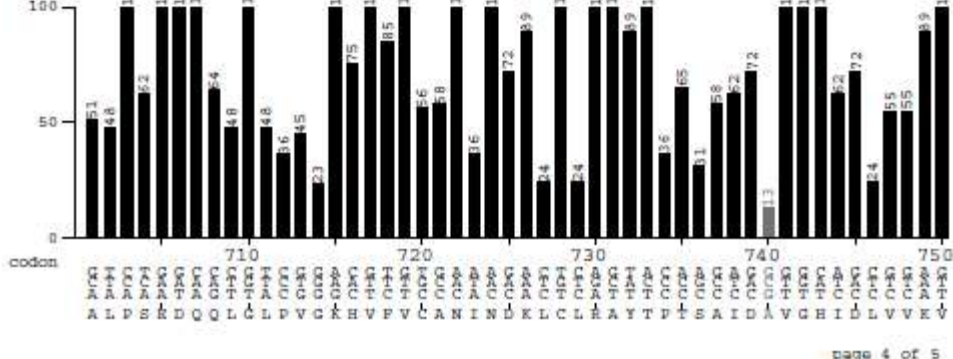
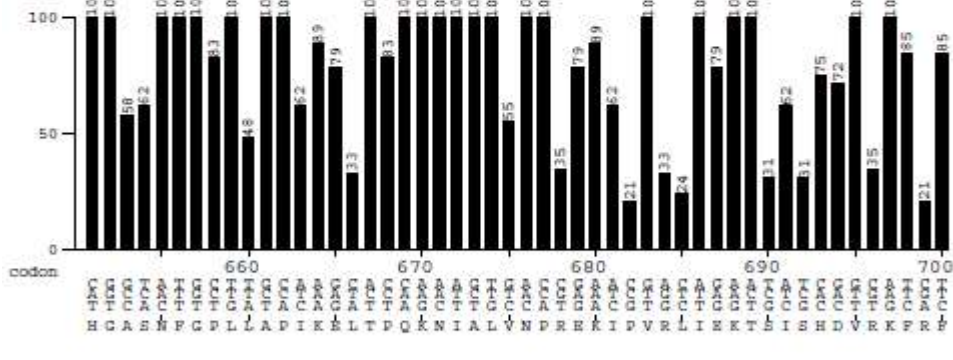
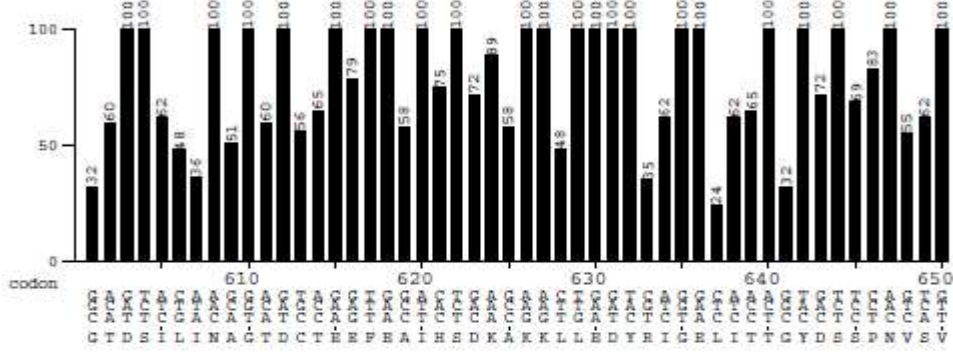
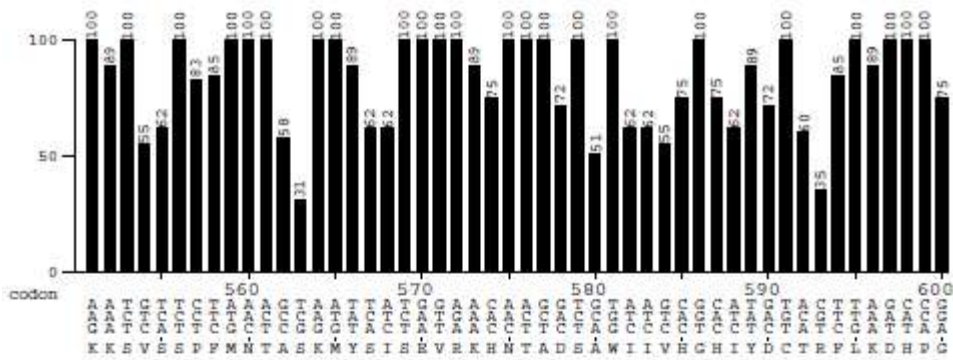
Ordinate (y-axis): relative adaptiveness <20% <10%



Codon usage frequency for expression of AtNR1-fl in *P. pastoris*.



Codon usage frequency for expression of AtNR1-fl in *P. pastoris*.



Appendix 2

Primers for PCR reactions

Function	Primer sequence	T _A	Restriction enzyme cut site
Spinach Mo-heme out of SoNRfl in pET21a into pQE80	11_MMo_So MoH into pQE_Pael_for: CATTTGATCGATgcatGCATGGCGGCGTC	59°C	Pael
	12_MMo_So MoH into pQE_Sall rc: CTGAGTTACCGGtCGActACGAGTCAG	59°C	Sall
So-NR-Mo-heme out of pQE80 (taking N-term His) into pPICZb	19_MMo_for_SoMoH_from pQE into pPICZ_EcoRI: CAA TTT CAC ACA GAA TTC ATT AAA GAG	52°C	EcoRI
	20_MMo_rc_SoMoH_from pQE into pPICZ_NotI : GGCTGcGcGgCcgCTACGAGTC	54°C	NotI
SoNR-fl out of pET21a into pQE80	23_MMo_for_SoNR_into pQE80_SacI: G ATA TAC ATA gaG CTc GCT ATa GCG GCG TC	60°C	SacI
	24_MMo_rc_SoNR fl_into pQE80_Sall : CCGCAAGCTTGTCGACttaAAAAATCAAC	58°C	Sall
SoNR-fl out of pQE80 (taking N-term His) into pPICZb	25_MMo_for_SoNR_into_pPICZ_KpnI: GAG GAG AAg gTA cCT ATG AGA GGA TC	53°C	KpnI
	26_MMo_rc_SoNR_into_pPICZ_NotI : CTTGGCTGgcGGcCGcCTTAAAAAATC	55°C	NotI
AtNR1-fl out of RAFL09 into pQE80	29_MMo_for_AtNR1corr_into_pQE80_KpnI : G TTC AAT CAC ggt ACC ATa GCG ACC TC	57°C	KpnI
	30_MMo_rc_AtNR1corr_into_pQE80_Sall : GCACAGAAgTcGAcCAAATCTAGAAGATTAAG	56°C	Sall
AtNR1-fl out of pQE80 (taking N-term His tag) into pPICZb	31_MMo_for_AtNR1_into_pPICZ_XhoI: GAG GAG AAc Tcg AgT ATG AGA GGA TCG C	56°C	XhoI
	32_MMo_rc_AtNR1_into_pPICZ_NotI : CTGCAGGgCGgCCgcATCTAGAAG	56°C	NotI
AtNR1-Mo-heme out of pQE80 (taking N-term His) into pPICZb	15_MMo_for_AtMoH1_pQE80_XhoI: GAG GAG AAc Tcg AgT ATG AGA GGA TCG	56°C	XhoI
	16_MMo_rc_AtMoH1_pQE80_NotI : TGG CTG Cgc GgC cgC TCA GGA AGA G	58°C	NotI
AtNR2-Mo-heme out of pQE80 (taking N-term His) into pPICZb	33_MMo_for_AtMoH2_into pPICZ_EcoRI: CAA TTT CAC ACA GAA TTCATTAAAGAGG	54°C	EcoRI
	34_MMo_rc_AtMoH2_into_pPICZb_XbaI : CCAAGCTCAtCTAgaTAAGCTTTCAAG	54°C	XbaI

ID positive transformed colonies of <i>Pichia</i> expressing <i>AtNR1-co-fl</i>	38_MMo_Optimized NR1_mid_regionF: GAGAGTTGTTGACTCCTGATC	52°C	n/a
	40_MMo_PCR_OptiNR1_Rev: CTCATCCAAGCTCTAACAG	52°C	n/a
ID positive transformed colonies of <i>Pichia</i> expressing CO SoNRfl	39_MMo_Optimized SoNR_mid_regionF:CTGGTTTCATTGGTGGTAGA ATG	53°C	n/a
	41_MMo_PCR_OptiSoNR_Rev: GAACCAACAGTTGTTCATCATAAC	52°C	n/a
Remove internal His tag from <i>AtNR1-co-fl</i> in pPICZa and remove C-term stop- re-insert into pPICZa using EcoRI and XhoI	50_MMo_for_NR1opti_EcoRI: CGAGGAATTCGAA ATG GCG ACA TCA GTC GAT AAC	64°C	EcoRI
	55_MMo-rc_removeCterm-stopNR1opti: CGGCTCGAGGTACCTaACAGATCCTCTTC	64°C	n/a
PCR I: Remove internal His-tag from <i>AtNR1-co-fl</i> and insert stop at C-term	50_MMo_for_NR1opti_EcoRI:CGAGGAATTCGAA ATG GCG ACA TCA GTC GAT AAC	64°C	EcoRI
	51_MMo_rev_NR1opti_cutMyc: GCGGCTCGAGGTACCGTTAAAAAGATAAGCAAGT C	66°C	n/a
PCR II: Insert N-term Prescission site into <i>AtNR1-co-fl</i> (however not properly coded)	52_MMo-for_add Presc to NR1: TTTTCTG TTC CAG GGG CCC ATGGCGACATCAGTCGATAAC	52°C	n/a
	53_MMo-rc_add Presc to NR1: GCGGCTCGAGGTACCG	54°C	n/a
PCR III: <i>AtNR1fl</i> Extend N-term by 6xHis tag and Yeast Kozak seq. insert into pPICZb using EcoRI and XhoI	54_MMo_for_addHistag: tttt gaa ttc gCT ATG gGA CAT CAC CAT CAC CAT CAC CTG TTC CAG GGG CCCATGGCGAC	55°C	EcoRI
	53_MMo-rc_add Presc to NR1: GCGGCTCGAGGTACCG	54°C	n/a
Excise NR1-Mo domain from NR1-fl in pQE80, replace into pQE80	29_MMo_for_AtNR1corr_into_pQE80_Kpnl: GTTCAATCACggtACCATaGCGACCTC	57°C	Kpnl
	45_MMo_rc_NR1-Mo_Sall: CTCTATGAGGCgTcgACTaGTTGGTCC	57°C	Sall
Excise NR1-FAD domain fragment from NR1-FI in pE80 and placement into pQE80p	Btq3 NR1FAD f BamH1 : C ATT GCT TTG Gat ccaaC CCA CGT GAG AAA ATC	63°C	BamH1
	Btq4 NR1FAD rc HindIII : G GCT GCA GGT CaA gCttAT CTA GAA GAT TAA G	60°C	HindIII
Excise NR2-FAD domain fragment from NR2-FI in pPICZb and placement into pQE80p	Btq1 NR2FAD f Pst1 : CT CCG GTT AGG AAC CTg cag TT GTT AAT CCC CG	63°C	PstI
	Btq2 NR2FAD rc HindIII : GCC GCG GCT CaA GcT tCC CTA GAA TAT CAA G	64°C	HindIII

Bacterial Strains

Strain	Genotype/Description	Function
Turbo competent <i>E. coli</i> (NEB)	F' proA ⁺ B ⁺ lacI ^q ΔlacZM15/fhuA2 Δ(lac-proAB) glnV galE15 galK16 R(zgb-210::Tn10)Tet ^S endA1 thi-1 Δ(hsdS-mcrB)5	Cloning/ Subcloning
<i>E. coli</i> DH5α	F ⁻ endA1 glnV44 thi-1 recA1 relA1 gyrA96 deoR nupG purB20 φ80dlacZΔM15 Δ(lacZYA-argF)U169, hsdR17(r _K ⁻ m _K ⁺), λ ⁻	Cloning/ Subcloning
<i>E. coli</i> XL-2 Blue (Stratagene)	endA1 supE44 thi-1 hsdR17recA1 gyrA96 relA1 lac [F' proAB lacI ^q ZΔM15 Tn10 (Tet ^r) Amy Cam ^r]	Cloning/ Subcloning
<i>E. coli</i> TP1004 (Tracy Palmer)	(As RK4353 Δ <i>mobAB</i> ::Kan). 'Unpublished. Similar to TP1000 but in a slightly different strain background that may synthesise more Moco.' Tracy Palmer http://www.lifesci.dundee.ac.uk/groups/tracy_palmer/moco.html	Expression of Moco- containing proteins
<i>E. coli</i> BL- 21 Rosetta (Novagen)	F- ompT hsdSB(rB- mB-) gal dcm (DE3) pRARE (CamR)	Expression of proteins

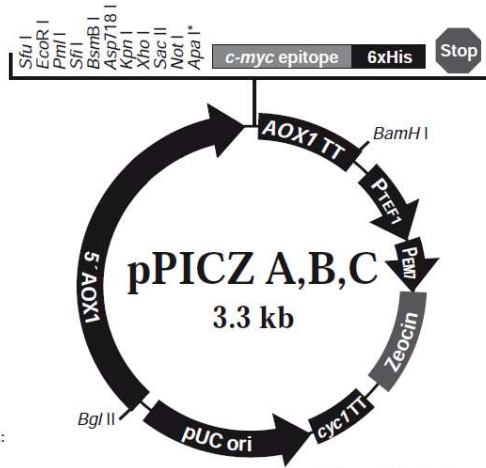
Yeast Strains

Strain	Genotype/Phenotype	Function
<i>Pichia pastoris</i> KM71H	arg4 aox1::ARG4 / Mut S, Arg+	Expression of proteins
<i>Pichia pastoris</i> GS115	his4 / His-, Mut+	Expression of proteins

Plasmids

Plasmid	Information	Reference/Source
pQE80	Used for expressing N-terminally His-tagged proteins in <i>E. coli</i> (Especially Moco-proteins in TP1004)	Qiagen
pJET2.1 blunt	Used for cloning and amplification of intermediate PCR cloning fragments	Thermo Scientific
pET21a	Expression of non-Moco proteins	Novagen
pPICZa, b, c	Expression of proteins in <i>P. pastoris</i>	Invitrogen

Map of pPICZ plasmids

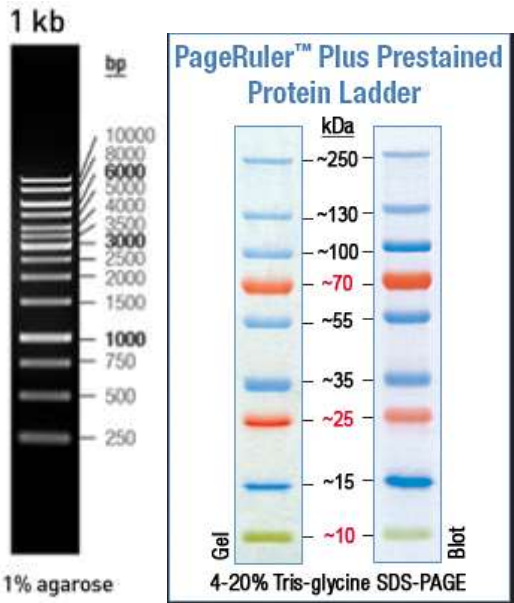


Comments for pPICZ A:
3329 nucleotides

5' AOX1 promoter region: bases 1-941
 5' end of AOX1 mRNA: base 824
 5' AOX1 priming site: bases 855-875
 Multiple cloning site: bases 932-1011
 c-myc epitope tag: bases 1012-1044
 Polyhistidine tag: bases 1057-1077
 3' AOX priming site: bases 1159-1179
 3' end of mRNA: base 1250
 AOX1 transcription termination region: bases 1078-1418
 Fragment containing TEF1 promoter: bases 1419-1830
 EM7 promoter: bases 1831-1898
 Sh ble ORF: bases 1899-2273
 CYC1 transcription termination region: bases 2274-2591
 pUC origin: bases 2602-3275 (complementary strand)

* The restriction site between *Not*I and the *myc* epitope is different in each version of pPICZ:
 Apa I in pPICZ A
 Xba I in pPICZ B
 SnaB I in pPICZ C

DNA Ladder and Protein MW marker:



Appendix 3

A standard curve of NO[•] generated on the NO-analyser was prepared by Daniel Bender as described (MacArthur et al., 2007). The following figure is copied from (Bender, 2017). This calibration curve was the basis of NO[•] quantification in this work.

Calibration of NO analyser

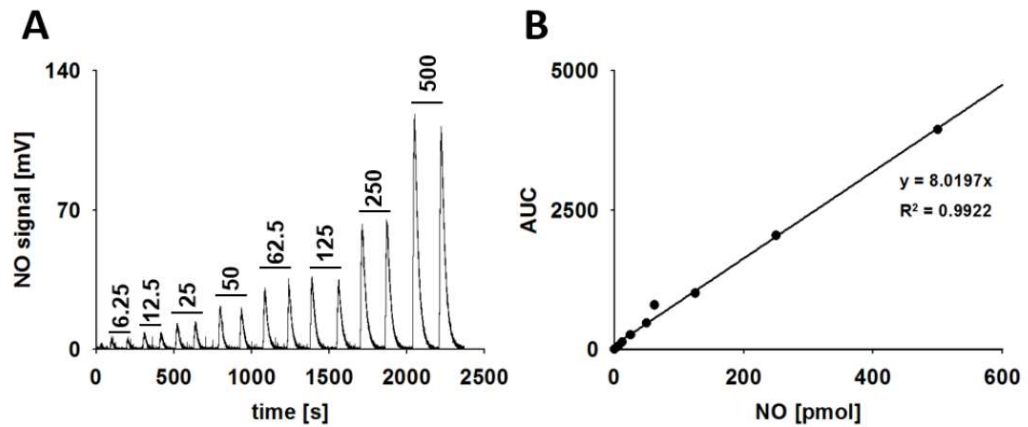


Figure: Calibration of the Sievers 280i NO analyser. **A:** Measurement of nitrite by tri-iodide-based gas phase chemiluminescence. 50 μ L of differing sodium nitrite concentrations (indicated as numbers over the peaks in pmol) were injected into 6 mL 60 mM potassium iodide and 51.2 mM iodine in 70% acetic acid at 37°C. **B:** Area under the curve of A calculated with OriginPro8.5 software versus the total amount of NO.

Acknowledgements

I would like to thank Prof. Dr. Günter Schwarz and Dr. Katrin Schrader for the opportunity to join the group. Katrin and Günter for their excellent guidance and all my colleagues for their encouragement and support. Thanks to Prof. Dr. Stanislav Kopriva for agreeing to be the second referee on my thesis and Prof. Dr. Kay Hofmann and Dr. Daniel Bender for being the chair of my thesis committee and observer respectively.

Thanks to my family for their love and support.

Erklärung

Ich versichere, dass ich die von mir vorgelegte Dissertation selbstständig angefertigt, die benutzten Quellen und Hilfsmittel vollständig angegeben und die Stellen der Arbeit – einschließlich Tabellen, Karten und Abbildungen –, die anderen Werken im Wortlaut oder dem Sinn nach entnommen sind, in jedem Einzelfall als Entlehnung kenntlich gemacht habe; dass diese Dissertation noch keiner anderen Fakultät oder Universität zur Prüfung vorgelegen hat; dass sie – abgesehen von unten angegebenen Teilpublikationen – noch nicht veröffentlicht worden ist sowie, dass ich eine solche Veröffentlichung vor Abschluss des Promotionsverfahrens nicht vornehmen werde. Die Bestimmungen dieser Promotionsordnung sind mir bekannt. Die von mir vorgelegte Dissertation ist von Prof. Dr. G. Schwarz am Institut für Biochemie der Mathematisch-Naturwissenschaftlichen Fakultät der Universität zu Köln betreut worden.

Köln den _____, Marie Mohn _____

Teilpublikationen:

Marie Mohn, Besarta Thaqi, and Katrin Fischer-Schrader. Isoform-specific NO synthesis by *Arabidopsis thaliana* nitrate reductase. Plants Special Edition NO, 2019